2001

Experimental study of the attenuation of acoustic emission signals in welded steel structures

Jacqueline Mayrosh
Lehigh University

Mayrosh, Jacqueline

Experimental Study of the Attenuation of Acoustic Emission Signals in Welded Steel Structures

January 2002

EXPERIMENTAL STUDY OF THE ATTENUATION OF ACOUSTIC EMISSION SIGNALS IN WELDED STEEL STRUCTURES

by

Jacqueline Mayrosh

A Thesis

Presented to the Graduate and Research Committee

of Lehigh University

in Candidacy for the Degree of

Master of Science

in

Department of Civil and Environmental Engineering

Lehigh University

Bethlehem, Pennsylvania

July 11, 2001

This thesis is accepted and approved in partial fulfillment of the requirements for the Master of Science.

JUN 11, 2001

Date

Dr. Stephen Pessiki

Dr. Arup SenGupta

Department of Civil and Environmental Engineering

ACKNOWLEDGEMENTS

This research was funded by the Pennsylvania Infrastructure Technology Alliance. The author wishes to express thanks to the principal investigator of this research, Dr. Stephen Pessiki, for his guidance and knowledge. The academic and professional growth he provided is greatly appreciated. The author also wishes to acknowledge the assistance provided by Mr. Scott Kopp of High Steel Structures, Inc., Mr. Robert Connor, and the staff of technicians at the ATLSS Engineering Center.

Above all, the author would like to thank her parents, family, and friends for their love, encouragement and support.

The support from the sponsor is gratefully acknowledged. The findings and conclusions presented in this report are those of the author, and do not necessarily reflect the views of the sponsor or the individuals acknowledged.

TABLE OF CONTENTS

LIST OF TABLES

LIST OF FIGURES

ABSTRACT

Acoustic emissions are transient elastic stress waves generated by the rapid release of energy from a localized source within a material. In steel structures subjected to fatigue loading, this localized source can be a crack tip. This research studies the attenuation of acoustic emissions as they propagate in typical welded steel plate girders. A series of specimens were fabricated to replicate the web and flange of the plate girder as well as typical welded details such as web and flange splices, the web-to-flange connection, and the stiffener-to-web connection. Simulated acoustic emissions were created by mechanical impact on the plate surface and were recorded with broadband displacement transducers. The displacement waveforms that result from impact were analyzed in the time domain using average waveforms created by repeated impact. The recorded waveforms were compared to determine the effect of the welded details on the amplitude and shape of recorded surface displacement waveforms. It was found that, for the materials and geometries treated in this study, attenuation of the surface displacements occurs due to the geometry of the plate girder. The roll direction has a dispersive effect in thin web plates but has little effect in the thicker flange. The groove welds used in the web and flange splices have no effect on the surface displacements. The welded connections affect both the amplitude and the shape of surface displacement waveforms that pass through

them. The web-to-flange connection and the stiffener-to-web connections cause a significant attenuation of the surface displacements.

CHAPTER 1

INTRODUCTION

1.1 INTRODUCTION

Acoustic emissions are transient stress waves generated by the rapid release of energy from localized sources within a material. The acoustic emission method is a nondestructive means of detecting and monitoring damage in structures and is particularly useful as a means to monitor structures subject to fatigue. As a crack propagates in a structure, transient elastic waves are generated by the rapid release of energy at a localized source, the crack tip (Matthews, 1983). The released energy propagates through the structure as stress waves. The stress waves are detected by transducers placed on the surface of the structure.

Acoustic emission testing has been standardized for certain applications. For example, the acoustic emission method is currently employed in proof-testing procedures for pressure vessels and in monitoring bucket trucks. These applications are standardized in ASTM 1419 and ASTM F915 respectively. Standardized test procedures do not currently exist for acoustic emission monitoring of civil-structural members.

This research focuses on the use of the acoustic emission method as a monitoring technique in civil-structural members, specifically in steel welded plate girders that are subject to fatigue cracking.

An acoustic emission originates at a crack tip as the crack propagates through the member. Transducers are placed on the structure to detect acoustic emission activity. Any obstruction between the source of the emission and the transducer may affect the emission as it propagates through the member. A variety of potential obstructions are present in welded plate girders. For example, welds present between the acoustic emission source and the transducer may attenuate the signal, causing a change in signal amplitude or the features of the signal. Because of this, a large number of transducers may be necessary to accurately assess the acoustic emission.

This report presents research that studies attenuation of the acoustic emission signals in welded steel structures. The study is conducted by introducing stress waves to a steel plate and evaluating the attenuation of the stress waves as they cross typical welded details commonly found in welded plate girders. With understanding of the attenuation of the stress waves by these welded details, the number of transducers necessary to employ the technique may be more accurately determined. This makes acoustic emission even more viable for monitoring of members subject to fatigue.

1.2 OBJECTIVE

The objective of this research is to experimentally study the attenuation of acoustic emission signals caused by details commonly used in welded steel plate girders.

1.3 SUMMARY OF APPPROACH

In this research, simulated acoustic emissions are introduced into steel plate specimens that contain welded details commonly found in steel plate girders. The simulated acoustic emissions are comprised of stress waves introduced into the plate by the impact of a steel sphere on the plate surface. The plates are small specimens with thicknesses ranging from 13 mm to 51 mm designed to reproduce the flange and web of the girder, a flange splice, a web splice, web-to-flange connection, and stiffener-to-web connection. The effect of each detail is determined by recording the surface displacements with transducers and comparing the surface displacement due to impact for each plate.

1.4 SUMMARY OF FINDINGS

Surface displacements of the various test specimens caused by mechanical impact are compared in both the amplitude and shape of the displacement waveform. The effect of the presence of welded details between the source location and the transducer is evaluated for the web splice, flange splice, stiffener-to-web connection, and web-to-flange connection. The effect of the orientation of the welds used in the details is also studied.

It was found that, for the materials and geometries treated in this study, attenuation of the surface displacements occurs due to the geometry of the plate girder. The roll direction has a dispersive effect in thin web plates but has little

effect in the thicker flange. The groove welds used in the web and flange splices have no effect on the surface displacements. The welded connections affect both the amplitude and the shape of surface displacement waveforms that pass through them. The web-to-flange connection and the stiffener-to-web connections cause a significant attenuation of the surface displacements.

1.5 OUTLINE OF REPORT

Chapter 2 presents the background information relevant to this study, including a brief review of the acoustic emission method, signal processing, and a review of plate vibration. A parameter study of all test variables is presented in Chapter 3. This parameter study is a systematic exploration of the influence of each physical component and variable in the test setup. Chapter 4 discusses the experimental program. This includes descriptions of the test plates, test setup, and testing procedures. The experimental results are presented in Chapter 5 and analyzed and discussed in Chapter 6. Finally, conclusions are presented and future research is suggested in Chapter 7.

1.6 NOTATION

The following notation is used in this report.

$2a$	=	impact-to-sensor distance (mm)
A_{IN}	=	amplitude of signal before filtering (V)
A_{OUT}	=	amplitude of signal after filtering (V)
C	=	capacitance in microfarads (μF)
D	=	flexural rigidity of plate
E	=	Young's modulus (kg/(m·s^2)
F_{CUT}	=	threshold frequency (Hz)
f	=	frequency of vibration (Hz)
f_s	=	sampling frequency (Hz)
G	=	shear rigidity (kg/(m·s^2)
h	=	drop height (mm)
N	=	number of data points
n	=	number of nodal diameters
R	=	radius of steel plate specimen (mm)
R′	=	radius of nodal circle
R_Ω	=	resistance in ohms (Ω)
r	=	radius of steel sphere (mm)
s	=	number of nodal circles
T	=	period (s)
t	=	thickness of specimen (mm)
$t_{c, exp}$	=	experimentally determined contact time (s)
$t_{c, theor}$	=	theoretical contact time (s)
ρ	=	mass density of a material (g/mm^3)
ω	=	angular frequency of vibration (rad/s)
ν	=	Poisson's ratio
Δf	=	frequency resolution (Hz)
Δt	=	sampling interval (s)

1.7 UNIT CONVERSIONS

The research in this report is presented in SI units. The following unit conversions can be used to convert to imperial units.

1 in.	=	25.4 mm
1 lb.	=	4.448 N
1 psi	=	6.895×10^3 kg/(m·s^2)
1 lb-s^2/in.	=	1.751×10^2 kg

CHAPTER 2

BACKGROUND

2.1 INTRODUCTION

This chapter provides background information pertinent to the study. As stated in Chapter 1, the objective of this research is to experimentally study the attenuation of acoustic signals in welded steel structures. Section 2.2 provides a general overview of some of the general features of acoustic emission testing to provide some context for the current study of attenuation of acoustic emission signals. Section 2.3 presents a general discussion of the attenuation of stress waves in objects, with emphasis on some of the attenuation mechanisms present in steel objects in particular. The stress waves of interest in this research are those caused by fatigue cracking. As explained more fully in Chapter 4, for the purpose of this research, the stress waves used in the tests reported here were created by mechanical impact instead of fatigue crack growth. Impact was used to provide a repeatable input with known characteristics. Section 2.4 discusses the characteristics of the stress waves generated by impact. As explained in Chapter 4, the test specimens treated in this study are circular plate specimens. Section 2.5 describes the mode shapes and frequencies of vibration of a free circular plate. The signal processing used in this report is presented in Section 2.6.

2.2 ACOUSTIC EMISSION TESTING

Acoustic emission testing is used to test a wide array of structures, and as noted in Chapter 1, application of the method has been standardized for certain particular applications. This section overviews some of the general features of acoustic emission testing to provide context for the current study of attenuation of acoustic emission signals. This section is necessarily brief, and the reader is referred to Nondestructive Testing Handbook Volume Five: Acoustic Emission Testing (ASNT, 1987) for more complete information about acoustic emission testing.

Figure 2.1 is a schematic drawing of a setup of an acoustic emission test. In this figure, the structure is under load, and an acoustic emission has been released from crack growth in the structure. The stress waves generated by crack growth propagate through the structure and their arrival is detected with a transducer. This transducer converts the mechanical disturbance at the surface of the structure into an electrical signal. This signal is either recorded in its entirety with the acoustic emission test system, or key features of the signal are recorded and the signal is then discarded.

Two types of transducers are used for acoustic emission testing. The most commonly used type of transducer is a resonant type transducer. A resonant type transducer, when excited by the arrival of the stress wave, will vibrate at its own natural frequencies of vibration. By design, resonant transducers are intended to respond most strongly at one particular frequency, and the intended

response of the transducer is described by this frequency (e.g. a 150 kHz transducer will have a dominant response at 150 kHz). A typical signal captured with a resonant type transducer is shown in Figure 2.2. The key features of this signal are noted in the figure. These features are described more fully in Nondestructive Testing Handbook Volume Five: Acoustic Emission Testing (1987). With a hit-based acoustic emission test system, these key features of the signal are recorded and the signal is discarded. Analysis of the key features of the signals, often presented in the form of correlation plots, is used to gain information about the condition of the structure under load.

The second type of transducer used for acoustic emission testing is a broadband type transducer. A broadband of transducer, when excited by the arrival of a stress wave, will provide an output voltage directly proportional to the input (surface displacement, velocity or acceleration, depending upon the construction of the transducer). The particular transducers used in this study, described more fully in Chapter 3, are broadband displacement transducers. They exhibit a flat response to normal surface displacement out to a frequency of 1 MHz. The transducers do have a resonance at a very low frequency of about 800 Hz. This low frequency resonance is removed by high-pass filtering.

In many applications, an array of two or more transducers is used to provide information about the source location of the source of an acoustic emission. The arrival times of the acoustic emission at the different transducers, along with the known wave speed in the test object, is used to calculate the location of the

source. In applications where the acoustic emission crosses boundaries such as welds or attachments, attenuation of the signal can complicate testing. An example of this is shown in Figure 2.3, using a linear arrangement of two transducers. In Figure 2.3(a), two transducers, located at A and B, are used to locate the source at C based on the arrival times of the acoustic emission at each transducer. The same situation is repeated in Figure 2.3(b), except that this case now also includes a welded attachment at D. If the attachment at D strongly attenuates the stress waves, then the arrival of the signal at B may be either greatly altered or not detected at all. Thus, the attenuation caused by the welded attachment at D has the potential to disrupt the ability to accurately locate the source at C. Suppose that the transducers at A and B are resonant type transducers. Attenuation of the stress waves by the attachment at D may also alter the features of the signal recorded with the transducer at B, (e.g. rise time, amplitude, etc.) and thus alter any analysis using correlation plots. The situation described in Figure 2.3 can be extrapolated to arrays of 3 or more transducers with multiple welds and attachments complicating the geometry of the test structure (as is the case in actual steel welded plate girders)

2.3 ATTENUATION OF STRESS WAVES

The term attenuation refers to the decrease in amplitude that occurs as a wave travels through a medium. Major factors that affect attenuation in welded steel structures include: (1) geometric spreading of the stress waves; (2) loss of

energy into adjacent media; (3) absorption of the wave in the form of damping or internal friction; (4) welds of other obstacles. Information in this section is primarily derived from the Nondestructive Testing Handbook Volume Five: Acoustic Emission Testing (ASNT, 1987).

Waves propagating in plates will undergo geometric attenuation if the source is small in size as compared to the source-to-transducer distance, 2*a*. As a wave propagates outward in all directions from a source, the wavefront is spread over a larger spherical area. Even in a lossless material (one in which mechanical energy is conserved) the amplitude of the signal must decrease in order for the wavefront to spread and have constant energy.

Attenuation from dispersion occurs because of the frequency dependence of speed for stress waves in some physical systems. Dispersion occurs when stress waves propagate in a solid medium and the wavelength is comparable with one or more dimensions. Dispersion effects are significant in the stress waves that comprise a typical acoustic emission event.

Boundaries and discontinuities can cause attenuation due to scattering and diffraction. Small voids cause the stress wave to be at least partially reflected. When a stress wave is scattered, the wave is partially reflected and partially transmitted past the void. Scattering is likely to occur in a material with inhomogeneous grain boundaries. Some energy propagates in all directions. When a wave encounters a sharp edge, such as a crack, energy passing the edge will be bent or diffracted downward. Scattering and diffraction cause a de-

crease (or an increase in some cases) of amplitude. The attenuation due to scatter and diffraction are difficult to calculate.

The rolling process used for steel plates may effect the boundaries and discontinuities in a steel member, causing a larger amount of scattering and diffraction. Inclusions in steel plates begin as spherical particles. As a plate is hot rolled to reduce thickness, the rolling elongates the metallurgical structure and inclusions parallel to the roll direction. Therefore, a thin plate and a thick plate produced from the same heat of steel will have differences in the inclusions because the thin plate will have undergone more extensive hot rolling (Roberts, 1983).

The discussion above focuses on lossless elastic media. However, real material is generally not conservative. The mechanical energy associated with motion and elastic deformation is not conserved, and energy is dispersed through various forms. Thermal energy results from thermal coupling. Mechanical energy is also lost through plastic deformations, the creation of new surfaces when a crack extends, or interactions with dislocation motion.

Losses in real materials are associated with friction and slip between surfaces, incompletely bonded inclusions or fibers in composites, or viscoelastic material behavior prevalent in plastics. The losses of mechanical energy will cause a decrease in the amplitude of a stress wave as it propagates through a medium. If the material is homogenous, the losses will occur uniformly as the stress wave travels through the medium.

The presence of a weld between the transducer and the emission source may cause attenuation of the acoustic signal since the weld may diffract or scatter the stress wave. One goal of this research to quantitatively evaluate the attenuation due to a weld or welded attachment.

2.4 CHARACTERISTICS OF STRESS WAVES GENERATED BY IMPACT

In this research, stress waves were imparted to a test specimen by mechanical impact of a steel sphere against the surface of the specimen. Impact was used to provide a repeatable input with known characteristics. This section discusses the characteristics of stress waves generated by impact.

2.4.1 Types of Stress Waves Generated by Impact

Mechanical impact on the surface of a solid generates three types of stress waves in the solid: dilatational waves, distortional waves, and surface waves. The three types of stress waves are shown in Figure 2.4. Dilatational waves, also known as primary or P-waves, and distortional waves, also known as secondary, shear, or S-waves propagate into the solid, radiating along hemispherical wavefronts. Surface waves, also known as Rayleigh or R-waves, radiate from the point source along a circular wavefront on the surface of the solid

Each wave is characterized by the direction of motion of the particles in the medium through which they propagate relative to the direction of the wave propagation, as shown in Figure 2.5. P-waves are associated with either tensile

or compressive stresses, and are characterized by particle motion parallel to the direction of wave propagation. Particle motion associated with P-waves is illustrated in Figure 2.5 (a). S-waves are associated with shear stresses, and are characterized by particle motion transverse to the direction of wave propagation, as illustrated in Figure 2.5 (b). Particle motion is in an elliptical pattern as the R-wave propagates along the surface of the solid (Figure 2.5 (c)).

The velocities of the stress waves can depend on the dimension of the solid relative to the wavelength. The velocity of each wave through an infinite elastic medium can be expressed as a function of the material properties of the medium, in particular the elastic modulus E, Poisson's ratio ν, and the material density ρ. The velocity of the P-wave, C_P, is given by the equation

$$C_P = \sqrt{\frac{E(1-\nu)}{(1+\nu)(1-2\nu)\rho}} \tag{2-1}$$

For steel, C_P=5960 m/s. The velocity of an S-wave through an infinite medium is given by the equation

$$C_S = \sqrt{\frac{G}{\rho}} \tag{2-2}$$

where G, the shear rigidity, is given by Equation 2-3:

$$G = \frac{E}{2(1+\nu)} \tag{2-3}$$

Combining Equations 2-2 and 2-3 yields Equation 2-4 for the velocity of an S-wave:

$$C_S = \sqrt{\frac{E}{2\rho(1+\nu)}} \tag{2-4}$$

For steel, C_s=3184 m/s. The velocity of the R-wave is approximated by Equation 2-5 (Sansalone, 1997):

$$C_R = \frac{0.87+1.12\nu}{1+\nu} C_s \tag{2-5}$$

For steel, C_R=2950 m/s.

As stress waves propagate through a material, the relative amplitude of particle displacements produced by a point impact will depend on the angle at which the wave travels from the point of impact. Figure 2.6 shows this variation in particle amplitude. In this figure, the waves are created by harmonic displacement input. This figure is based on work done by Miller and Pursey (1954, 1955).

2.4.2 Contact Time and Hertz Theory of Elastic Impact

In the experiments described later in this report, stress waves are introduced into the test specimens by mechanical impact—dropping a steel sphere onto the surfaces of the specimens. The time that a sphere remains in contact with a plate during impact is a function of the material properties of the sphere and plate, as well as the energy the sphere has when it strikes the plate. The contact time can be computed using the Hertz theory of contact. The contact time, t_c, of a steel sphere on a steel plate is given by the equation (Goldsmith, 1960)

$$t_c = 4.583\left[\frac{(\delta_1 + \delta_2)m_1}{\sqrt{r_1 v_0}}\right]^{\frac{2}{5}} \tag{2-6}$$

where m_1 and r_1 are the mass and radius of the steel sphere and δ_1 and δ_2 are functions of the material properties of the sphere and plate respectively and are given by Equation 2-7:

$$\delta = \frac{(1-\nu^2)}{E\pi} \tag{2-7}$$

A 2 mm diameter steel sphere is used as an impact source in the work described in Chapter 4. The test specimens are also made of steel. Equation 2-7 leads to values of $\delta_1 = \delta_2 = 1.40 \cdot 10^{-9}$ mm·s^2/kg. The velocity at contact, v_o, is calculated by the equation

$$v_0 = \sqrt{2gh} \tag{2-8}$$

where h is the drop height when the sphere has an initial velocity of zero. The contact time can be expressed as a function of the sphere radius, r, and drop height h, with Equation 2-9:

$$t_c = \frac{0.005157r}{h^{0.1}} \tag{2-9}$$

Because the drop height in the tests for this study is generally 0.150 m, the term in the denominator that is dependent on drop height has a value of 0.827, yielding Equation 2-10 for contact time.

$$t_c = 0.00623r \tag{2-10}$$

This equation gives the contact time solely dependent on the radius of the sphere.

2.5 MODE SHAPES AND VIBRATION OF A FREE CIRCULAR PLATE

A free circular plate subject to impact will vibrate in modal shapes that depend on the geometry of the plate. Each modal shape that is excited has a frequency associated with it. The deformed shape of the plate consists of the superposition of the deformed shapes of each excited frequency. The modes of vibration of the circular plate are reviewed here to aid in interpreting the results presented later in this report.

It is noted here that, although it is necessary to support the plate specimens in the laboratory, it is assumed that these supports have a negligible effect on the frequencies of vibrations that occur in the plate due to impact. The plate is assumed to act as a free plate in space, with no constrained boundaries or surface stresses.

Plate vibration is characterized by the locations on the plate where zero displacement occurs (nodes). The locations of zero displacement occur in patters of circles and diameters. Each mode shape is characterized by the numbers and of nodal circles, s, and nodal diameters, n, and their relative locations on the plate. The normal modes of vibration were first determined by Chladni, beginning with the fundamental mode when n=2, s=0 (Ravenhall, 1973). An n=1 mode does not exist because dynamic equilibrium can not be maintained. The natural

angular frequencies, ω, are given by Weaver, Timoshenko, and Young (1990) for a Poisson ratio of 0.33 by the equation

$$\omega = \frac{\alpha}{R^2}\sqrt{\frac{D}{\rho t}} \tag{2-11}$$

where R is the diameter of the plate, t is the plate thickness, ρ is the mass density. The flexural rigidity of the plate, D, is given by the equation

$$D = \frac{Et^3}{12(1-\nu^2)} \tag{2-12}$$

and α is a constant corresponding to a combination of nodal diameters and nodal circles. Table 2.1 shows values of α for the first twelve modes of vibration for a circular plate as determined by Weaver, Timoshenko, and Young (1990). The frequency is calculated from the angular frequency with Equation 2-13:

$$f = \frac{\omega}{2\pi} \tag{2-13}$$

The test specimens used in this research and presented in Chapter 4 consist of circular plates with a diameter of 915 mm and thickness of either 13 mm or 51 mm. Table 2.2 (a) gives the theoretical frequencies excited for each mode of vibration for the 13 mm thick plate. Table 2.2 (b) gives this information for the 51 mm thick plate.

The nodal diameters are equally spaced, and Rao (1999) gives the location of the nodal circles, as a ratio of the plate radius for the first eighteen modes of vibration in Table 2.3. The table gives values of R′/R, where R is the plate radius and R′ is the radius of the nodal circle. Mode shapes for the first 18 modes

of vibration of a free circular plate are found in Figure 2.7. A sample calculation determining the natural frequencies and location of nodal circles is presented in Appendix A.

In this research, the stress waves will be created by impact of a steel sphere on a steel plate. The sphere diameter will have an effect on the modes of vibration excited by impact. Large diameter spheres will cause low frequencies to be excited, but at high amplitudes. Spheres with smaller diameters will cause a relatively higher frequency content by exciting higher modes of vibration, but sacrificing amplitude (Sansalone, 1997). A pencil break will excite the highest frequencies, but at small amplitudes. Impact with a sphere results in a force time function that is parabolic. Figure 2.8 shows the force time functions for 2 mm and 5 mm diameter spheres. The distribution of frequencies corresponding to the impact of each of the two spheres on a steel plate is shown in Figure 2.9. The frequencies at $1.5/t_c$, $2.5/t_c$, $3.5/t_c$, etc., have amplitudes of zero. The large diameter sphere excites low frequencies at high amplitudes, while the smaller sphere excites a broader range of frequencies at lower amplitudes.

The pencil break most closely simulates the acoustic emissions generated in steel members by fatigue cracking (Matthews, 1983). Results are difficult to reproduce using the pencil breaks as an input signal. Therefore, a steel sphere of small diameter is used. This sphere excites sufficiently high frequencies at amplitudes large enough to allow analysis of the signal.

2.6 SIGNAL PROCESSING

In this research, the stress waves created by impact are recorded. The transducer converts the surface displacements to a proportional voltage signal. The voltage signal is passed through a filter to an oscilloscope. The oscilloscope discretizes the signal and records the time-history of the surface displacements as a digital waveform. Each waveform is composed of N discrete points sampled Δt, giving a total recorded response time of $N^*\Delta t$ seconds.

The signal can be analyzed in two ways: time domain analysis and frequency domain analysis. Both techniques are used in this report. Chapter 3 uses frequency domain analysis in the parameter study. Time domain analysis is used to compare waveforms obtained from the test specimens in Chapter 6.

2.6.1 Time Domain Analysis

Time domain analysis identifies similarities between two signals. When evaluating the similarities in digital signals using time domain analysis, wave shapes and amplitudes for a group of signals are compared. Examples of attributes of the waveform that may differ among signals include: (1) the arrival time of the signal; (2) an increase or decrease in the amplitude at a given position in the signal; or (3) the pattern of waveform.

A change in the arrival time of the signal may mean that the signal is somehow slowed in one direction by an attribute of the material the wave has passed through. For example, in a steel plate, the roll direction during manufac-

turing may cause a lag in arrival time. If stress waves are passed through an obstruction, a weld for example, the obstruction may affect the relative amplitude of the peaks of the signal or change the appearance of the signal altogether.

2.6.2 Frequency Domain Analysis

In this report, analysis of the discrete signal in the frequency domain involves transforming the time domain signal to the frequency domain using a Fourier transformation. Fourier analysis is based on the principle that a general periodic function can be expressed as the superposition of a series of sine and cosine terms.

A function, f, is termed periodic if there exists an positive number *2p* such that for every t in the domain of f, f(t+2p) = f(t*)*. For the purposes of this discussion, a time function with period of 1 second is given by Equation 2-14 and shown in Figure 2.10 (a).

$$f(t) = 2\sin(2\pi t) + \frac{1}{2}\sin(8(2\pi t)) \qquad (2\text{-}14)$$

The Fourier transformation, F(a), is a function of the input function, *f(t)*. The Fourier transformation resolves the function, f, into the sum of a series of sine terms. The results of the transformation can be plotted in an Amplitude versus Frequency plot called the frequency amplitude spectrum or frequency domain. Frequencies that are present in the function appear as peaks in the frequency amplitude spectrum. The Fourier transformation of a continuous signal is given by Equation 2-15:

$$F(a) = F(f(t)) = \int_{-\infty}^{\infty} f(t)e^{-iat}dx \qquad (2\text{-}15)$$

In the signal processing used in this research, discrete signals are used. That is, an analogue signal is recorded at N discrete values sampled at a sampling interval, Δt. The resulting frequency spectrum is dependent on the sampling interval used to descritize the signal. The sampling frequency is calculated by Equation 2-16 and is dependent on the sampling interval.

$$f_s = \frac{1}{\Delta t} \qquad (2\text{-}16)$$

The difference between adjacent frequency values on the frequency axis of the frequency spectrum, Δf, is related to the sampling frequency by Equation 2-17.

$$\Delta f = \frac{f_s}{N} \qquad (2\text{-}17)$$

The equation for the Fourier transformation of a discrete signal is given in Equation 2.18.

$$F(k\Delta f) = \sum_{n=0}^{N-1} f(n\Delta t)e^{-i(2\pi k\Delta f)(n\Delta t)}, \text{ for } k=0, 1, 2, \ldots, N\text{-}1 \qquad (2\text{-}18)$$

Figure 2.10 (b) shows the theoretical Fourier transformation of the function presented in Equation 2-14 and shown in Figure 2.10 (a). A peak occurs at the frequency of each sine component of the function. The first term of Equation 2-14, 2sin(t), has a frequency of 1/(1 s) = 1 Hz. The amplitude of the peak at 1 Hz is equal to 2, the amplitude of the sine wave corresponding to this term of

the function. A second peak occurs at 8 × (1/(1 s) = 8 Hz, corresponding to the second term of Equation 2-14. The amplitude of this peak is equal to 0.5.

Acoustic emission signals in the time domain, either real or simulated as in this research, are not necessarily periodic in nature. Nonetheless, to analyze the signals, it is assumed periodic with a period N*Δt, where N is the number of data points sampled, and Δt is the sampling interval. The sampling interval is chosen to achieve an accurate portrayal of the input signal. A large value of Δt may cause aliasing, or undersampling. Figure 2.11 shows the effects of aliasing on a sine wave recorded at different sampling intervals. The affect of aliasing on an analyzed signal is generally the appearance of a lower frequency content than is actually occurring (Sansalone, 1997).

Signals resulting from acoustic emissions are generally complex, as are their frequency spectra. A typical time domain signal is shown in Figure 2.12 (a), and its frequency spectrum is shown in Figure 2.12 (b). The time domain signal consists of 1000 points and has a sampling interval of 1μs. The series of peaks in the frequency domain are no longer simple linear spikes. They now have width, called leakage. The leakage is caused because the signal is in fact not periodic. Sharp disruptions occur at the beginning and end of the record. These sharp breaks and the lack of full cycles of the signal require a higher frequency response. Leakage can be reduced by windowing the signal. In effect, windowing uses gradual functions to decrease the influence of the beginning and end of

the signal, where the sharp breaks occur. More information on leakage and windowing is found in Santamarina (1998).

2.7 SIGNAL FILTERING

As explained in Chapter 3, a high-pass filter is used to remove a low frequency component, caused by resonance of the transducer, from the captured displacement waveform. The high-pass filter is a basic resistor-capacitor circuit shown in Figure 2.13. The cut-off frequency of the filter is determined by the equation

$$F_{CUT} = \frac{159000}{R_{\Omega}C} \tag{2-19}$$

where R_{Ω} is the resistance in ohms and C is the capacitance in microFarads.

The filter is a passive filter which requires no power supply, in effect taking its operating power from the signal that is passed through it. This causes the filter to slightly attenuate the entire signal, but greatly attenuate the portion of the signal that is below the threshold value (Horn, 1992).

s \ n	0	1	2	3
0	--	--	5.25	12.23
1	9.08	20.52	35.28	52.91
2	38.52	59.86	83.91	111.30
3	87.80	119.03	154.01	192.10
4	157.00	198.25	242.74	290.70

Table 2.1 Values of α for a circular plate with free boundary conditions.

s \ n	0	1	2	3
0	--	--	3.97	9.24
1	6.86	15.50	26.65	39.96
2	29.09	45.21	63.38	84.07
3	66.32	89.90	116.32	145.09
4	118.58	149.74	183.34	219.57

(a)

s \ n	0	1	2	3
0	--	--	0.5	1.2
1	0.9	1.9	3.3	5.0
2	3.6	5.7	7.9	10.5
3	8.3	11.2	14.5	18.1
4	14.8	18.7	22.9	27.4

(b)

Table 2.2 Frequencies of vibration for a 915 mm diameter plate: (a) 13 mm thick; (b) 51 mm thick.

s \ n	0	1	2	3
1	0.680	0.780	0.820	0.850
2	0.840	0.871	0.890	0.925
	0.391	0.497	0.562	0.605
3	0.893	0.932	0.936	0.930
	0.591	0.643	0.678	0.704
	0.257	0.351	0.414	0.460
4	0.941	0.946	0.950	0.951
	0.691	0.723	0.746	0.763
	0.441	0.498	0.540	0.572
	0.192	0.272	0.330	0.347

Table 2.3 Location of nodal circles, R′/R, for a free circular plate.

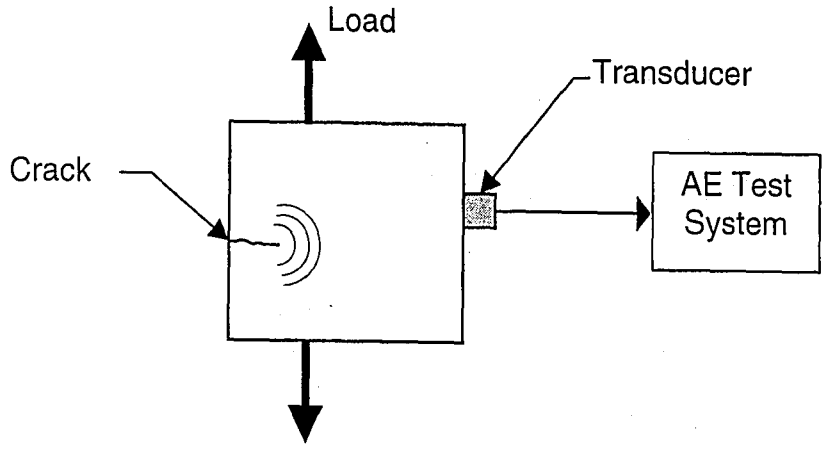

Figure 2.1 Schematic drawing of an acoustic emission test setup.

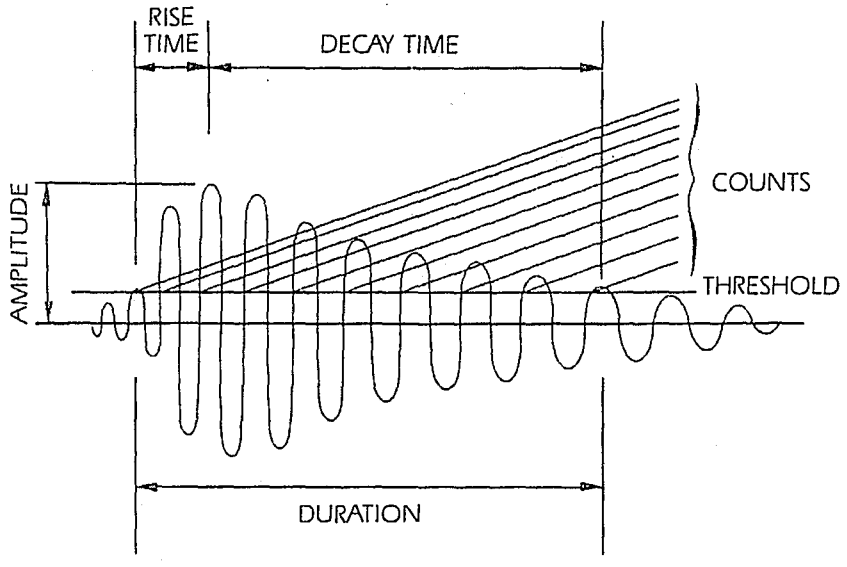

Figure 2.2 Typical acoustic emission as captured with a resonant transducer (ASNT, 1987).

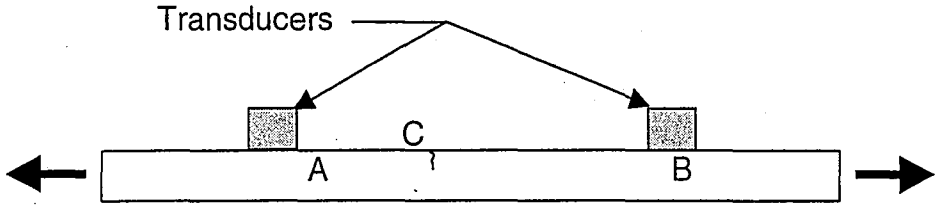

(a)

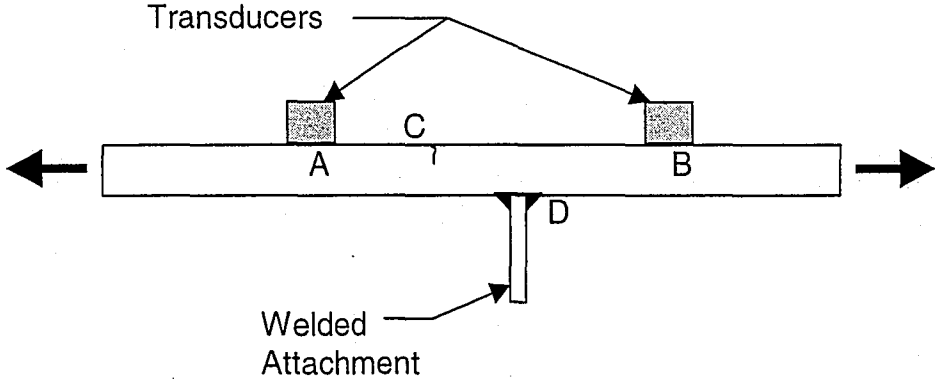

(b)

Figure 2.3 Acoustic emission source location: (a) in a plain plate; (b) with waves potentially disrupted by a welded attachment.

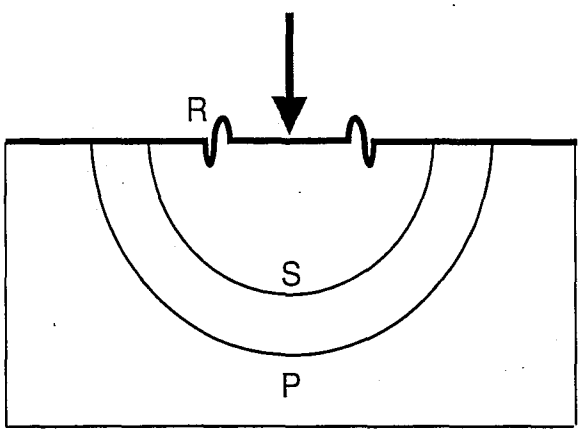

Figure 2.4 Wavefronts of P-, S-, and R-waves caused by a point impact.

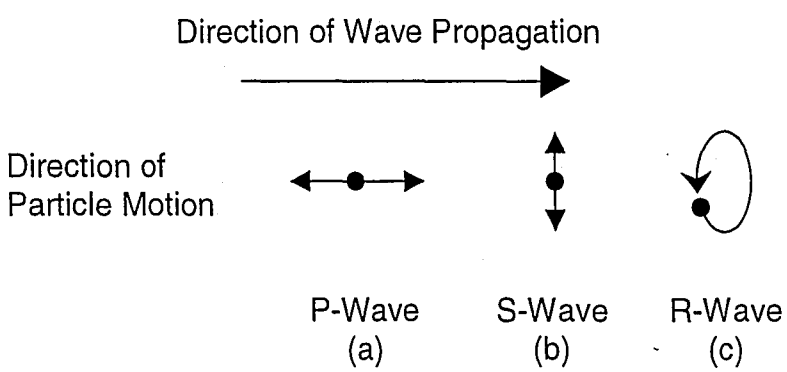

Figure 2.5 Particle motion associated with: (a) P-waves; (b) S-waves; and (c) R-waves.

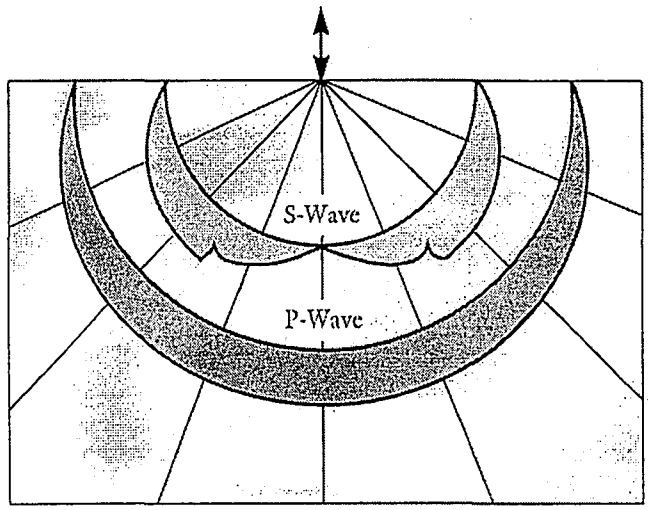

Figure 2.6 Relative amplitudes of particle displacements along P- and S- wave-fronts produced by a point impact (Sansalone, 1997).

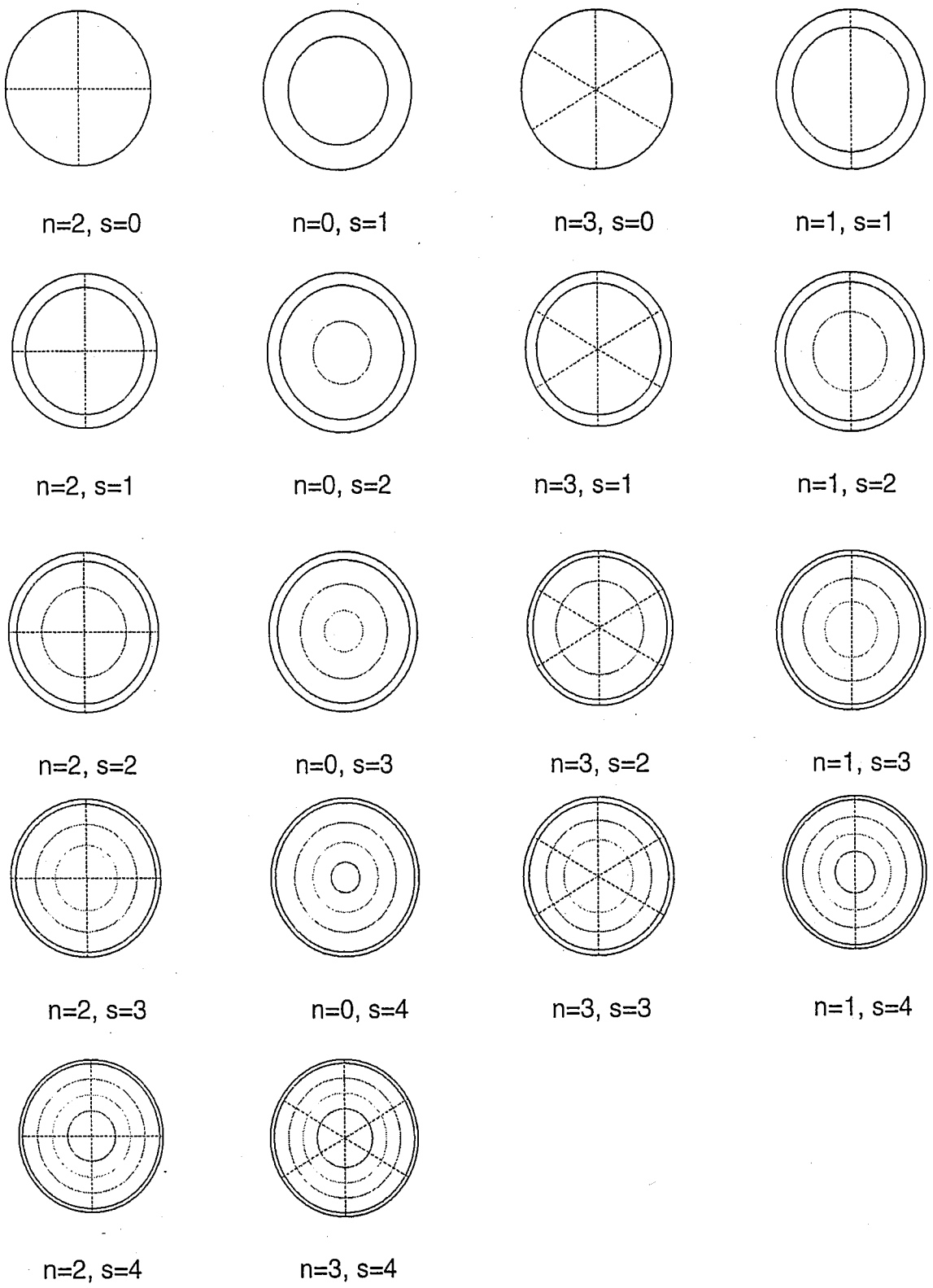

Figure 2.7 Mode shapes for the first 18 modes of vibration of a free circular plate.

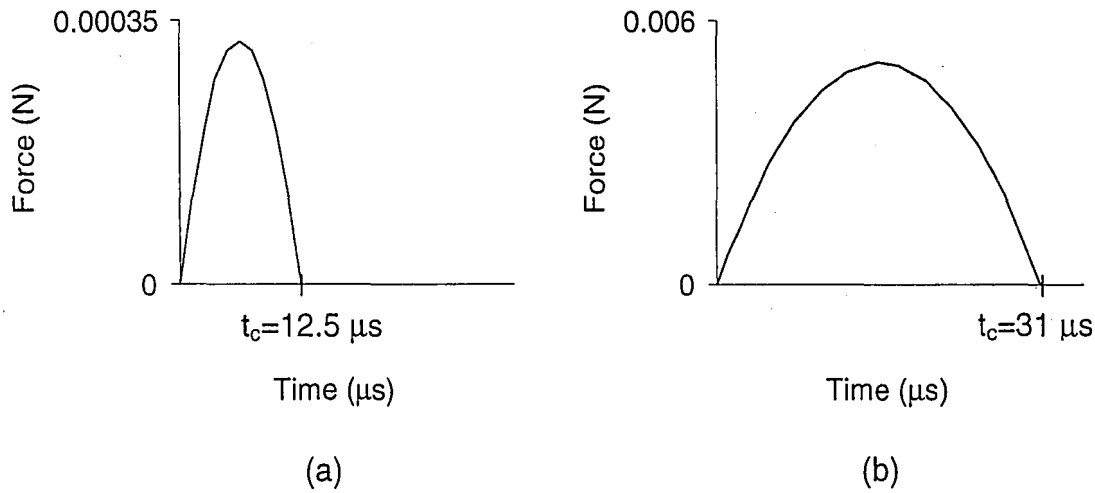

Figure 2.8 Force time functions for: (a) 2 mm diameter sphere; (b) 5 mm diameter sphere.

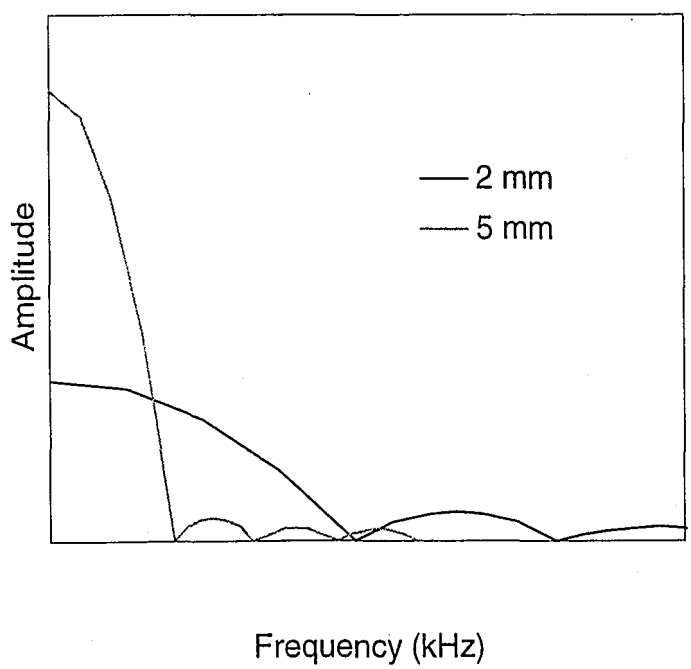

Figure 2.9 Effect of sphere diameter on the frequencies excited by impact.

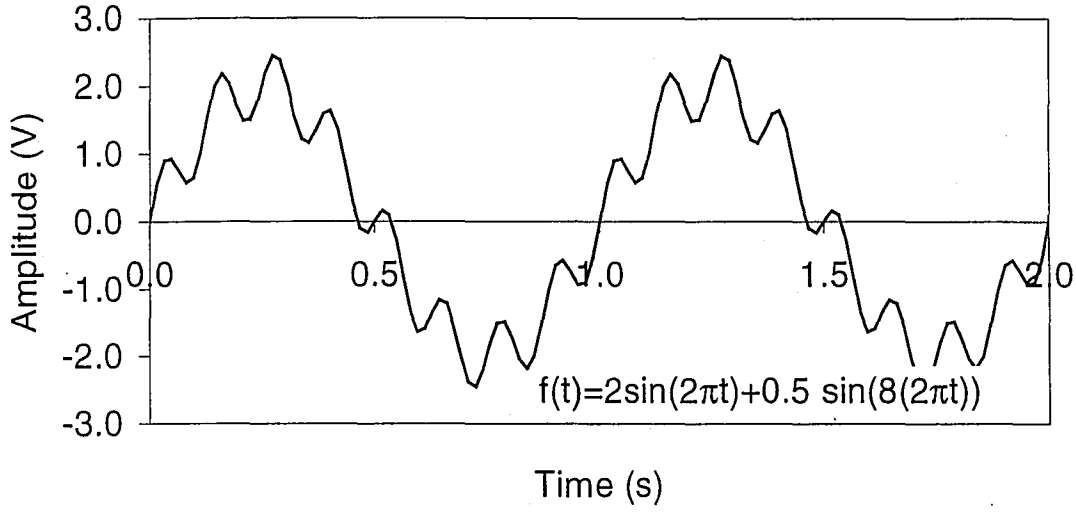

(a)

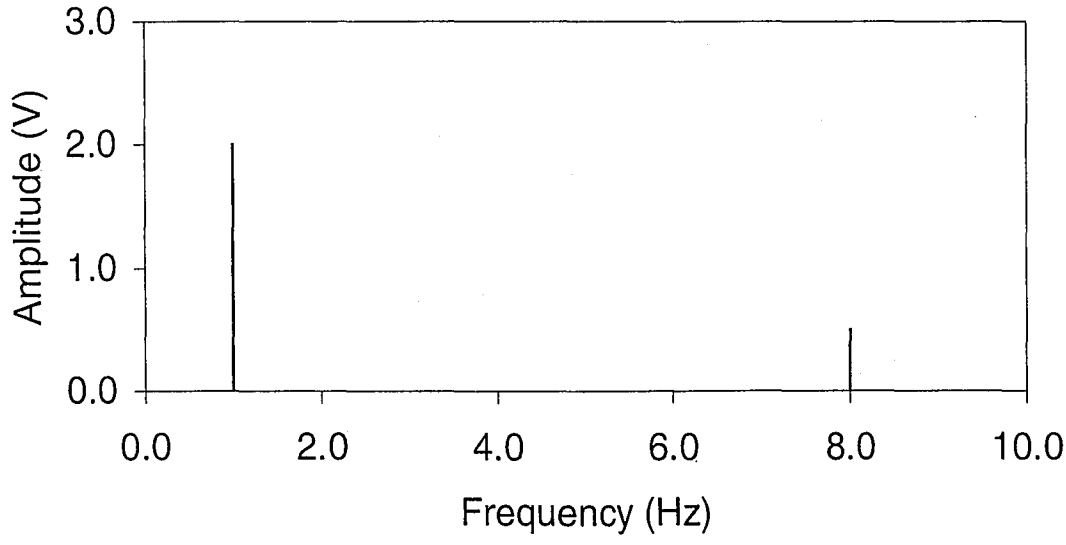

(b)

Figure 2.10 The function f(t): (a) the time domain; (b) the frequency amplitude spectrum.

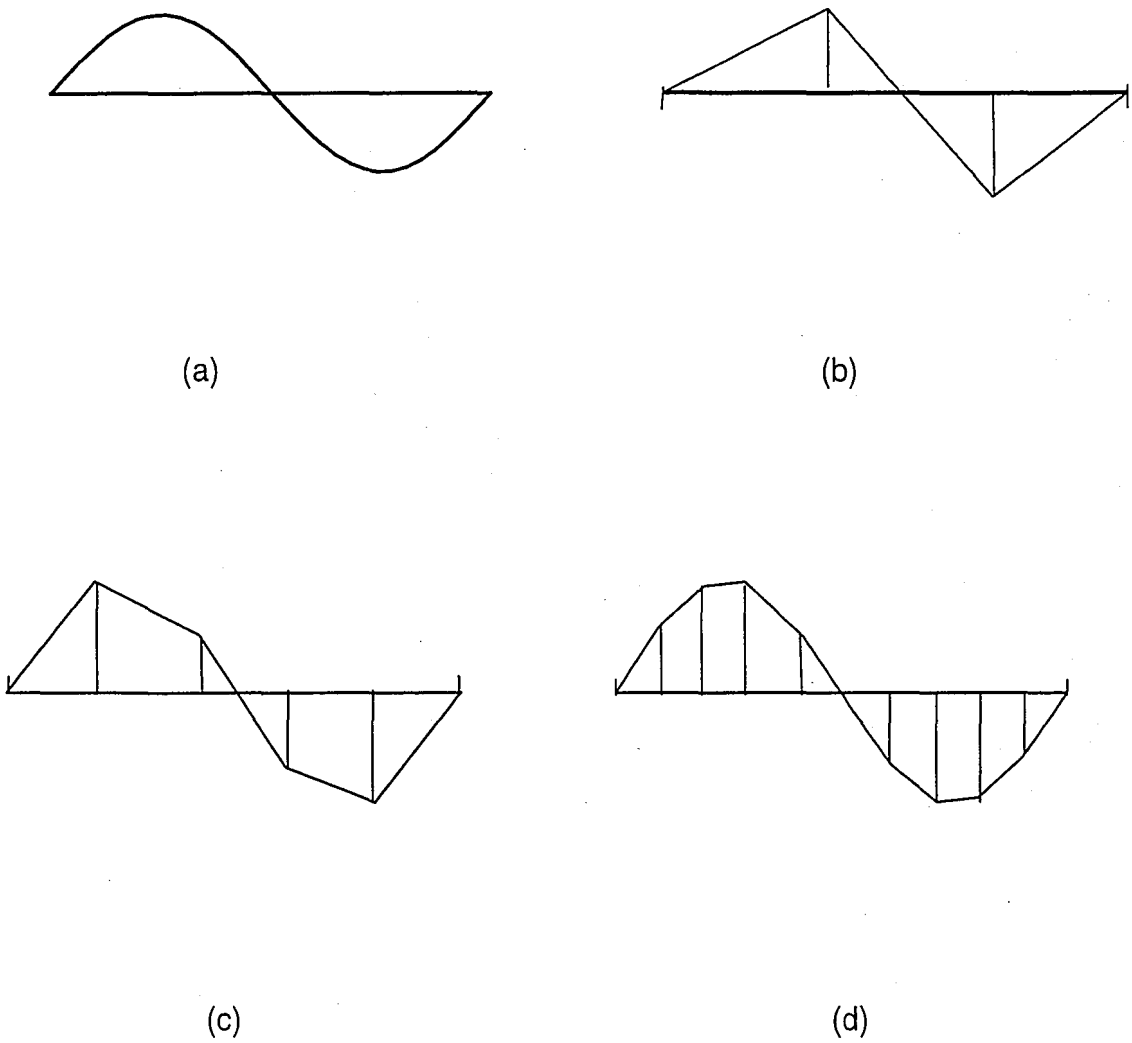

Figure 2.11 Sampling interval and the effect of aliasing on a sine wave: (a) continuous signal; (b) Δf =3 samples per second; (c) Δf =5 samples per second; Δf =10 samples per second.

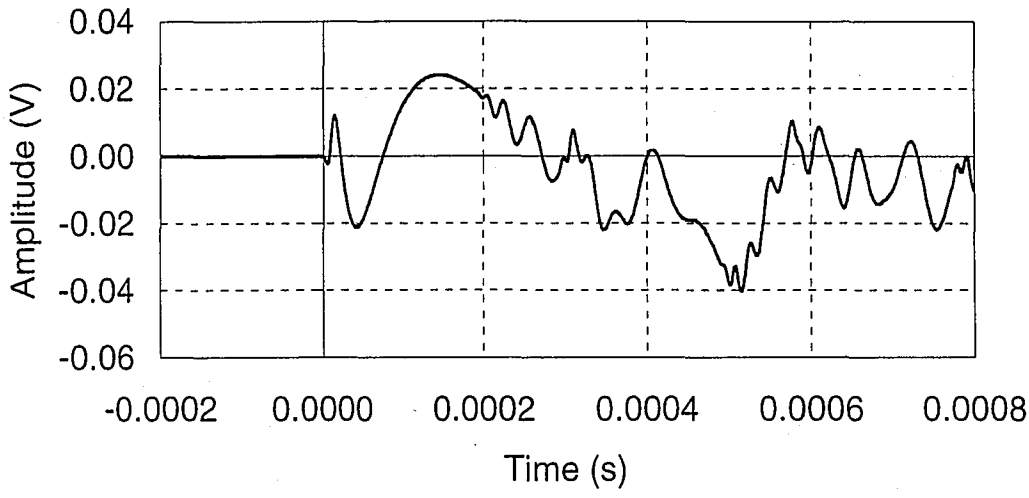

(a)

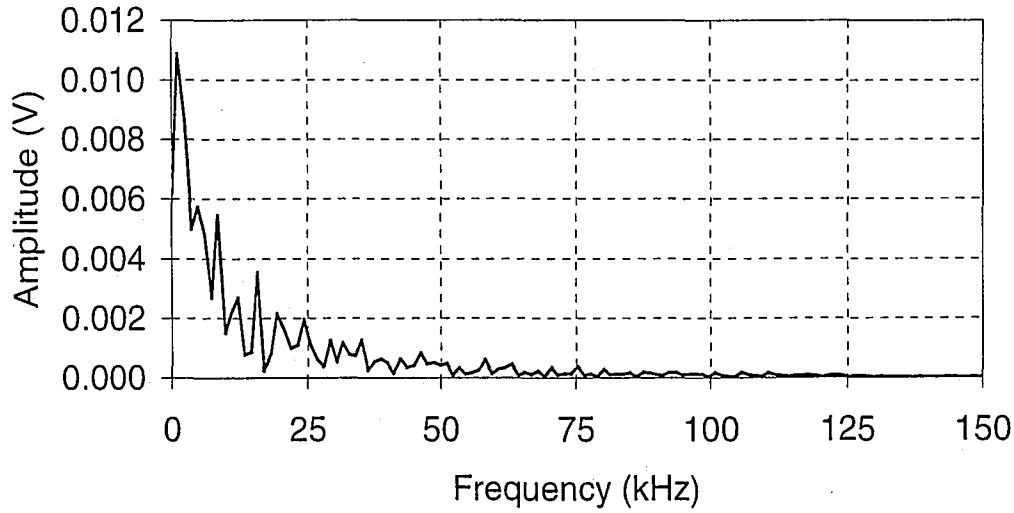

(b)

Figure 2.12 Typical acoustic emission signal recorded by a piezoelectric transducer: (a) in the time domain; (b) transformed to the frequency domain.

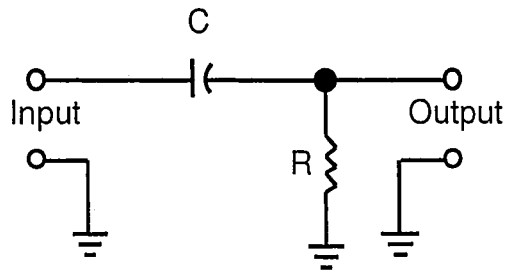

Figure 2.13 Electrical circuit for a high-pass filter.

CHAPTER 3

PARAMETER STUDY

3.1 INTRODUCTION

The tests performed in this research to experimentally evaluate the attenuation of acoustic signals caused by details commonly used in welded steel plate girders are described in detail in Chapter 4. As explained in Chapter 4, impact is used to impart stress waves into the test specimens. A schematic of a typical test is shown in Figure 3.1. Impact is generated on a circular plate specimen at the position marked X, and the stress waves that are imparted at this point propagate to the transducers positioned at A and B. In Figure 3.1, the stress waves that propagate to the transducer positioned at A travel parallel to the weld, and the stress wave that propagate to transducer B travel perpendicular to the weld and must cross the weld. Thus, the stress waves that propagate to the transducer positioned at A travel a different path from the stress waves that propagate to the transducer at B. The path traveled by the stress waves to each transducer is the intended variable in the specimen.

Figure 3.2 shows the general test setup for the acoustic emission testing in this report. The impact is made by dropping a steel sphere of known diameter from a known height onto a steel plate, creating a simulated acoustic emission that travels to each of two transducers. The transducers convert the surface displacements to voltage signals with voltages proportional to displacements.

These analogue signals travel to filters via coaxial cables. After filtering, the resulting signals travel to a two-channel oscilloscope through coaxial cables. The oscilloscope digitizes the analogue signals. Each transducer is powered with a power supply as shown in Figure 3.2. There are several physical components (e.g. transducers, filters, cables, power supplies, etc.) and operator-specified test variables (e.g. sampling frequency, voltage ranges, etc.) that comprise the test system used in this study. In order to determine that the differences in waveforms captured with transducers A and B are attributed to the paths traveled, and not to some physical component or operator-specified test variable in the test system, it is necessary to systematically explore the influence of each of these parameters (physical components and test variables) on the recorded waveforms. This chapter presents this systematic exploration of these parameters. All of the parameters of the test system are identified and varied in a controlled manner to determine what effect, if any, they have on the recorded waveforms.

Section 3.2 describes the test setup and the general testing procedure for the parameter study. The test parameters are separated into three categories—oscilloscope parameters, input parameters, and hardware parameters. Each of these categories of parameters is presented in Sections 3.3, 3.4, and 3.5.

3.2 PARAMETER STUDY TEST SETUP AND PROCEDURE

Common test setup and procedure are used throughout parameter testing. This section presents the general setup and procedure. Variations from this

setup and procedure in order to isolate a particular parameter are noted in each section.

Figure 3.3 shows the test setup used in the parameter study. The plate used in the study has dimensions 350x117x65 mm. The plate is impacted at A and the transducer is positioned at B. The distance between the impact and the transducer, 2*a*, equals 100 mm for each parameter. Five impacts are made on the plate at the specified location, A, and recorded at the transducer location, B. One parameter is then varied. For example, the coupling of the transducer with the test plate is varied. Five more impacts are performed and recorded. All other variables in the test setup (i.e. transducer, filter, sampling interval, etc.) remain unchanged.

The way the oscilloscope is triggered by an input to being recording also be varied. The triggering mechanism for the oscilloscope can be varied. A trigger level is set. The trigger level is a specified voltage that the signal must cross to qualify as a valid trigger. The sensitivity of the trigger is adjusted using the sensitivity window. The window is a range of voltages and the signal must begin outside and pass through the window to be considered a valid trigger. Both the sensitivity and the trigger were adjusted for each signal. "OR" triggering was used for this study. "OR" Triggering allows a signal from either input channel of the oscilloscope to trigger a sweep on both channels when it qualifies as a valid trigger. Dual slope triggering was also used, allowing the signal to have a positive or negative slope when it triggers the oscilloscope. Once triggered, the os-

cilloscope records a waveform in the time domain that contains 1000 data points at a sample interval of Δt.

In the parameter study presented in this chapter, each displacement waveform is comprised of one thousand points sampled at a sampling interval, Δt, of 5 μs. The sampling interval is chosen to decrease the frequency interval, and increase the resolution of the plot in the frequency amplitude spectrum. The voltage range displayed on the output window (Section 3.3.2) and the trigger and sensitivity levels are adjusted for each signal. Any derivation from the procedure presented here is noted in the appropriate section.

3.2.1 Signal Processing Procedures

As stated in Section 3.1, frequency domain analysis is used in this chapter. The Fourier transformation is obtained by using the Fast Fourier Transformation (FFT) Snapshot feature of the digital oscilloscope. This function transforms the recorded signal in the time domain to the frequency amplitude spectrum and displays the spectrum on the output screen.

In order to use the FFT Snapshot feature, the signal recorded by the oscilloscope must consist of 1000 discrete points. Prior to the Fast Fourier Transformation, the oscilloscope's FFT Snapshot function adds nulls to pad the signal to 2048 points. The resulting FFT is 1025 points long, but only the first 1000 points are displayed on the screen.

The test setup requires the response of a plate to mechanical impact to be recorded using each channel of the oscilloscope and compared. The five impacts will create waveforms that travel to each of the channels. Therefore, five trials will produce a total of ten signals, five at each channel.

Impact recorded by one transducer produces a time domain signal that is transformed to the frequency amplitude spectrum by the FFT. The frequencies at which peaks occur in the frequency amplitude spectrum, and amplitudes that occur at those frequencies, are recorded for the impact. Five impacts are made at each location. At each frequency, the average amplitude is calculated from the amplitudes of the five trials. The average amplitudes of the frequency amplitude spectra recorded by the first channel is referred to as Signal 1. The average amplitude is also calculated for the five frequency amplitude spectra created from the five waveforms recorded by the second channel of the oscilloscope and referred to as Signal 2.

When evaluating the differences in two signals, the average amplitude values at a given frequency are compared using an amplitude ratio. The amplitude ratio is computed by dividing the average amplitude of Signal 1 by the average amplitude of Signal 2. The results of the average amplitude ratio are plotted for each frequency. An average amplitude ratio equal to one indicates the parameter has no effect on the signal.

If the amplitude ratio does not equal one, the amplitudes are normalized. The average amplitude values are normalized by dividing each average ampli-

tude value by the average amplitude of a selected frequency. The normalization frequency is selected to be a frequency that appears consistently for all impacts. Normalized average amplitude ratios are computed by dividing the normalized average amplitudes of Signal 1 by the normalized average amplitudes of Signal 2. Normalized average amplitude ratios equal to one indicate that the effect of the parameter can be removed by normalizing the amplitudes. Normalized ratios that are constant, but not equal to one, indicate that the normalized signal must be adjusted by the ratio value to remove the effect of the parameter. An inconsistent ratio shows an unpredictable effect of the parameter.

Once the effect of the parameter is determined, any necessary normalization or adjustment of the signal to eliminate the effect of the parameter is known and can be used for the tests described in Chapter 4. Following is a summary of the significance of the analysis results.

- Average amplitude ratio equal 1 for all frequencies: Parameter has no effect on the signal.
- Normalized average amplitude ratio equal 1 for all frequencies: The effect of the parameter can be removed by normalizing the frequency amplitude spectra by the amplitude of a frequency that appears consistently.
- Normalized average amplitude ratio equals a constant other than 1: The frequency amplitude spectra must be adjusted by the constant to remove the effect of the parameter.

- Normalized average amplitude ratio does not equal a constant: The effect of the parameter is unpredictable.

3.3 OSCILLOSCOPE PARAMETERS

Oscilloscope parameters are defined as those variables specific to the oscilloscope settings. The oscilloscope parameters in this study are the input channel and the voltage range.

3.3.1 Input Channel

Figure 3.4 shows the test setup for determining the effect of the input channel. An impact is created with a 3 mm steel sphere at A and the stress waves travel to the transducer at B. The signal is split after the transducer so that the identical signal can travel to each input channel of the oscilloscope. As shown in Figure 3.4, no filter was used in this test. All other parameters were identical for the two channels.

The waveform was recorded by each channel of the oscilloscope. The average amplitude values for Channel 1 and Channel 2 are shown in Figure 3.5 (a). Figure 3.5 (b) shows the amplitude ratio of Channels 1 and 2 (Channel1 / Channel 2). This plot shows the amplitude ratio equals one for each frequency except for the lowest frequency, at 1.8 kHz. At this frequency, the amplitude ratio is slightly below one. The reason for the discrepancy in amplitude at this frequency is unknown. However, the frequency of 1.8 kHz is lower than the frequencies

that are of importance in the research. Therefore, the input channel has no effect on the signal recorded by the oscilloscope.

3.3.2 Voltage Range

The oscilloscope has the capability of a varying range of voltages it will record. The range can be set to discrete values between ±0.003 V and ±12 V. As long as the input signal has an amplitude less than the specified range, the signal will be captured in its entirety. If the input signal has amplitude greater than the selected voltage range, that part of the signal with an amplitude greater than the selected range will not be recorded by the oscilloscope (i.e. the signal will be clipped).

A test setup identical to that used for the input channel (Figure 3.4) is used to determine the effect of the voltage range. Figure 3.4 shows an impact that travels to a transducer. The analogue signal is split to each channel of the oscilloscope. To evaluate the effect of clipping, a display range that best displays the input signal is determined for the impact of a 2 mm sphere. Channel 1 of the oscilloscope will use this voltage range. The voltage range of Channel 2 is varied from its minimum range of ±0.3 V, which is assumed to severely clip to the signal, to a range of ±6.0 V. When a voltage range of 6.0 V is used, the maximum voltage that can be displayed is significantly greater than the maximum voltage of the signal. The impact is repeated with Channel 2 set to preset voltage ranges.

An FFT is performed on each channel of the oscilloscope. The frequencies and their amplitudes are recorded. An amplitude ratio is computed by dividing the amplitude of a frequency recorded by Channel 1 (with the consistent voltage range) by the amplitude of the same frequency at the other display ranges.

Figure 3.6 shows the amplitude ratio of frequency amplitude spectra (Channel 1 / Channel 2) generated from an impact recorded with Channel 1 having a voltage range of ±1.2 V, and Channel 2 having voltage ranges equal to some of the preset ranges available. At each frequency, the amplitude ratios calculated from the impacts with ranges less than 1.2 V are less than one. Figure 3.6 shows that amplitude ratios calculated from impacts will the voltage range of Channel 2 greater than or equal to 1.2 V are equal to one. This shows that a voltage range larger than necessary does not adversely effect the displacement waveform. However, a voltage range that does not fully capture the displacement waveform has adverse effect on the signal.

Figure 3.7 (a) shows a typical displacement waveform, with a voltage display of 3 V. Figure 3.7 (b) shows the same signal, with the voltage display set to 0.6 V. The portions of the signal with an amplitude higher than 0.6 V or lower than –0.6V are assigned an amplitude of 0.6 V or –0.6 V, respectively.

As stated earlier, when signals are clipped, the oscilloscope considers all amplitudes that are greater than the maximum value in the display range to be equal to that maximum value. This alters the frequency content of the signal,

causing inaccurate analysis of the waveform. A voltage range that is substantially larger than the amplitude of the signal does not adversely affect the analysis of the signal. To eliminate the effect of the voltage range, the voltage range must be selected so the signal is not clipped.

3.4 INPUT PARAMETERS

Input parameters are defined as those variables that will affect the stress waves imparted to the plate. The input parameters are the diameter of the steel sphere used for impact and its contact time with the plate, and the drop height of the steel sphere. The frequency content and amplitudes of the signal can be controlled by varying the impact. As discussed in Chapter 2, the ideal impact would create a stress wave with high frequency content at low amplitudes, similar to the stress waves that may be produced by crack propagation. Possible impacts include dropping a steel sphere of various diameters on the specimen or by breaking 0.5 mm pencil lead on the specimen. The parameter study varies the sphere diameter and drop height, focusing on how the contact time and the simulated acoustic signal are affected.

3.4.1 Drop Height

Impacts on the plate specimens in this study are made by releasing a steel sphere from a rest position at a given height h above the plate. The height from which the steel sphere is dropped directly affects the energy input into the

test specimen from the impact. The energy input influences the amplitude of the signal at each frequency. Because the steel spheres are manually dropped onto the plate, it is possible for slight discrepancy in the drop height to occur. The parameter study shows the effect of this discrepancy on the stress waves introduced to the plate.

The test setup to study the influence of drop height is as shown in Figure 3.8. A steel sphere with a 3-mm diameter is dropped from a height, h, onto the surface of the plate at location A. The stress wave travels to the transducer located at B, and is recorded by the oscilloscope. No filter is used. The drop height is varied to 75, 150, and 300 mm. Five impacts are made at each drop height.

Figure 3.9 (a) shows the average amplitude at each excited frequency for drop heights of 75, 150, and 300 mm. The plot of average amplitude values shows that the frequencies excited are independent of the drop height. The amplitude is directly proportional to drop height. For a given frequency the amplitude is lowest for a drop height of 75 mm and highest for a drop height of 300 mm.

To determine whether the effect of an inadvertent change in drop height can be removed, the amplitude values are normalized by the amplitude value at 5.43 kHz. Figure 3.9 (b) shows the normalized average amplitude values. The graph shows that the normalized amplitude values at any frequency are the

same for each drop height. Therefore, the effect of the drop height can be removed through the process of normalization.

3.4.2 Contact Time and Sphere Diameter

A second means of varying the amplitude of the input signal is by adjusting the impact by varying the diameter of the sphere used or by using a pencil break. The diameter of the sphere used for impact will affect the energy input into the system upon impact. The diameter of the sphere will influence the frequency content, amplitude, and contact time.

The contact time of a steel sphere on a steel plate is a function of the sphere diameter. The theoretical calculation of the contact time is given by Equation 2-10. For a 5 mm diameter steel sphere dropped on a steel plate from a drop height of 150 mm, the contact time is calculated to be 31 μs.

The contact time can be observed experimentally by studying the signal in the time domain. For this test setup, the transducer is positioned as close as possible to the impact point. The *a* value is at its minimum value of 30 mm (the radius of the transducer plus the radius of the tube used to guide the impact). The initial R-wave caused by impact can be observed without the obstruction of the P- and S-waves. Figure 3.10 shows a typical signal in the time domain created by the impact of a 5-mm diameter steel sphere on a steel plate from a drop height of 150 mm. The R-wave arrival is characterized by a small amplitude positive peak followed by a larger amplitude negative peak. The duration of this

negative peak corresponds to the contact time of the sphere on the steel plate. The contact duration is denoted on Figure 3.10 as 28 μs. This value agrees well with the theoretically calculated value of 31 μs.

3.5 HARDWARE PARAMETERS

Hardware parameters are the physical components of the test setup. The hardware parameters in this research are the transducer, shield, filter, and power source. In order to compare signals recorded with different locations, the hardware used at each location must behave identically.

3.5.1 High-pass Filter

As discussed in Section 2.2, the resonant frequency of the transducer has an amplitude potentially greater than that of the input signal. This can cause the input signal to be masked. The transducers used in this study have natural frequencies of approximately 800 Hz. Two high-pass filters were constructed to remove low frequency content from the signal.

The high-pass filters are constructed of a resistor and capacitor in series, as shown in Figure 2.13. The high-pass filters contain a 1 kΩ resistor in series with a 0.15 μF capacitor. The cut-off frequency of the filter, as given by Equation 2-14, is 1 kHz.

The actual attenuation curve of a filter does not have a sharp cut-off at F_{CUT}. Figure 3.11 shows the test setup to determine the filter attenuation curves.

A signal of known frequency and amplitude, created using a function generator, was passed to the filter. The signal from the function generator is split so the signal is input to the oscilloscope with Channel 1 recording the filtered signal and Channel 2 recording the signal in its original state. The amplitude of the generated signal is held constant at 1 mV while the frequency is increased incrementally from 0.1 to 10 kHz.

The amplitude of each signal is measured in the time domain and is recorded. The amplitude of the input (unfiltered) signal, A_{IN}, and the amplitude of the output or filtered signal, A_{OUT}, are compared by computing an amplitude ratio. The amplitude ratio represents the attenuation as a fraction of the input amplitude for each frequency. The amplitude ratio is computed as A_{OUT} divided by A_{IN}. An attenuation curve is constructed by plotting the amplitude ratio versus frequency.

Figure 3.12 shows the attenuation curve for the high-pass filters constructed. The curves show that the attenuation of the signal is nearly identical for each filter. This shows that the filters will have an identical effect on signals passed through them and will not contribute to differences in waveforms.

3.5.2 Power Source

In the original configuration, the transducer is powered by a 9V battery contained in the shield unit. The voltage of this power source may affect the performance of the transducer. As the battery's voltage decreases with use, the

signal recorded by the transducer may be adversely effected. To eliminate the effect of a variable power source, the 9V batteries were replaced with a constant power supply. This power supply provided a constant 9V excitation to each transducer for all testing.

3.5.3 Shields

The shield is used to protect the transducer from ambient noise and provide housing for the power source. The two shields provided identical responses.

3.5.4 Transducer

Two broadband piezoelectric transducers are used in this study, Transducer A (TA) and Transducer B (TB). The transducers, shown in Figure 3.13, are described in Proctor (1982). TA and TB are tested to discover any difference inherent to them. Two issues are present when dealing with the response of the transducers: (1) Will the transducer react consistently to identical impacts if it remains stationary throughout testing, and (2) Will the transducer react consistently to identical impacts if it is repositioned between impacts.

These questions lead to the testing of the transducers in two stages. The first stage required the transducers to remain stationary throughout the testing. Figure 3.8 shows the test setup used to determine if the transducer behaves consistently to impact. The impact at A is created by dropping a 3 mm diameter

steel sphere from a drop height of 150 mm. TA, positioned at B, receives the signal. The signal is filtered by the 1 kHz filter and passed to the oscilloscope. Five impacts are made and TA remains unmoved throughout the impacts. TA is removed from the plate and TB is carefully placed at point B. Five impacts are made with TB stationary between impacts. Each waveform is transformed to the frequency domain with the FFT snapshot function of the digital oscilloscope.

Figure 3.14 shows the amplitudes recorded for each trial with TA. At each frequency, the amplitude for each trial is near identical. Therefore, there is a high level of repeatability when the transducer is stationary between trials.

The second set of trials required the transducers to be repositioned between each trial. This movement of the transducer may cause the transducer to have a different coupling with the surface of the plate. The test setup and procedure is the same as it was to determine the consistency of the transducer response, with the exception that after each impact the transducer is picked up and replaced in the same location on the plate. Five impacts are made with using TA, and five impacts are made with TB.

The signal resulting from each impact is transformed to the frequency domain. Figure 3.15 (a) shows the amplitudes of the excited frequencies for each of the four trials using TA. The amplitudes for each trial differ and this shows that the signal is affected by the placement of the transducer. Figure 3.15 (b) shows the amplitudes from the excited frequencies for the four trials using TB. Although

the frequencies excited for each trial are the same, the amplitudes vary greatly as the transducer is repositioned on the plate.

The amplitudes for TA and TB are normalized by the amplitude value at 13.58 kHz, and the results are presented in Figure 3.16 (a) and Figure 3.16 (b), respectively. At high frequencies, the normalized amplitude values are equal for all impacts. At the lowest frequency recorded, 1.37 kHz, the amplitude values become closer in magnitude, but are not equal. Because the frequencies that are of interest in this study are larger than the lowest value, 1.37 kHz, the inconsistency at this low frequency will not effect the results in later sections of this report.

The consistent amplitudes shown in Figure 3.16 allow the average normalized amplitude to be calculated at each frequency for TA and TB. With these average normalized amplitudes, the average normalized amplitude ratio versus frequency can be plotted. Figure 3.17 shows this plot, with the average normalized amplitude ratio calculated as the normalized average amplitude of TA divided by that of TB (TA/TB). The normalized amplitude ratios in Figure 3.17 are equal to or close to one. This shows the effect of the coupling of the transducer and the plate can be eliminated by normalizing the signal.

3.6 SUMMARY

Chapter 3 presents a study of the parameters of the test setup. Each parameter is isolated and its affect is determined. The parameters are separated

into three categories: oscilloscope parameters, input parameters, and hardware parameters.

The oscilloscope parameters refer to those setting controlled by the oscilloscope, such as the input channel input voltage range. It was found that the input channel has no effect on the recorded signal. The display range need be chosen carefully to allow for the maximum amplitude of the signal without clipping the signal.

Input parameters refer to the variation in the signal due to the impact. Sphere diameter and drop height are the two main ways to control the input. Spheres are used for impact because they allow good repeatability. Small diameter spheres are used for impact in subsequent chapters to allow for a broad range of frequencies at sufficient amplitudes to be excited in a test plate. The behavior of the plate responding to impact is verified by observing the contact time of a steel sphere on a plate and comparing the observed contact time with a theoretical value. Effects of variation of the drop height are small, and large variation can be removed through normalization.

Hardware parameters refer to the physical test equipment such as transducers, filters, and the power supply. Attenuation curves are generated for the high-pass filters to assure consistent behavior. The filter removes the resonance of the transducer. Repeatable results are obtained with a stationary transducer, and problems in transducer coupling with the plate are eliminated through normalization.

All variables in the test setup have been determined and accounted for. Any variation in response in the testing described in Chapter 4 is due to the path length of the signal, and not inherent to the test setup.

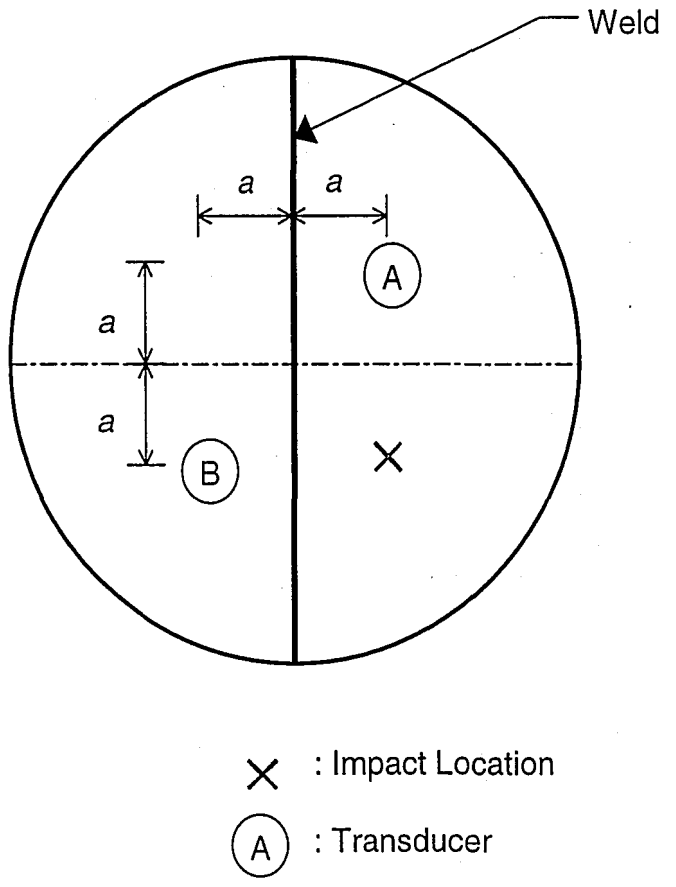

Figure 3.1 Schematic drawing of a typical test setup.

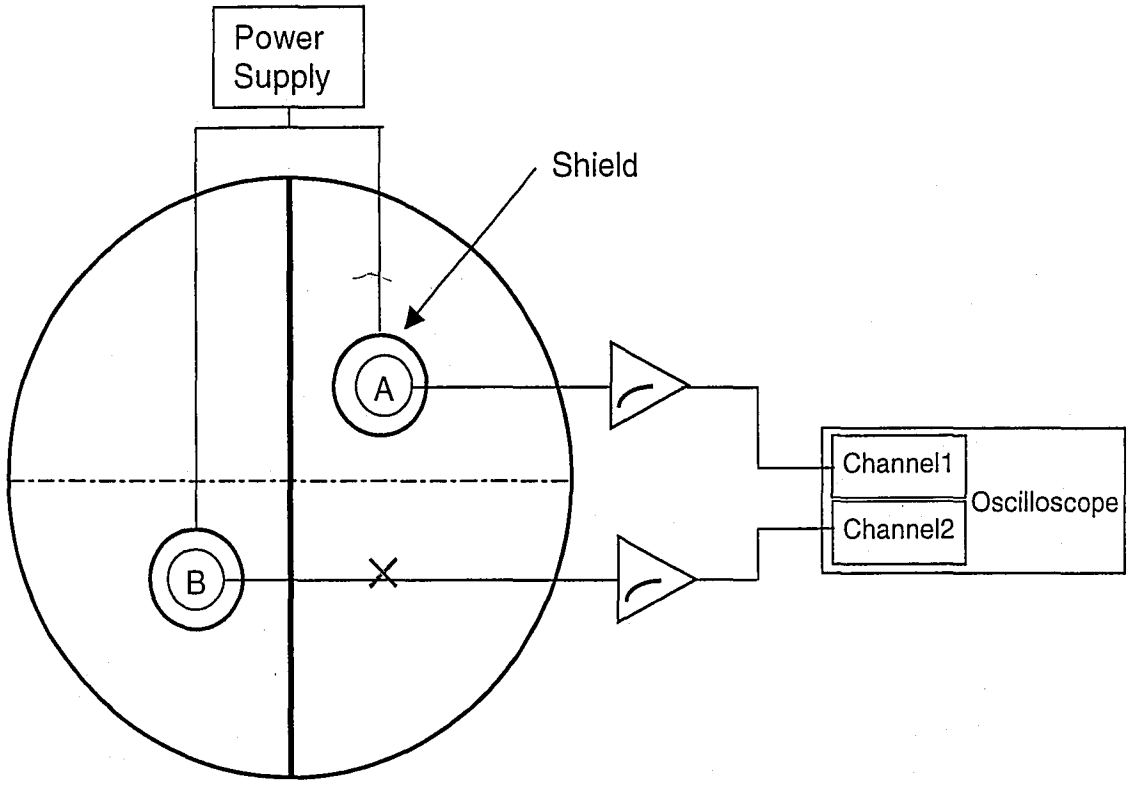

Figure 3.2 Schematic drawing of the test setup.

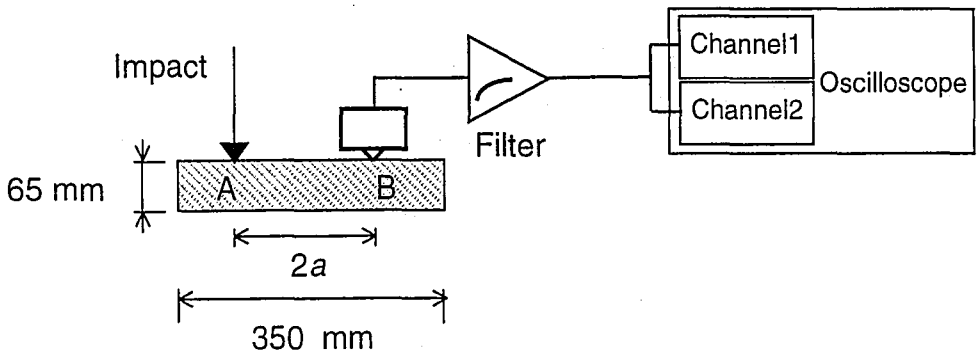

Figure 3.3 General test setup for parameter study.

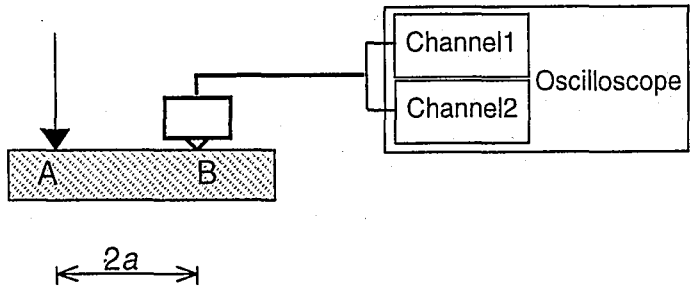

Figure 3.4 Test setup for isolating the effect of the oscilloscope input channel.

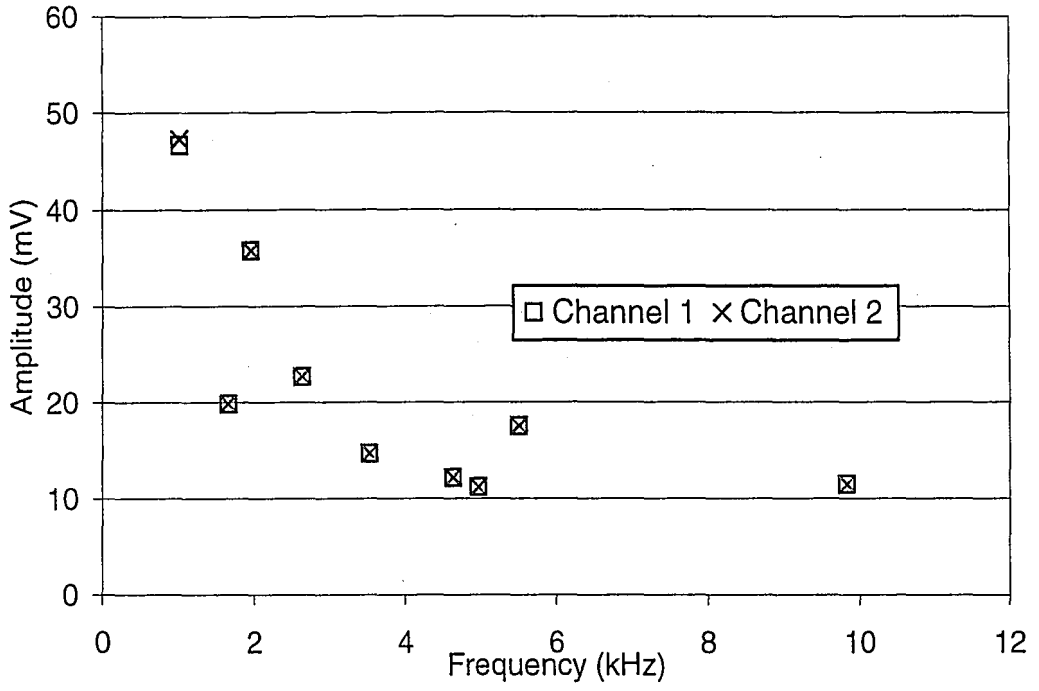

(a)

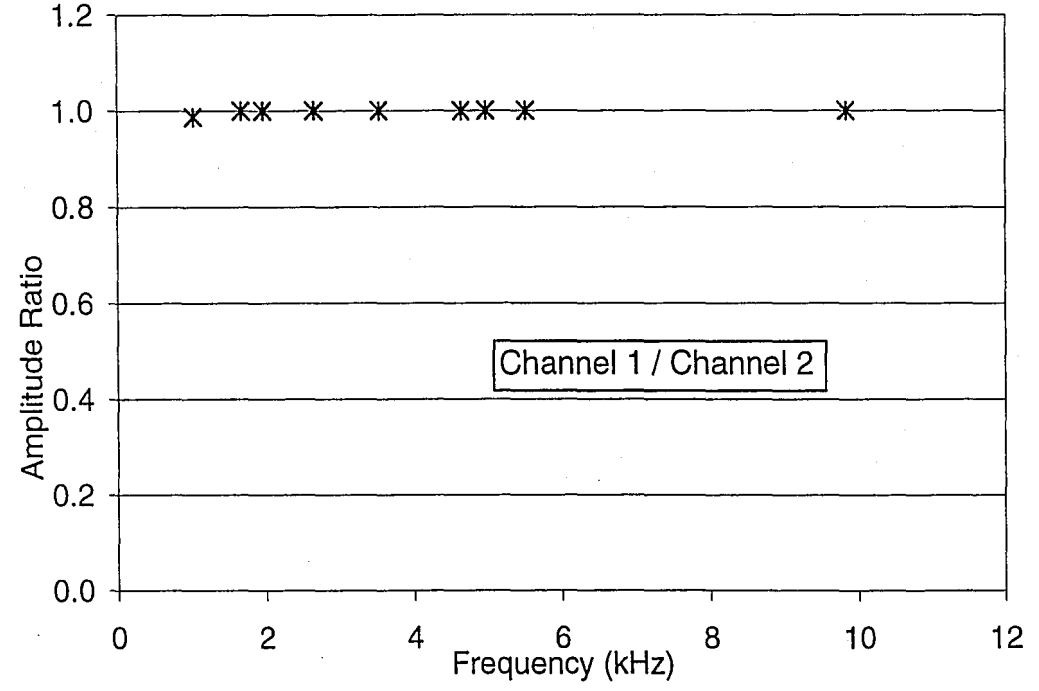

(b)

Figure 3.5 Effect of input channel on recorded signals: (a) plot of average amplitude versus frequency for each channel; (b) plot of amplitude ratio versus frequency.

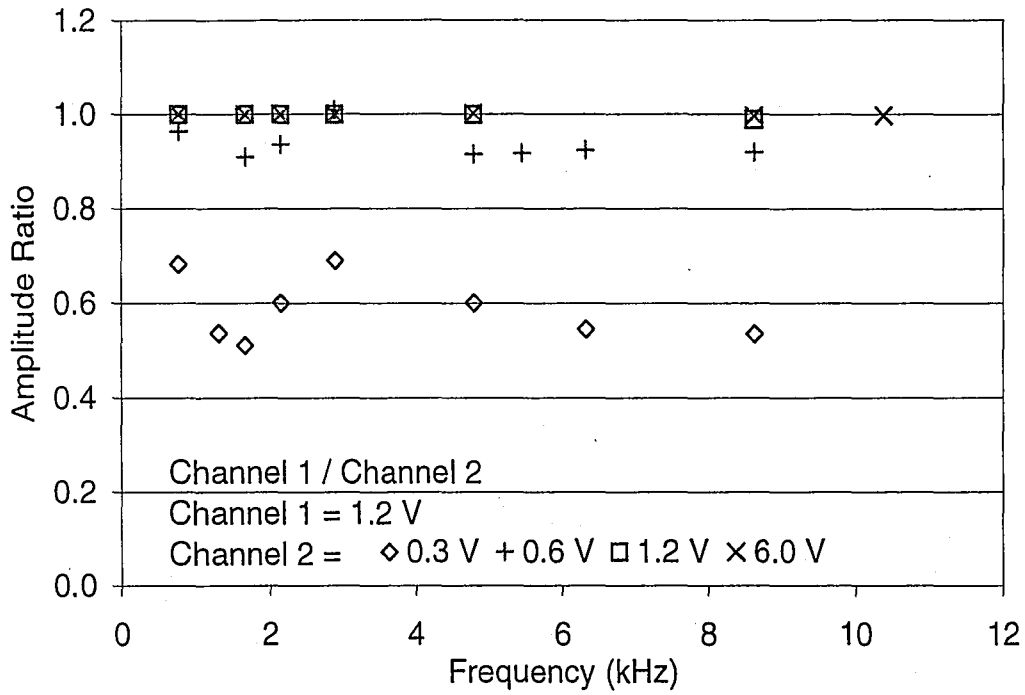

Figure 3.6 The effect of the voltage range in the frequency amplitude spectra with various voltage ranges.

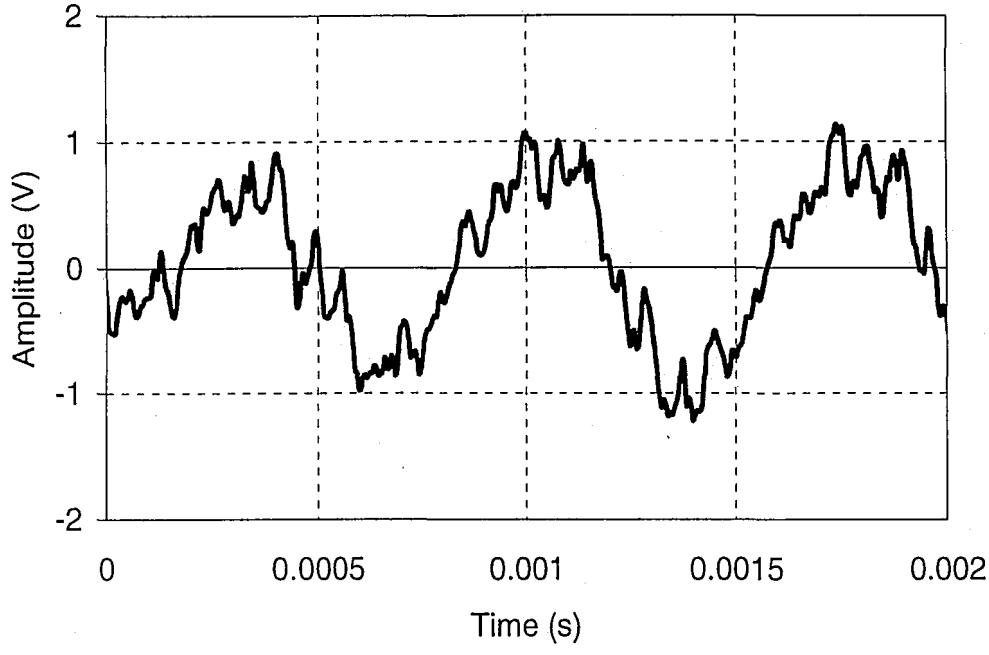

(a)

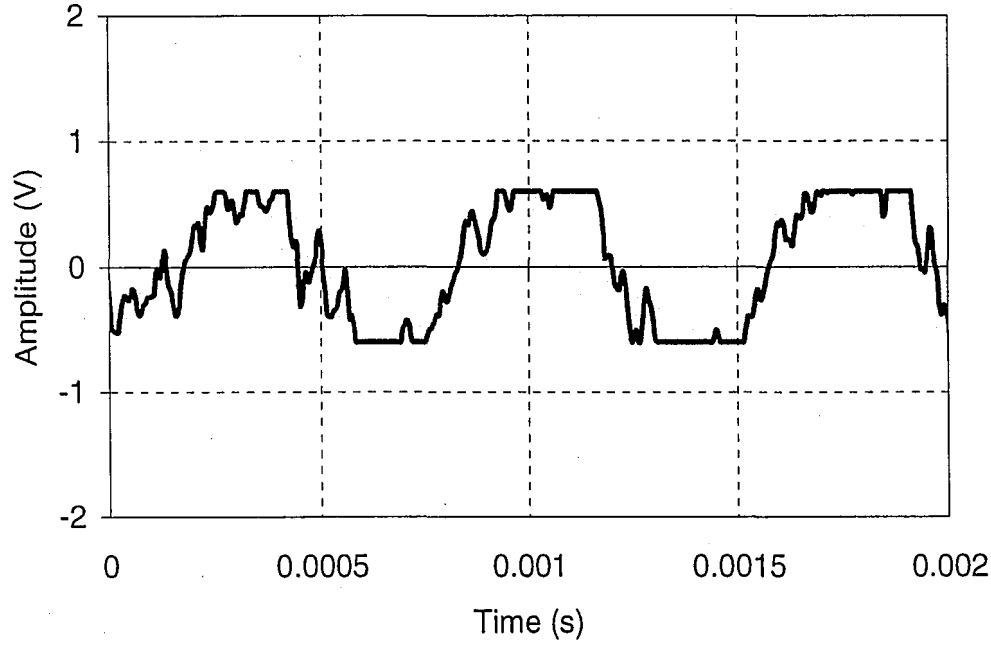

(b)

Figure 3.7 Effect of signal clipping on displacement waveforms.

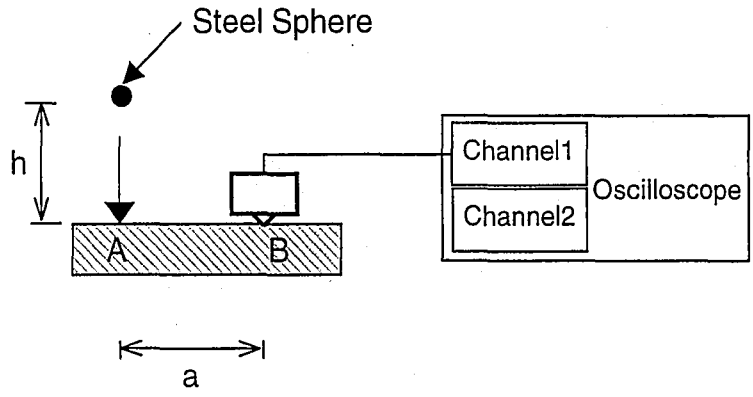

Figure 3.8 Test setup isolating the effect of the drop height of the steel sphere and the effects of the transducer.

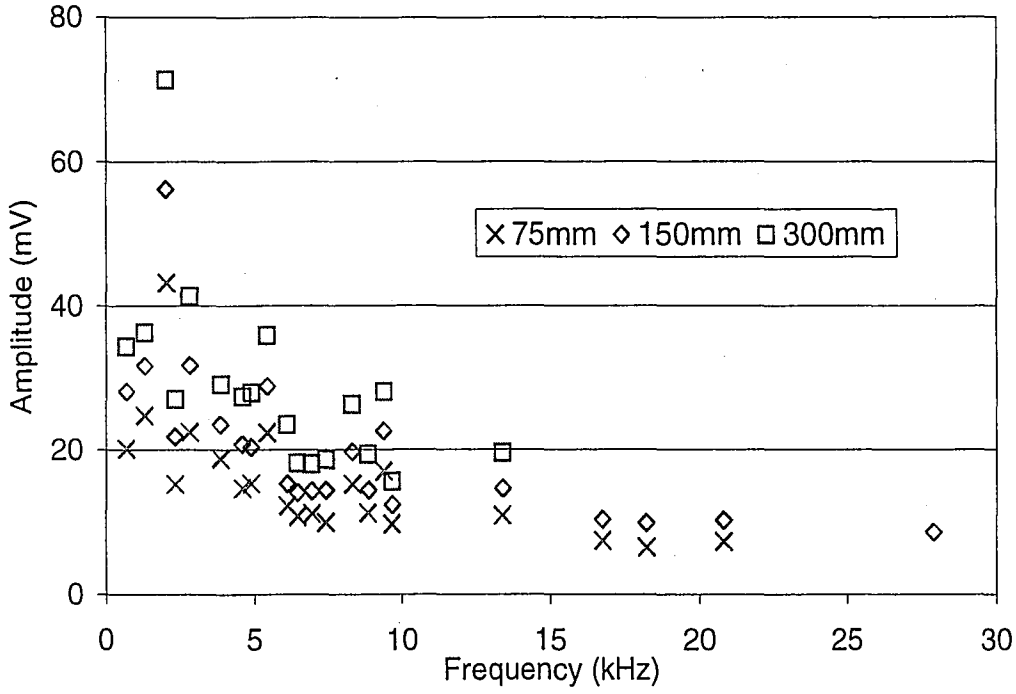

(a)

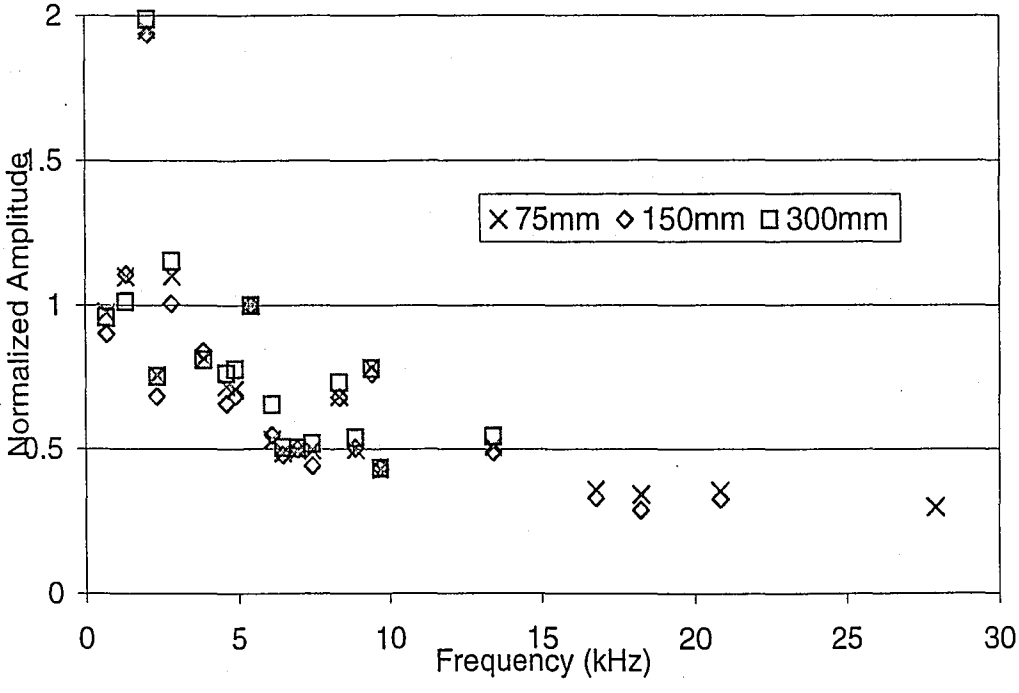

(b)

Figure 3.9 The effect of drop height in the frequency domain for drop heights of 75, 150, and 300 mm: (a) average amplitude; (b) normalized average amplitude, normalized by the amplitude at 5.43 kHz.

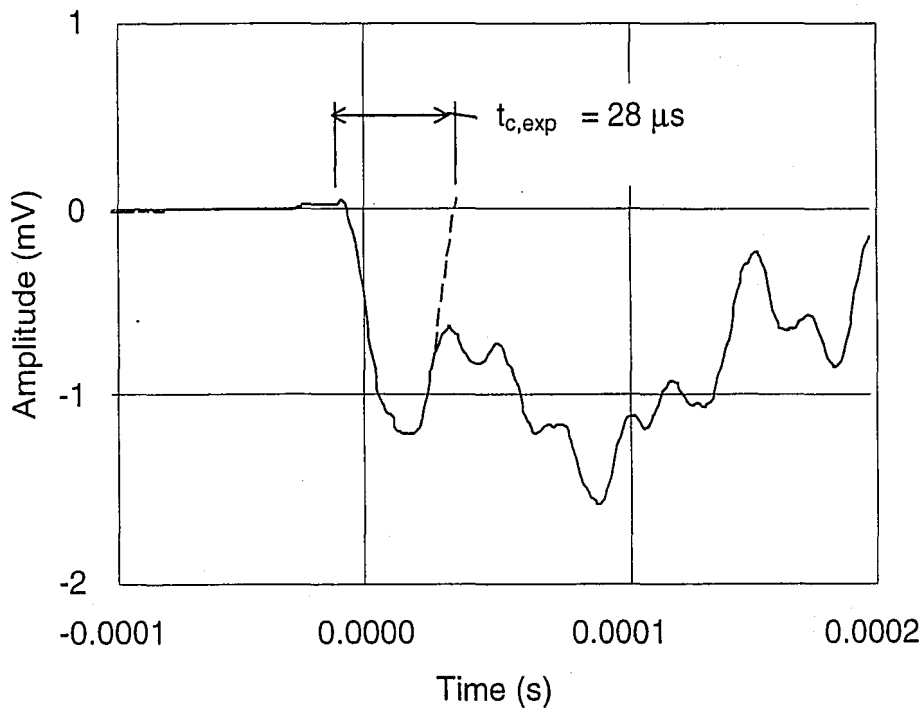

Figure 3.10 The experimental contact time, $t_{c,exp}$, of a steel sphere on a steel plate as determined from the time domain plot of the waveform and compared with the theoretical value, $t_{c,theor}$.

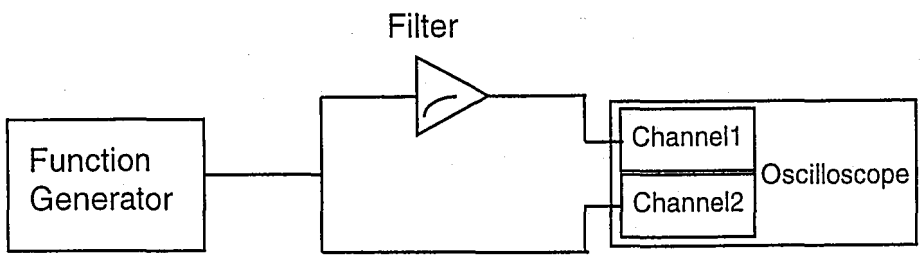

Figure 3.11 Test setup to determine the attenuation of a high-pass filter.

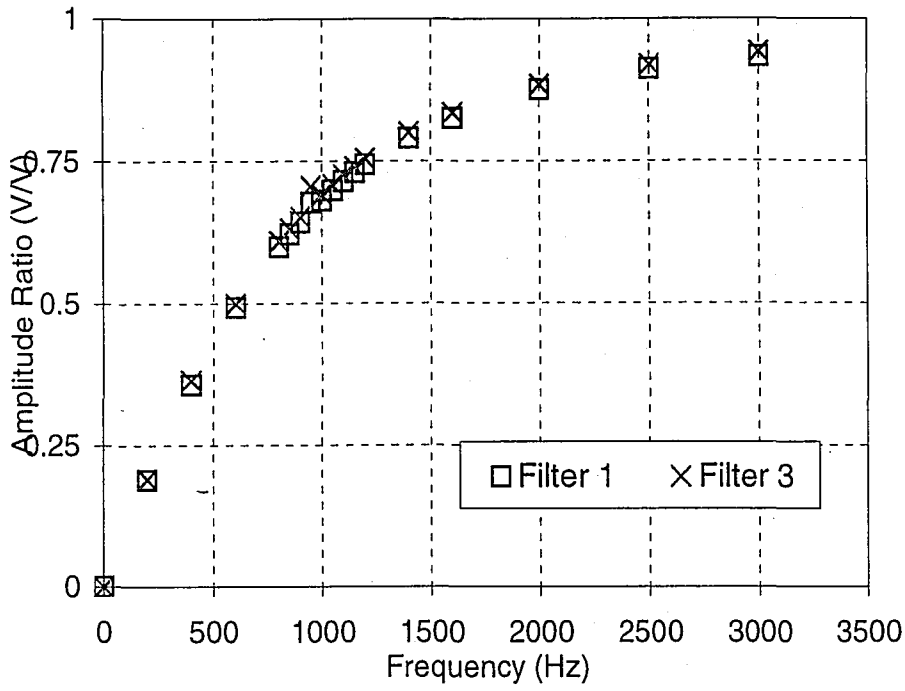

Figure 3.12 Attenuation curves for the high-pass filter.

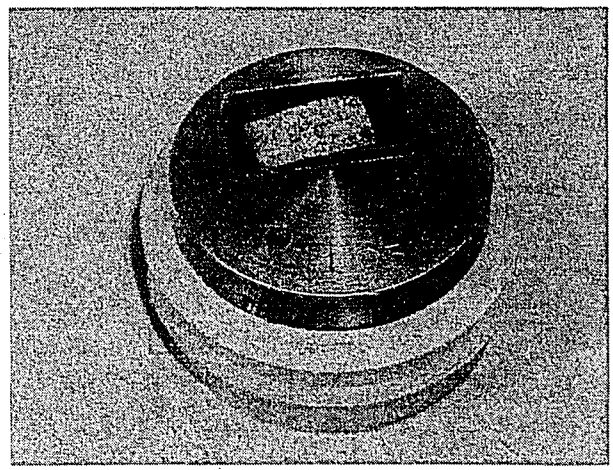

Figure 3.13 Broadband piezoelectric transducer.

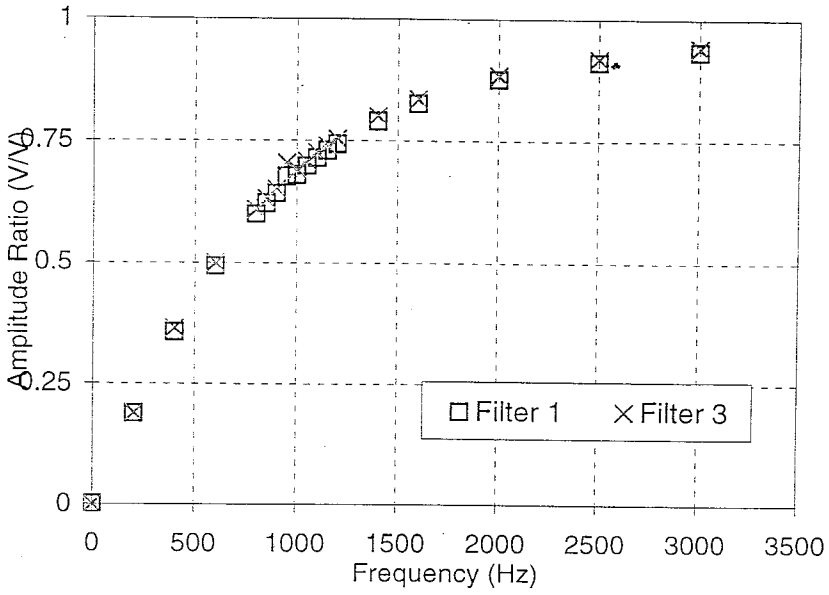

Figure 3.12 Attenuation curves for the high-pass filter.

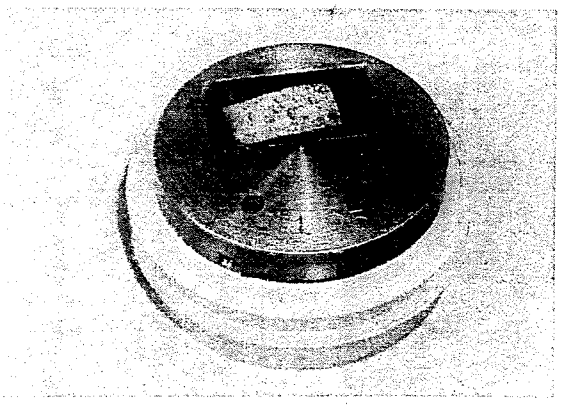

Figure 3.13 Broadband piezoelectric transducer.

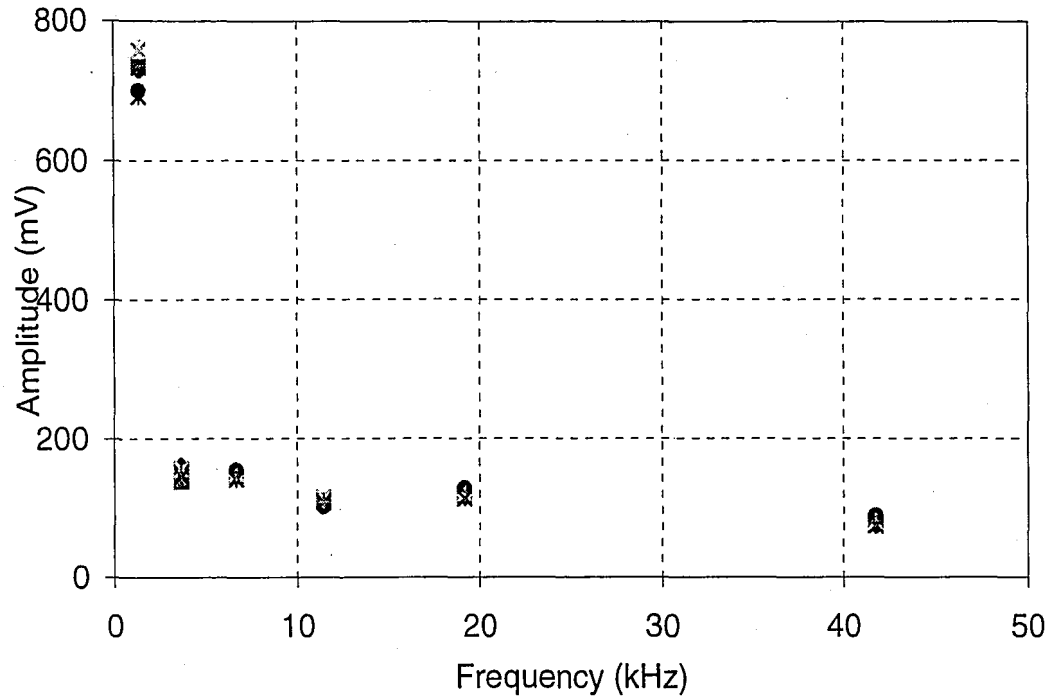

Figure 3.14 Repeatable response of a stationary transducer: amplitude versus frequency for five successive impacts.

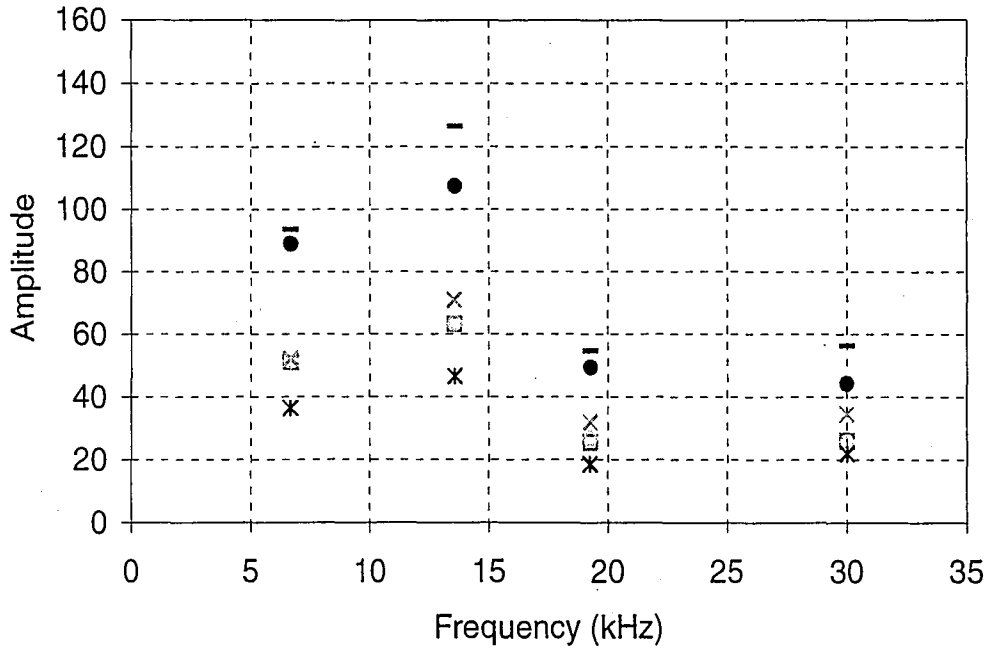

(a)

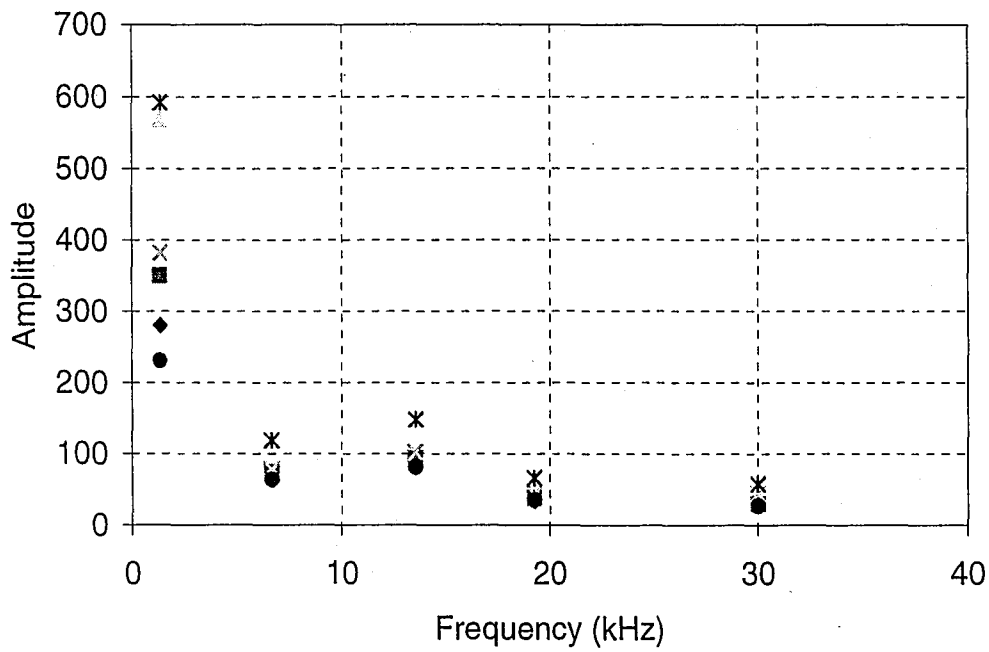

(b)

Figure 3.15 Frequency response generated by five impacts with transducers repositioned after each impact: (a) TA; (b) TB.

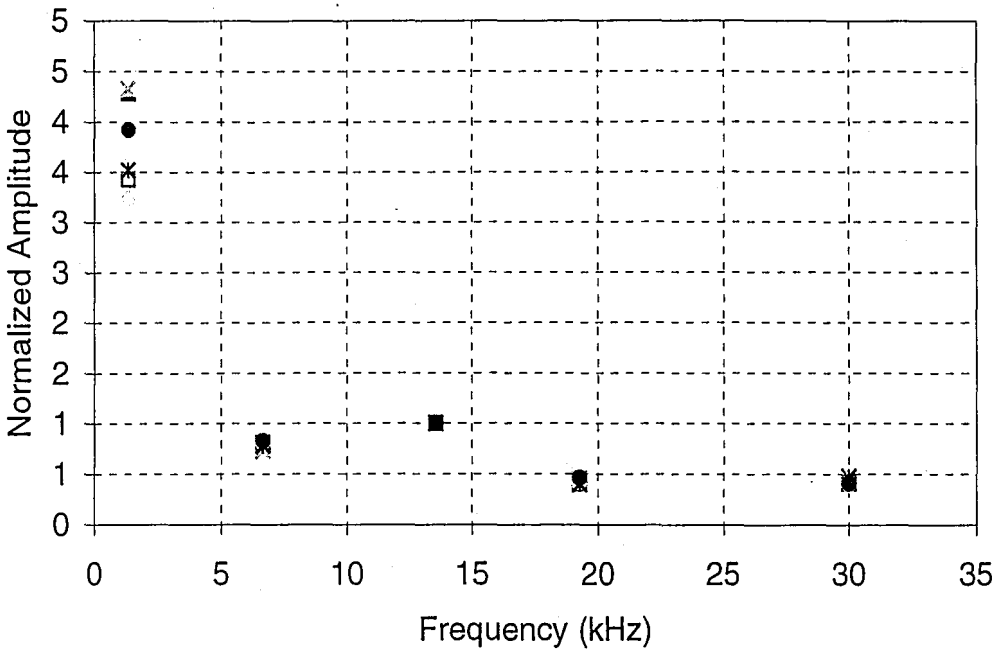

(a)

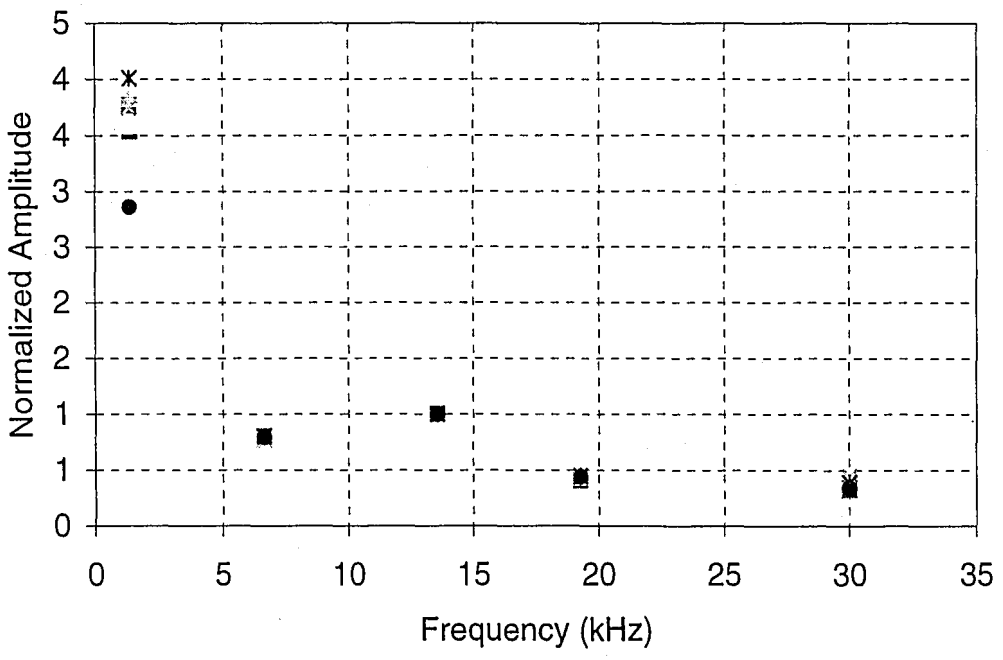

(b)

Figure 3.16 Normalized response to five impacts when transducers are repositioned after each impact, normalized by the amplitude at 13.6 kHz: (a) TA; (b) TB.

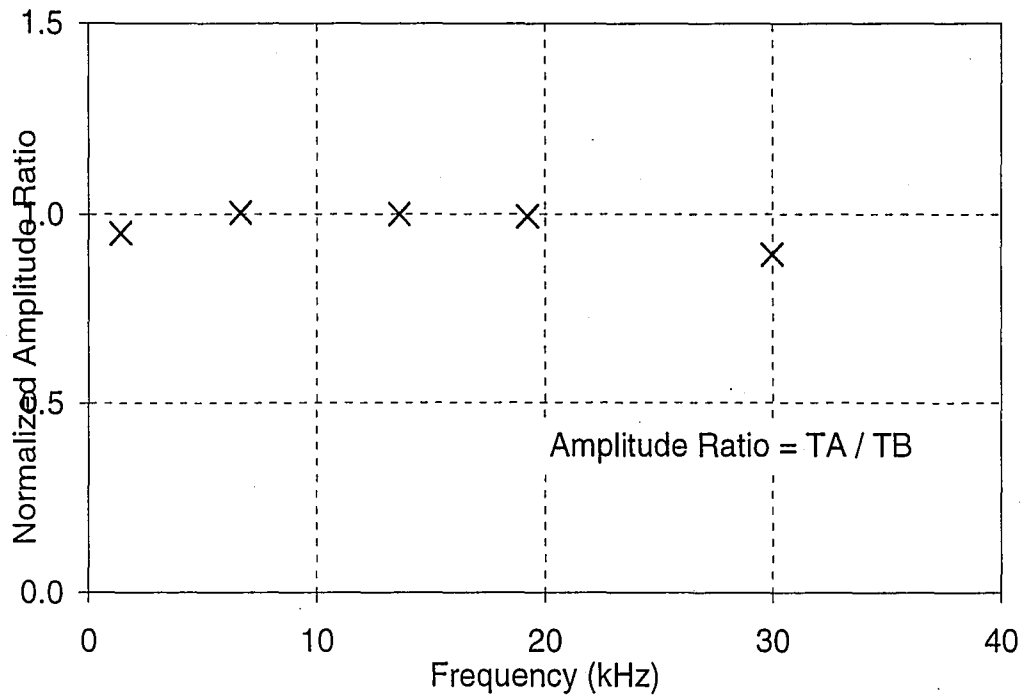

Figure 3.17 Normalized amplitude ratio versus frequency for the frequency response of TA and TB to impact with the transducers repositioned after each impact.

CHAPTER 4

EXPERIMENTAL PROGRAM

4.1 INTRODUCTION

This chapter presents the experimental program. Section 4.2 presents a prototype steel welded plate girder and describes its typical features. The specimens used in this research are intended to replicate these features of the welded plate girder. Section 4.3 describes the specimens and their fabrication. The experimental setup and the testing procedure are given in Section 4.3.

4.2 TYPICAL FEATURES OF WELDED PLATE GIRDERS

Figure 4.1 is a drawing of a typical welded steel plate girder. Welded steel plate girders typically have webs with thickness ranging from 10 to 25 mm. The flange thickness is generally between 20 and 100 mm. The web and flange are joined with a fillet weld along both sides of the web. The web and flange plates are oriented with the roll direction parallel to the span. Because plate girders tend to have long spans, it is often necessary to create the web or flange from multiple lengths of steel plate. The steel plates are spliced together using single or double bevel groove welds. The thickness of the web or flange may change at this splice. To prevent local buckling of the compression flange of the plate girder, stiffeners are attached to the web and compression flange of the girder. The stiffener thickness typically ranges from 6 to 40 mm. The stiffeners are at-

tached to the web and flange of the girder with fillet welds. Other details typically present in a welded steel plate girder, such as cover plates or other welded attachments, are not treated in this research.

4.3 SPECIMEN DETAILS AND FABRICATION

Figure 4.2 shows ten 915 mm diameter plate specimens treated in this study. These plates reproduce the details commonly founded in welded plate girders shown in Figure 4.1. The details of each plate specimen and the features of the prototype plate girder it is intended to model are discussed in the following paragraphs. Table 4.1 summarizes the welded plate girder detail that each test plate is intended to reproduce.

P1 represents the web of a welded plate girder and P2 represents the flange of a welded plate girder. Figures 4.2 (a) and (b) show schematic diagrams of P1 and P2. P1 has a thickness of 13 mm, a value within the range of web thickness for a plate girder, and P2 has a thickness of 51 mm, a common thickness for the flanges of a plate girder. P1 and P2 are control specimens, and have no welded details. The roll direction of each plate is known and is shown in the figures.

P3 and P4 model web and flange splices in welded plate girders where the open side of the weld bevel is upward. Figures 4.2 (c) and (d) show schematic diagrams of P3 and P4. P3 models a splice in the web of a girder. Two 13 mm thick plates are joined using a single V groove weld. The groove weld is ori-

entated perpendicular to the roll direction. This is consistent with the web splice in the typical welded steel plate girder shown in Figure 4.1.

P4 models a splice in the flange of a plate girder. A double beveled groove weld running along its diameter connects the two 51 mm plates. The roll direction of P4 is perpendicular to the weld, consistent to the welded plate girder in Figure 4.1.

Bevel welds are used to splice the web and flange of the welded steel plate girder. Because the weld is beveled, the same weld condition will not occur on each side of the plate. P3′ and P4′ represent the cases when the bevel is on the opposite side of the plate. Figure 4.2 (e) and (f) show plates P3′ and P4′. Plates P3′ and P4′ have thickness 13 and 51 mm respectively, and the roll direction for both plates is perpendicular to the groove weld. The plates are, in fact, the same plates as P3 and P4, with impact occurring on the opposite side.

P5 models a stiffener-to-web connection. Figure 4.2 (g) shows a schematic diagram of P5. The circular plate is used to model the web, and the welded attachment along the diameter represents the stiffener. The circular plate representing the web is the same as to P1. The attachment that models the stiffener has a thickness of 6.4 mm and a height of 150 mm. The stiffener is attached to the web using a 7 mm continuous fillet weld on both sides. The roll direction of P5 is perpendicular to the stiffener. This same orientation would be found in an actual welded plate girder.

P6 models the web-to-flange connection of a welded steel plate girder. Figure 4.2 (h) shows a schematic diagram of P6. The circular plate represents the flange of a girder, and the attachment along the diameter models the web. The circular plate representing the flange has a thickness of 51 mm. The double fillet welded attachment represents the flange with a thickness of 13 mm. The height of the attachment representative of the web is 150 mm. A 7 mm continuous double fillet weld is used for the web-to-flange connection. The welded attachment of P6 is parallel to the roll direction.

P5′ and P6′ also model the stiffener-to-web and web-to-flange connections. These specimens represent the case where the welded attachment is located on the opposite side of the plate as P5 and P6. P5′ and P6′ have the same fabrication details as P5 and P6, respectively, and are shown in Figure 4.2 (i) and (j). In fact, P5′ and P6′ are the same identical plates as P5 and P6, except that testing is performed on the opposite surfaces. For clarity, they are presented with the separate identifiers P5′ and P6′.

All specimens were ASTM 709 Grade 50 steel. The specimens were created by Bethlehem-Lukens Plate and fabricated at High Steel Structures, Inc. All welds are prequalified by the American Welding Society (AWS) and conform to the minimum and maximum weld sizes as dictated by AISC-LRFD Section J (1998). All welds conform to the American Welding Society Bridge D1.5 Bridge Welding Code (1995). The single V groove welds for P3 and P4 conform to AWS W71 specifications (1995). The fillet welds for P5, P6, P5′, and P6′ conform to

AWS W33 specifications (1995). Weld soundness was verified both with ultrasonic and magnetic particle testing. This is standard practice for bridge elements as well.

Circular plates are used in this research because the patterns of vibration are well understood and can be predicted. The modes of vibration for a circular plate are presented in Chapter 2. Another reason for the specimens being circular is that a symmetric geometry can be produced. Section 4.3 discusses the symmetric setup and response of the test system.

4.4 EXPERIMENTAL SETUP AND PROCEDURE

A common test setup is used for each specimen and is shown in Figure 4.3. Each plate rests on wood supports during testing. The supports are assumed not to influence the vibration of the plate. This assumption was verified by experimenting with different configurations of the wood supports.

For the purpose of discussion, the plate is divided into 4 quadrants. As shown in Figure 4.3, the transducers and impact location are arranged symmetrically with respect to the weld detail and roll direction. Transducer A (TA) is placed in quadrant Q1. Transducer B (TB) is placed in quadrant Q3. Impacted is made in Q2 or Q4. The impact creates stress waves that propagate to the transducers.

A general discussion of the test setup parameters and its components is given in Chapter 3. The test parameters common to all plates include a steel

sphere diameter of r= 2 mm, drop height of h=150 mm, sample interval of Δt=1μs, and a record length of 1000 samples. A signal is received by TA and TB, each signal is filtered using a 1-kHz high-pass filter, and captured and processed using a two-channel oscilloscope. At each impact location, signals generated from five impacts are recorded in the time domain. Chapter 5 presents the waveforms recorded in this research.

The circular plates are chosen to simplify the patterns of vibrations and to produce a symmetric response to the point impact. The transducers and impact are placed a distance *a* from the center of the plate as shown in Figure 4.3. Upon impact, stress waves are assumed to radiate spherically from the source. When the waves encounter a boundary, they are reflected and refracted. Figure 4.4 shows two possible travel paths for two rays along the waves that travel from an impact location to the transducer location. One wave travels from the impact at A directly to the transducer at C. Another wave will travel from A and be reflected off the boundary of the plate at point B and then travel to the transducer at C. Thus, the displacements recorded at C will be due to waves traveling along path AC and also along path ABC. Only the signal recorded before the arrival of the reflected waves (path ABC) will show the effect of the plate geometry on the wave AC. The location of the transducers and impact (the distance 2*a*) is chosen to maximize the duration of the recorded signal for path AB before reflected waves arrive. This will occur when the value of 2*a* is minimized.

The value of *a* is limited by the processing of the steel plates. The welding process creates a heat-affected zone in the steel plate. The surface of the plates with welds or welded attachments has an irregular surface due to welding approximately 50 mm to each side of a weld. Because of the surface disturbance, consistent coupling can not be made between the transducer and the steel plate. For this reason, the value of *a* is chosen as 70 mm in this study to avoid coupling problems.

If *a* equals 70 mm, the distance between the impact and the transducer (path AC in Figure 4.4) is 140 mm. Given the speed of the P-wave in steel (C_P= 5960 m/s), the wave will have a travel time of 23.5 μs. The shortest reflected wave (traveling along path ABC) will have a travel time of 284.5 μs. This means that the reflected waves will arrive 261 μs after the arrival of the unreflected wave. Therefore, including a pretrigger of 200 μs, the first 461 μs of the signal will be free of the influence of waves reflected off plate boundaries, and useful in evaluation. It is noted here that pretrigger is considered negative time and all time durations given in this report begin at zero unless otherwise noted. The comparisons made in this report will primarily focus on the beginning of the signal, before the reflected waves arrive.

The transducers and impact are arranged such that the path length from impact to TA is identical in geometry to the path length from impact to TB. The roll direction or the presence of a welded attachment are the intended variables inserted into the paths traveled by the stress waves. Signals are said to travel

either *parallel* or *perpendicular* to the roll direction. Waves that propagate across welds or welded attachments are referred to as *obstructed*. Waves not propagating across the weld or welded attachment are referred to as *unobstructed*. For example, Figure 4.5 shows a circular plate with a weld. An impact in Q2 creates stress waves that travel parallel to the roll direction to TB, located in Q3. Waves travel perpendicular to the roll direction to TA, located in Q1. The groove weld causes the wave recorded in Q3 to be obstructed, while the wave recorded by Q1 is unobstructed. Therefore, the waveform recorded by TA in Q3 is said to be "parallel to the roll direction obstructed by the weld", and the waveform recorded by TB in Q1 is said to be "perpendicular to the roll direction unobstructed by the weld."

In order to make reliable measurement, good acoustic coupling has to be maintained between the steel plate and the impact and receiver. Residual surface coatings from fabrication and dirt from storage on the surface of the plate can interfere with the contact the transducer, shield, and impact make with the plate. Care was also taken that the impact and receiver locations are free of mill scale. Locations of impact and receiver were thoroughly cleaned prior to testing.

The circular plates will respond similarly to impact resulting in the waves of the same class (i.e. parallel or perpendicular, obstructed or unobstructed). Impacts in Q2 and Q4 produce waves that are similar in class from each impact. A plate impacted in Q2 will produce a wave traveling to Q1 that is the same class of waves as that traveling to Q3 by an impact in Q4. The same is true for waves

traveling to Q3 from an impact at Q2 and to Q1 from an impact at Q4. Waveforms generated in all plates from impacts in Q2 and Q4 are presented in Chapter 5.

Plate	Description
P1	Web
P2	Flange
P3	Web splice
P3′	Flange splice
P4′	Web splice with bevel on opposite side
P5	Flange splice with bevel on opposite side
P6	Stiffener-to-web connection
P7	Web-to-flange connection
P6′	Stiffener-to-web connection on opposite side of plate
P7′	Web-to-flange connection on opposite side of plate

Table 4.1 Description of test specimens.

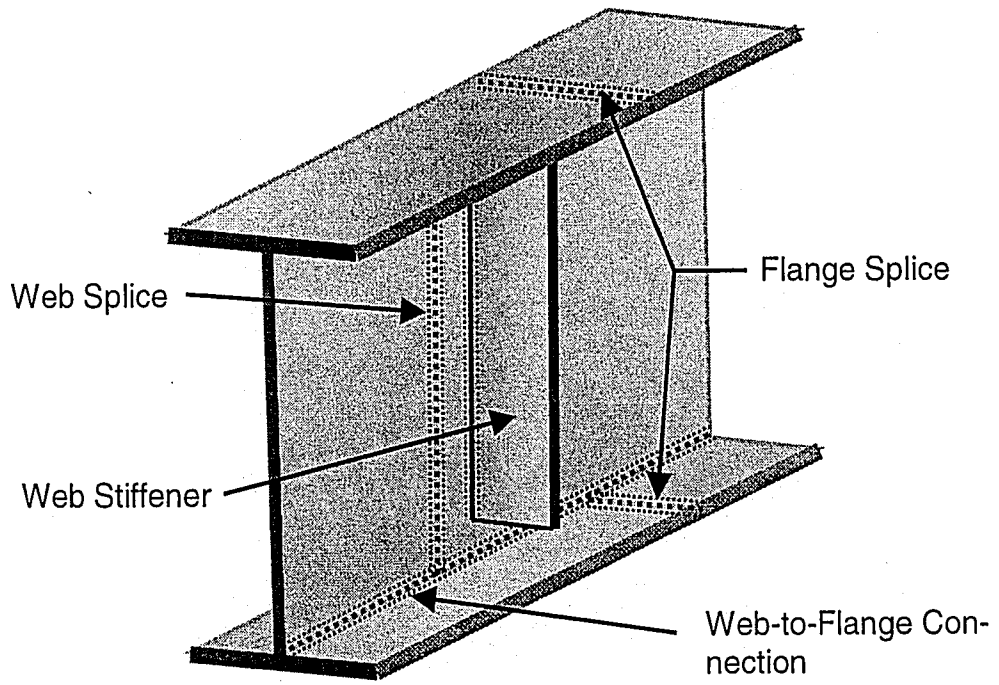

Figure 4.1 Prototype plate girder.

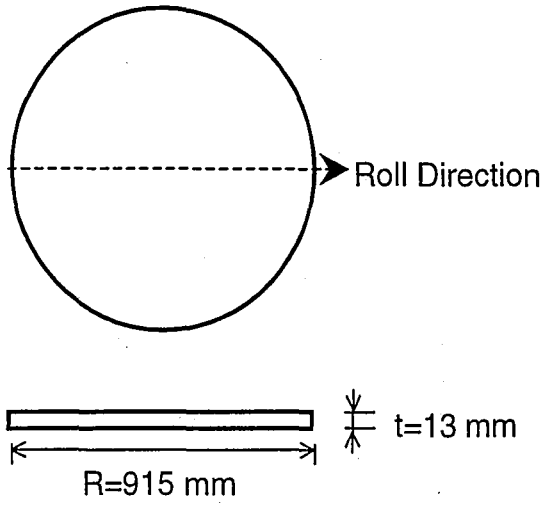

(a)

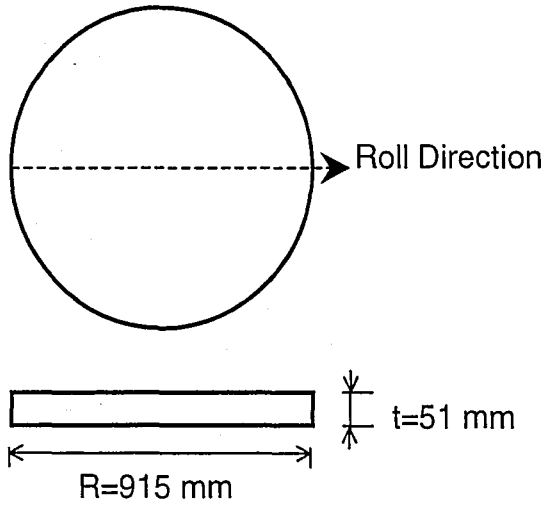

(b)

Figure 4.2 Plate specimens: (a) P1: plain web plate; (b) P2: plain flange plate;

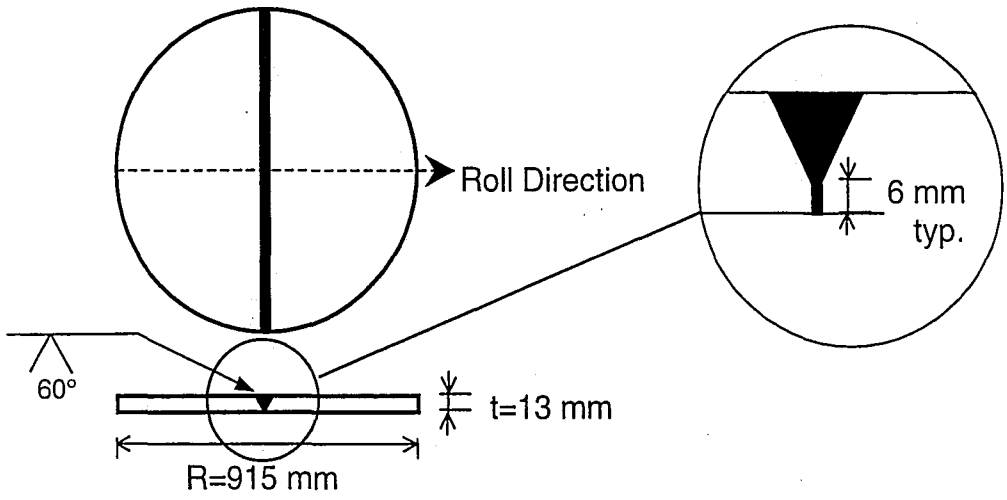

(c)

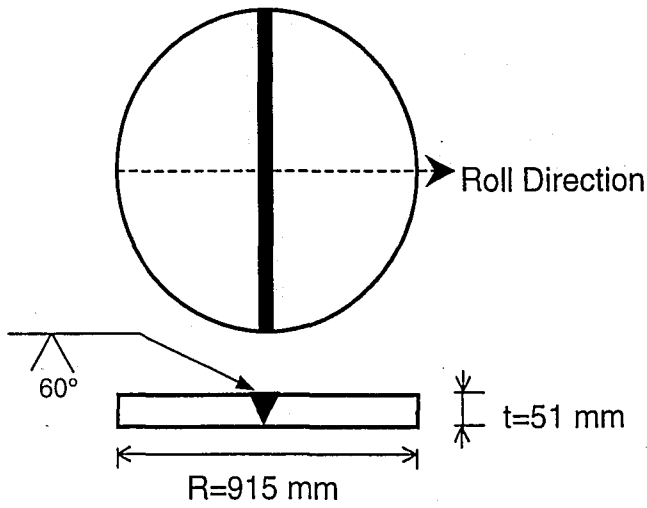

(d)

Figure 4.2 (continued) Plate specimens: (c) P3: web splice plate with bevel on test side; (d) P4: flange splice plate with bevel on test side;

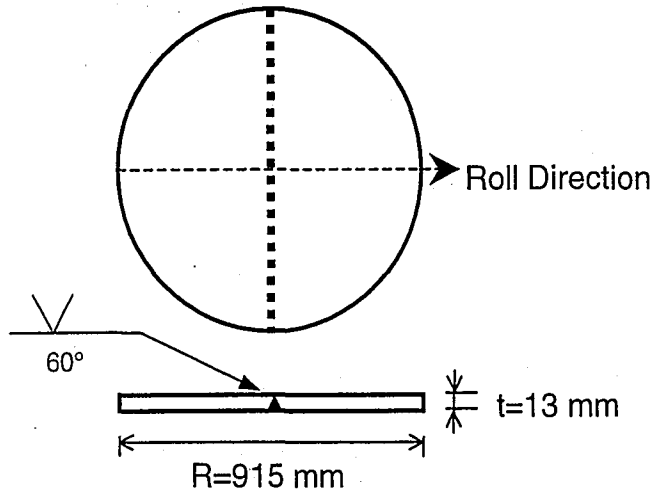

(e)

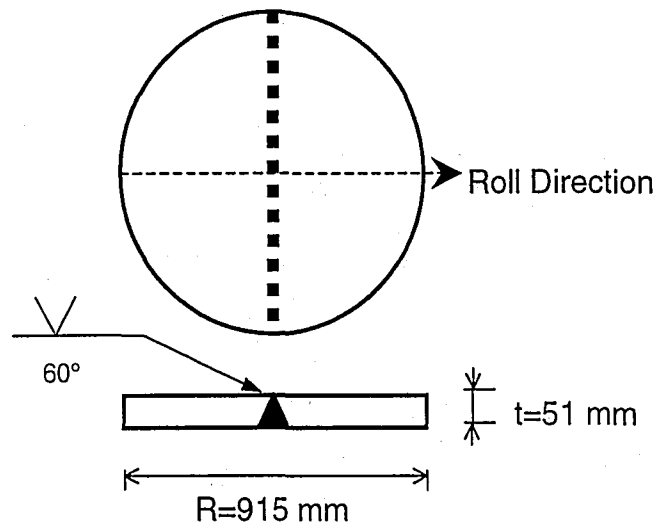

(f)

Figure 4.2 (continued) Plate specimens: (e) P3': web splice plate with bevel on opposite side; (f) P4': flange splice plate with bevel on opposite side;

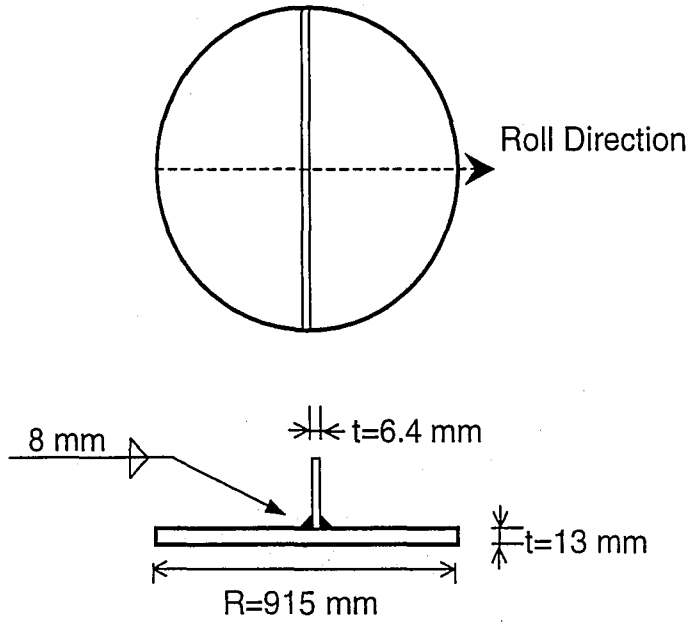

(g)

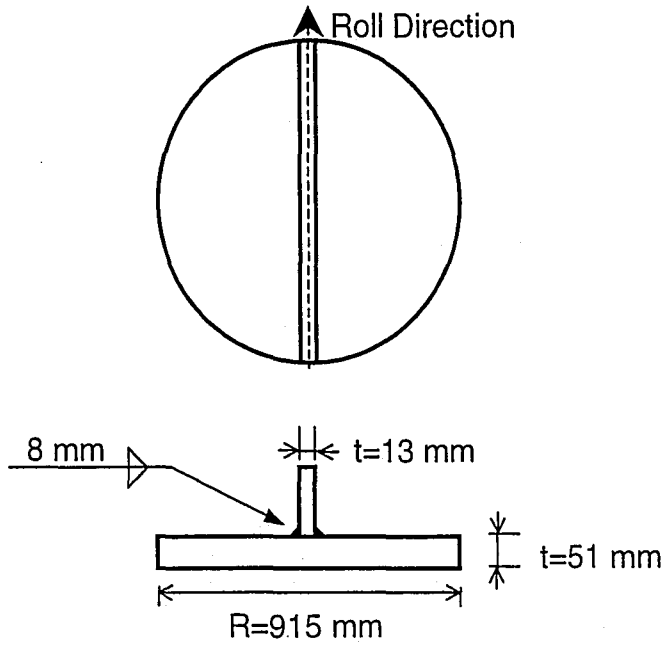

(h)

Figure 4.2 (continued) Plate specimens: (g) P5: stiffener-to-web connection; (h) P6: web-to-flange connection;

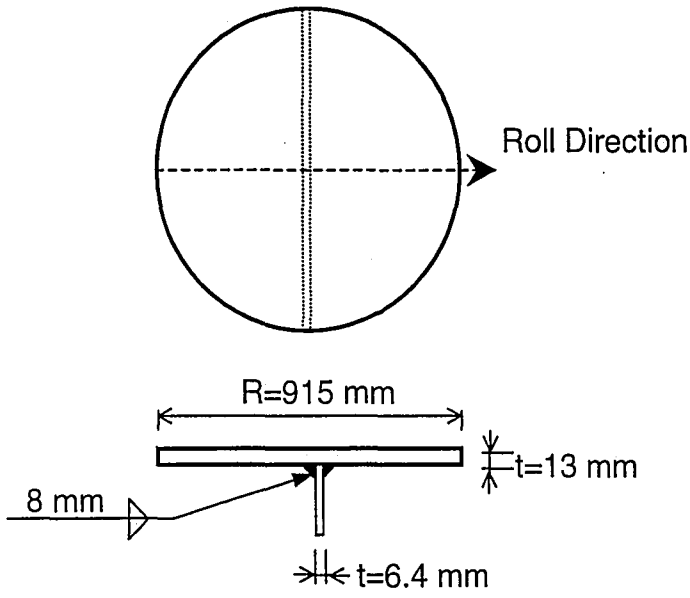

(i)

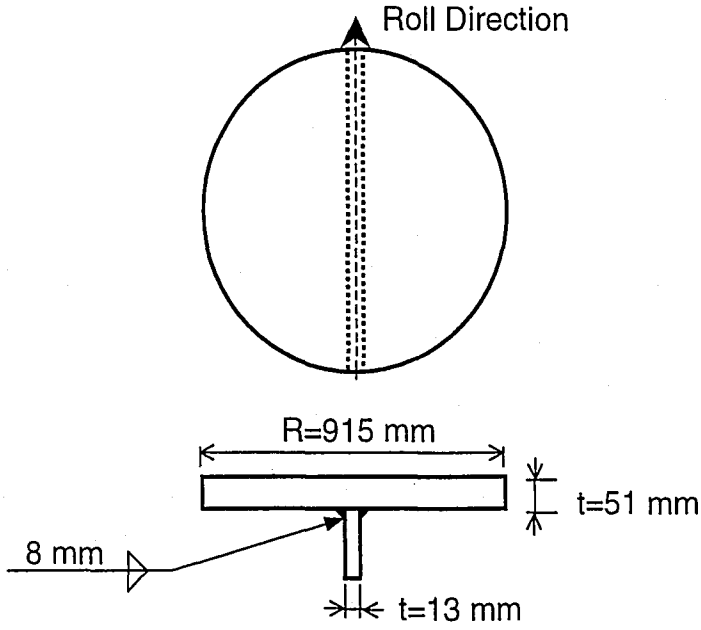

(j)

Figure 4.2 (continued) Plate specimens: (i) P5': stiffener-to-web connection on opposite side; (j) P6': web-to-flange connection on opposite side.

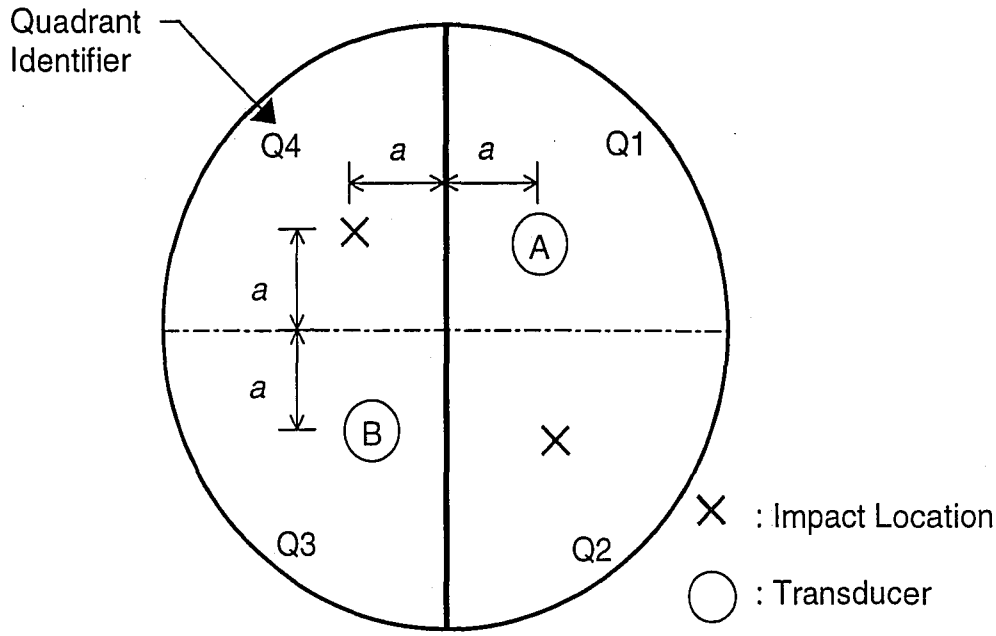

Figure 4.3 Experimental setup.

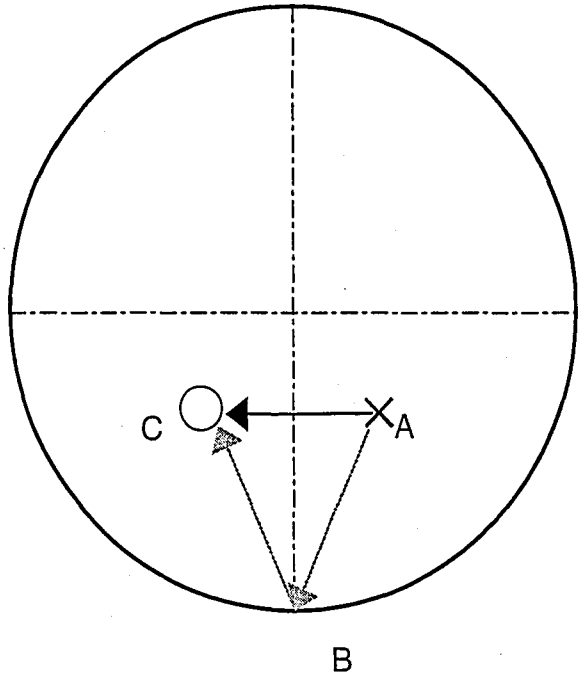

Figure 4.4 Two possible travel paths for a stress wave originating from an impact at A and traveling to a transducer at C.

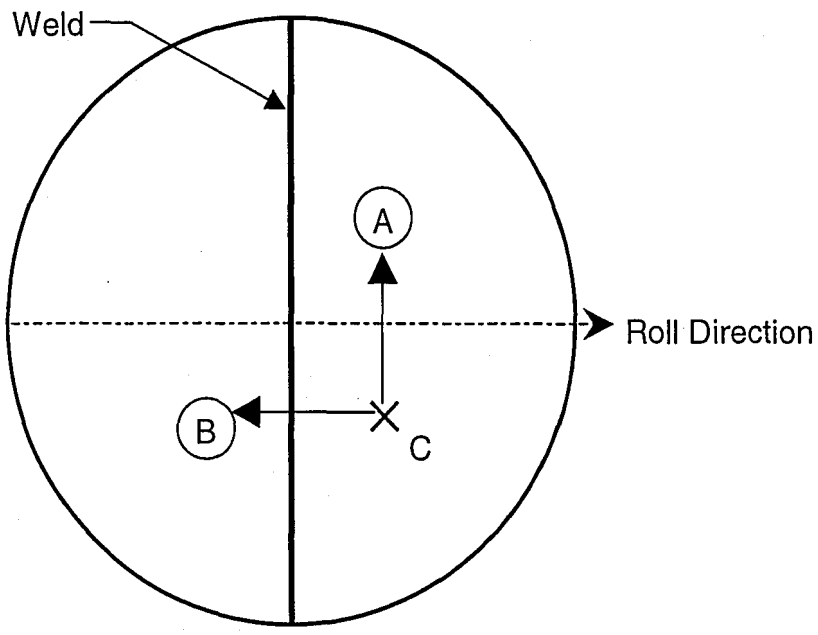

Figure 4.5 Stress waves generated by an impact in Q2: stress wave AC travels parallel to the roll direction obstructed by the weld; stress wave BC travels perpendicular to the roll direction unobstructed by the weld.

CHAPTER 5

EXPERIMENTAL RESULTS

This chapter presents the experimental results in the form of surface displacement waveforms obtained from the tests of each plate. Chapter 6 presents a discussion of the results presented here.

As explained in Chapter 4, Transducer A and Transducer B were positioned at Q1 and Q3 and impacts were made in Q2 and Q4. Data was gathered from five impacts at Q2 and five impacts at Q4. Thus, a total of twenty waveforms are presented for each plate (ten impacts total times two transducers). All twenty waveforms for a particular plate are presented in a four-part figure. The results for plates P1 through P6′ are presented in Figures 5.1 through 5.10 respectively. In each figure, the waveforms are arranged as follows:

(a) Waveforms generated by impact in Q2 and recorded by Transducer A in Q3.

(b) Waveforms generated by impact in Q2 and recorded by Transducer B in Q1.

(c) Waveforms generated by impact in Q4 and recorded by Transducer A in Q3.

(d) Waveforms generated by impact in Q4 and recorded by Transducer B in Q1.

Each figure includes a schematic drawing of the test setup, with the quadrant of the impact marked with an "x" and the quadrant with the transducer marked with an "o". Also noted in each schematic is the direction of roll of the plate material and the orientation of the welds or attachments. Finally, Table 5.1 summarizes the parameters associated with the test of each plate.

Plate	Description	Transducer		Voltage Range (V)
		Q1	Q3	
P1	Web Plate		A	3.0
		B		
P2	Flange Plate		A	0.6
		B		
P3	Web Splice		A	3.0
		B		
P4	Flange Splice		A	0.6
		B		
P3'	Web Splice (bevel opposite side)		A	3.0
		B		
P4'	Flange Splice, (bevel opposite side)		A	0.6
		B		
P5	Stiffener-to-Web Connection		A	3.0
		B		
P6	Web-to-Flange Connection		B	0.6
		A		
P5'	Stiffener-to-Web Connection (opposite side)		A	3.0
		B		
P6'	Web-to-Flange Connection (opposite side)	A		0.6
			B	

Table 5.1 Test parameters for each test plate.

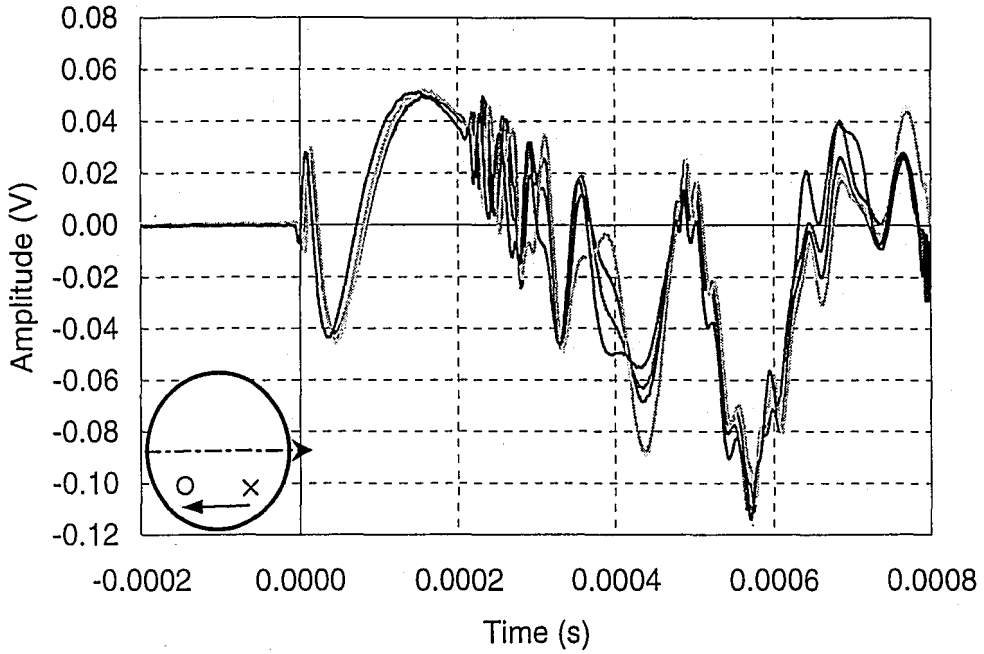

(a)

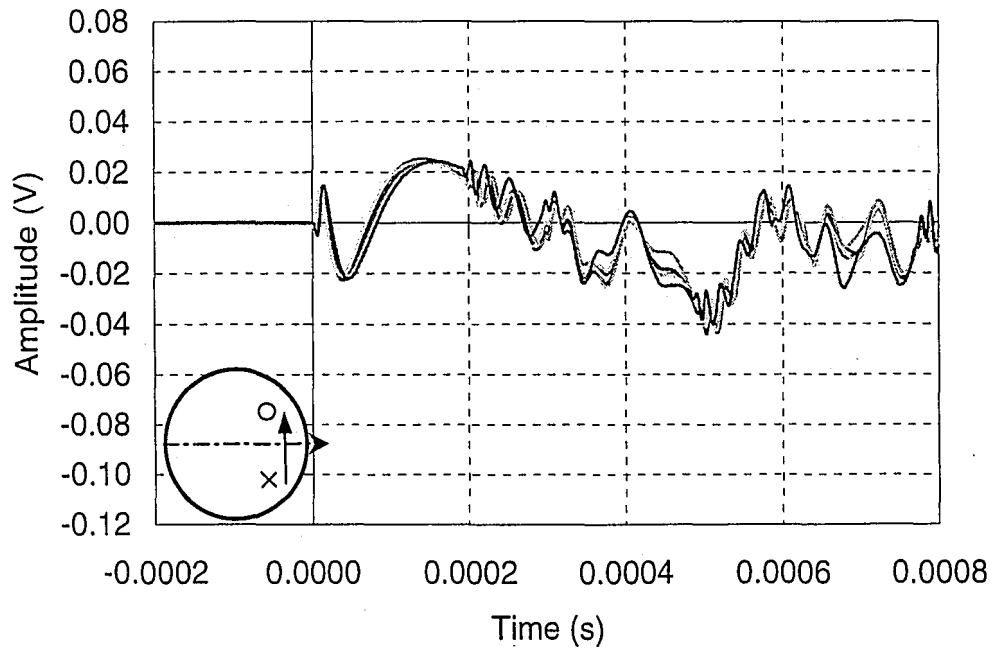

(b)

Figure 5.1 Waveforms for P1 (web plate): impact in Q2 (a) parallel to the roll direction; and (b) perpendicular to the roll direction;

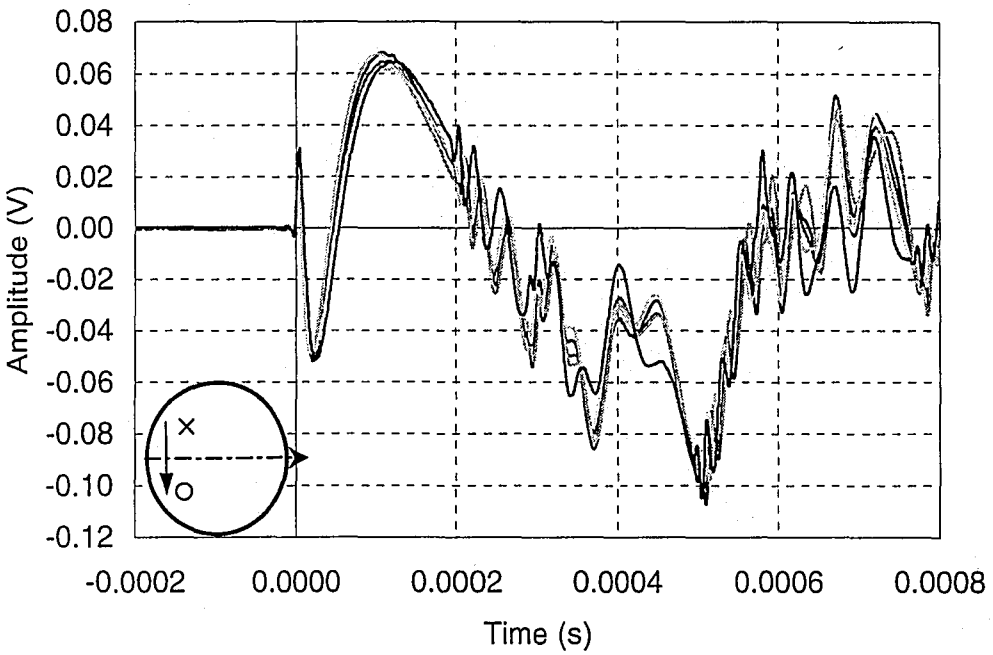

(c)

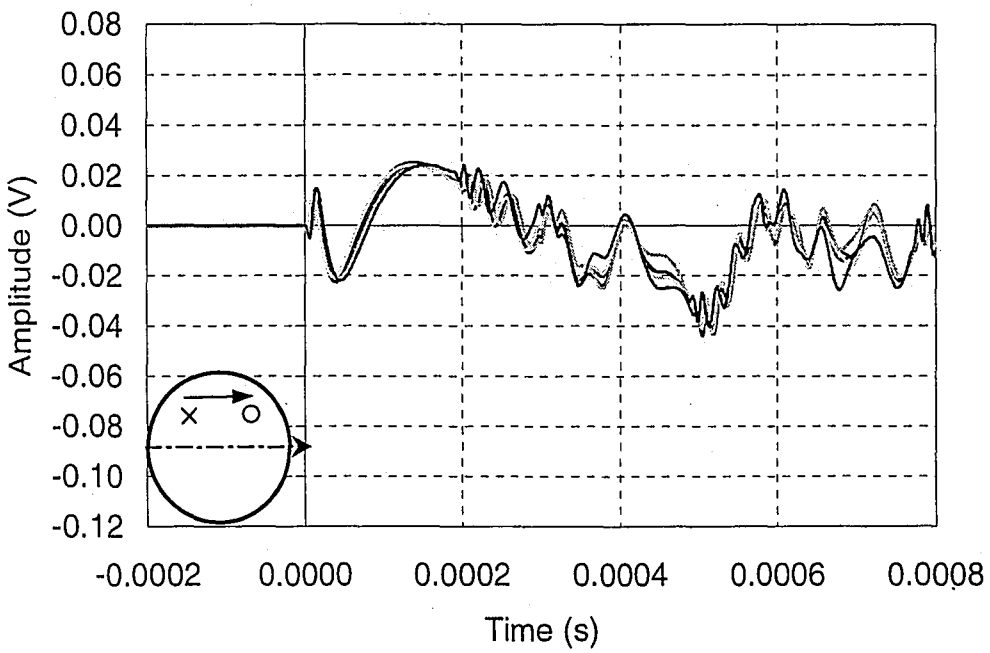

(d)

Figure 5.1 (continued) Waveforms for P1 (web plate): impact in Q4 (c) perpendicular to the roll direction; and (d) parallel to the roll direction.

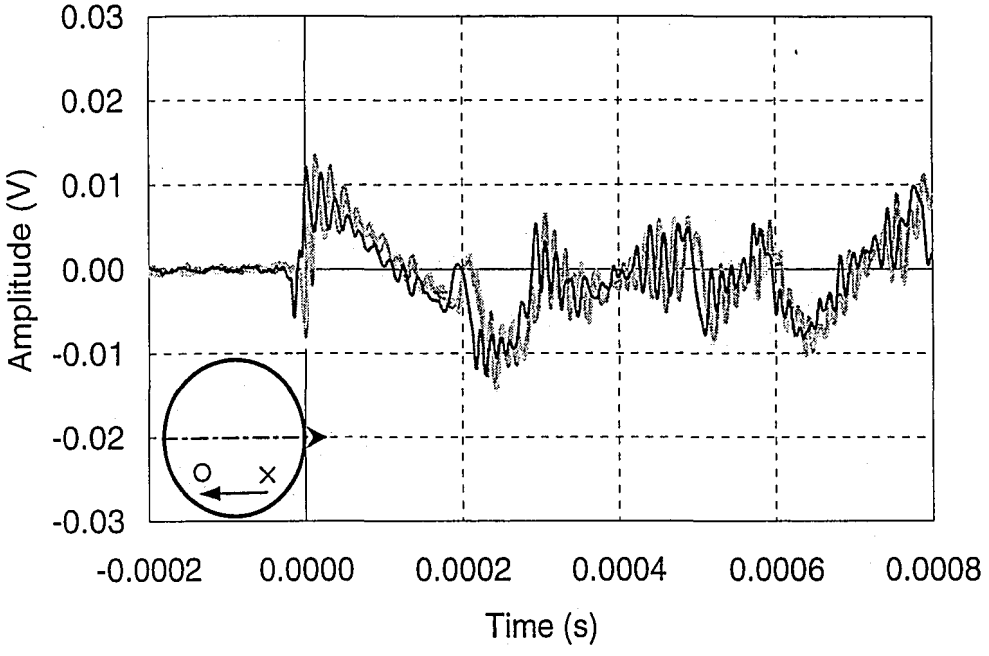

(a)

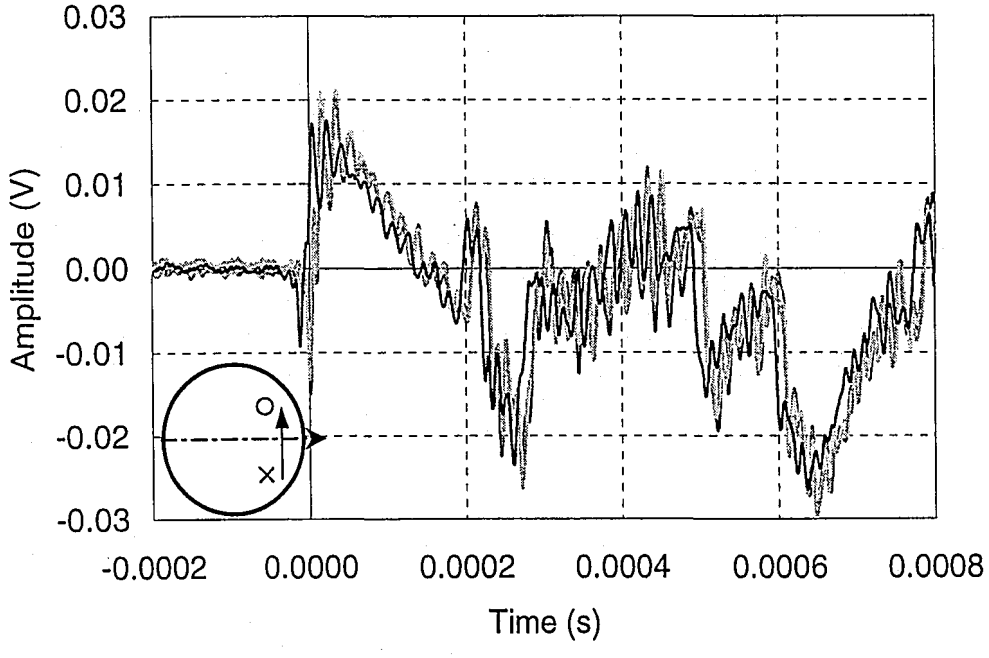

(b)

Figure 5.2 Waveforms for P2 (flange plate): impact in Q2 (a) parallel to the roll direction; and (b) perpendicular to the roll direction;

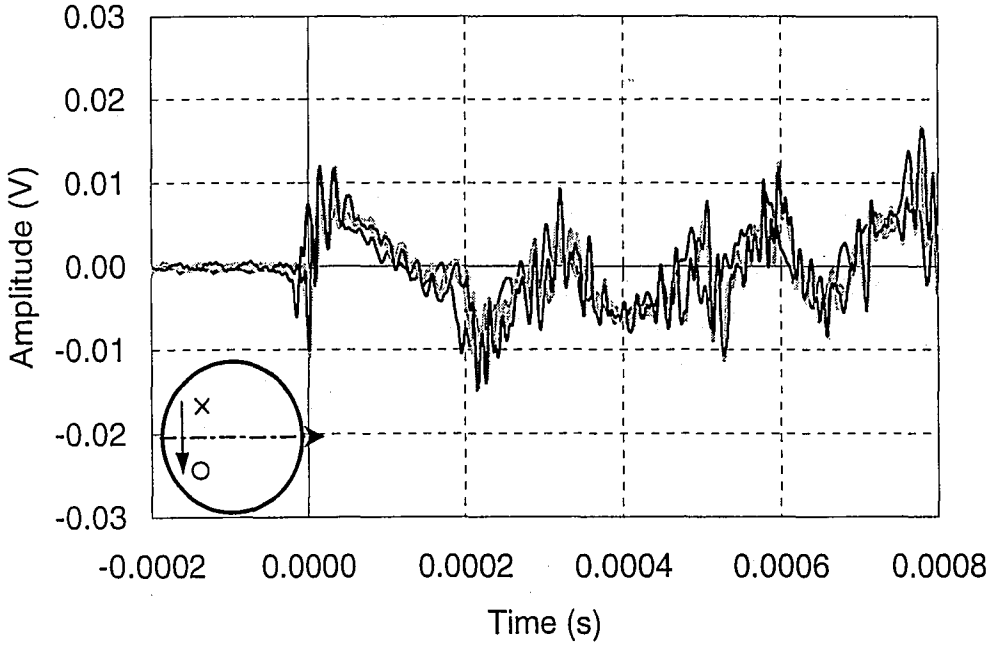

(c)

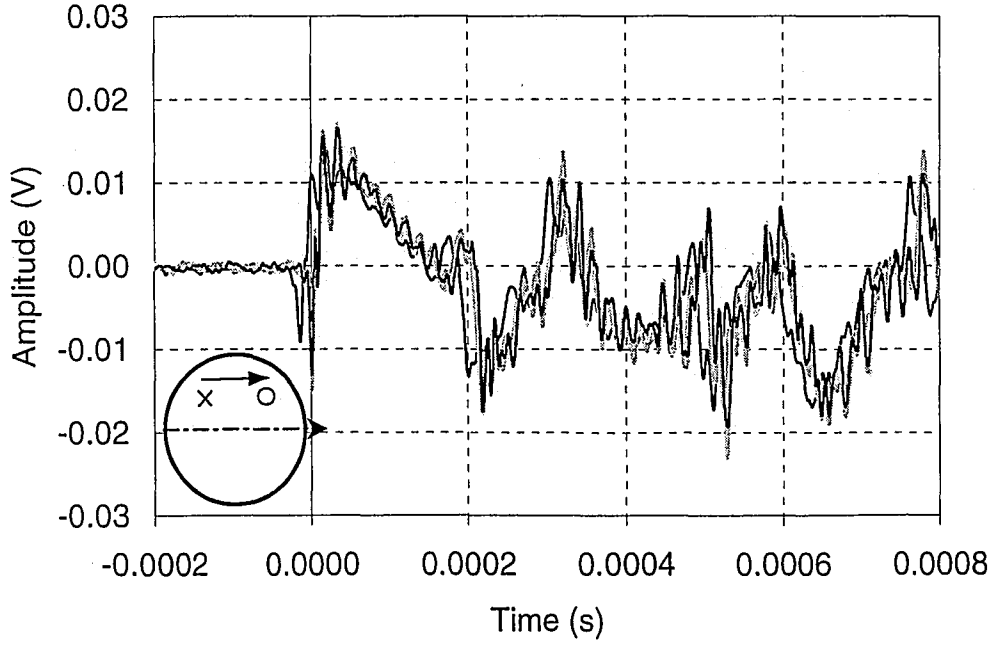

(d)

Figure 5.2 (continued) Waveforms for P2 (flange plate): impact in Q4 (c) perpendicular to the roll direction; and (d) parallel to the roll direction.

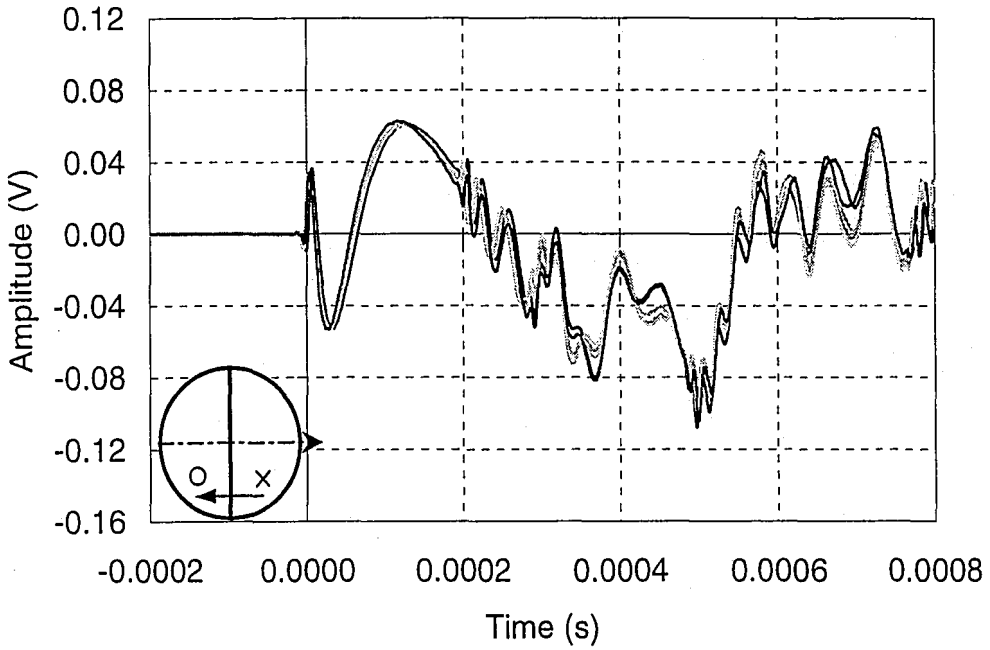

(a)

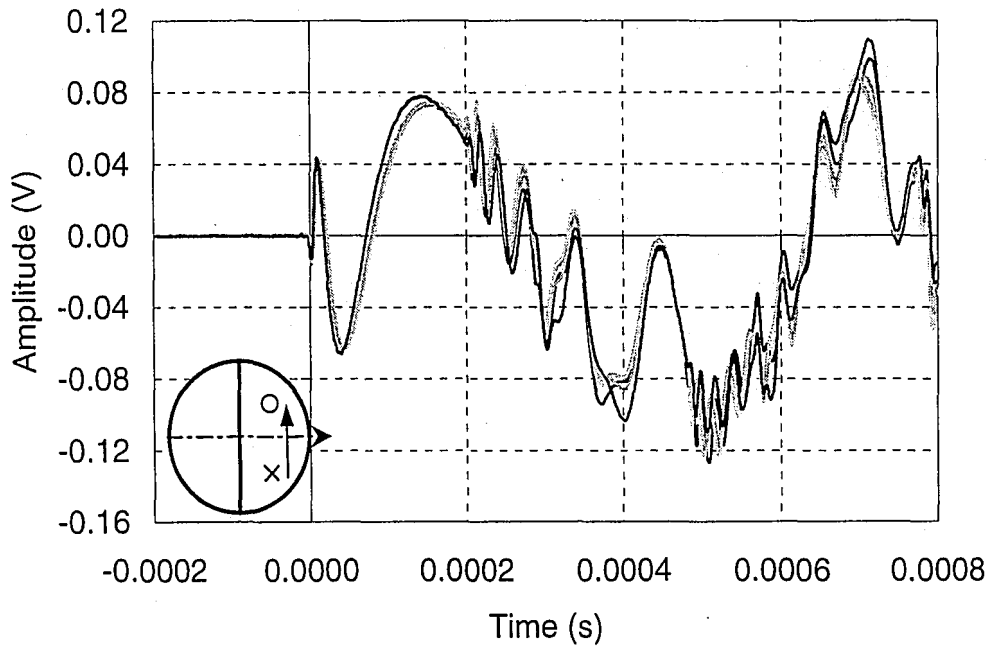

(b)

Figure 5.3 Waveforms for P3 (web splice): impact in Q2 (a) parallel to the roll direction; and (b) perpendicular to the roll direction;

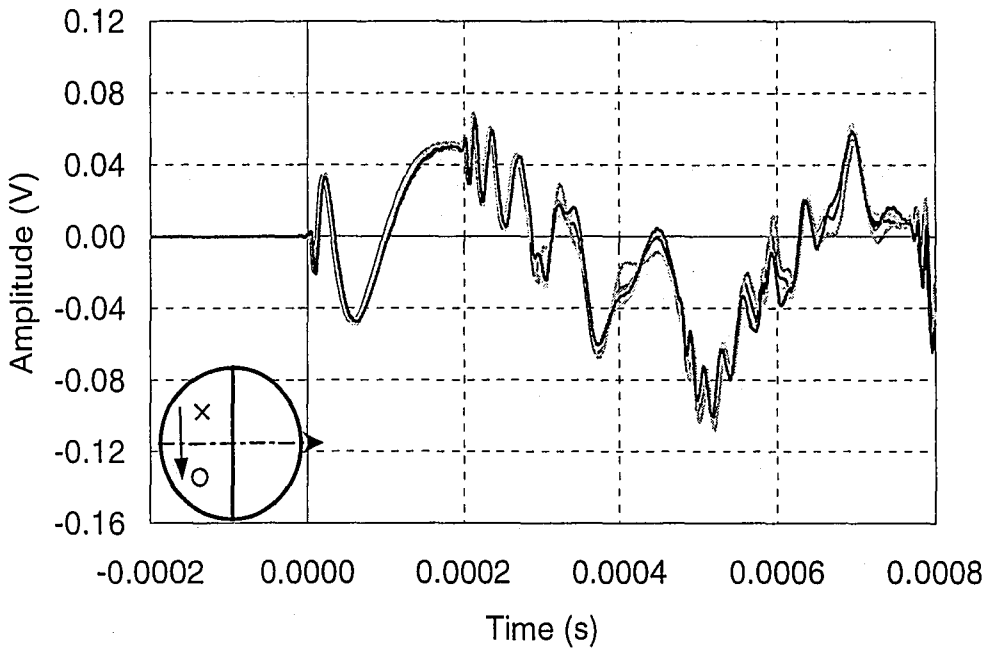

(c)

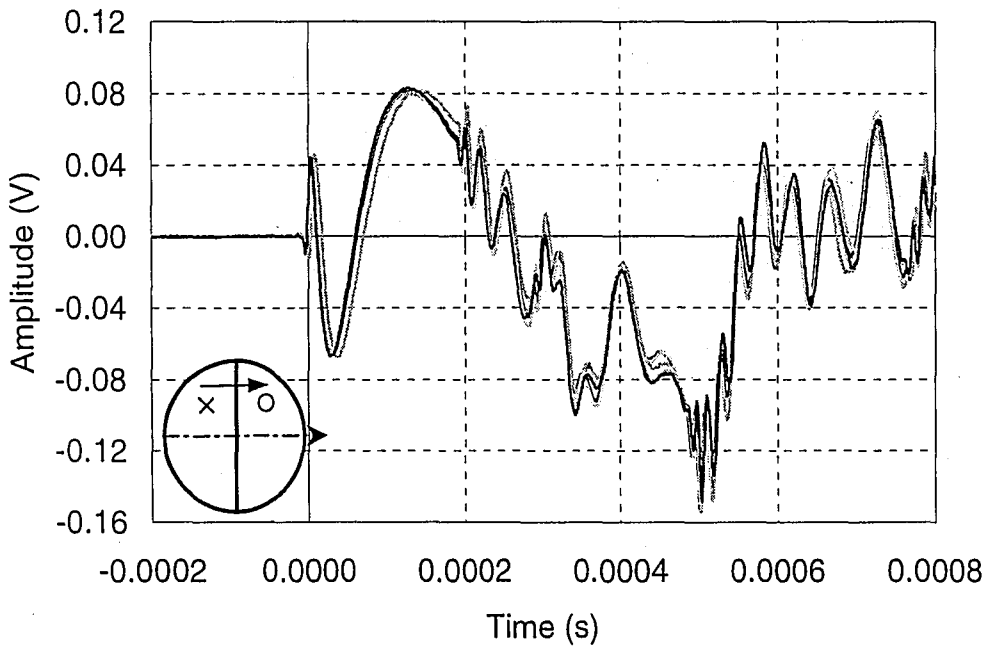

(d)

Figure 5.3 (continued) Waveforms for P3 (web splice): impact in Q4 (c) perpendicular to the roll direction; and (d) parallel to the roll direction.

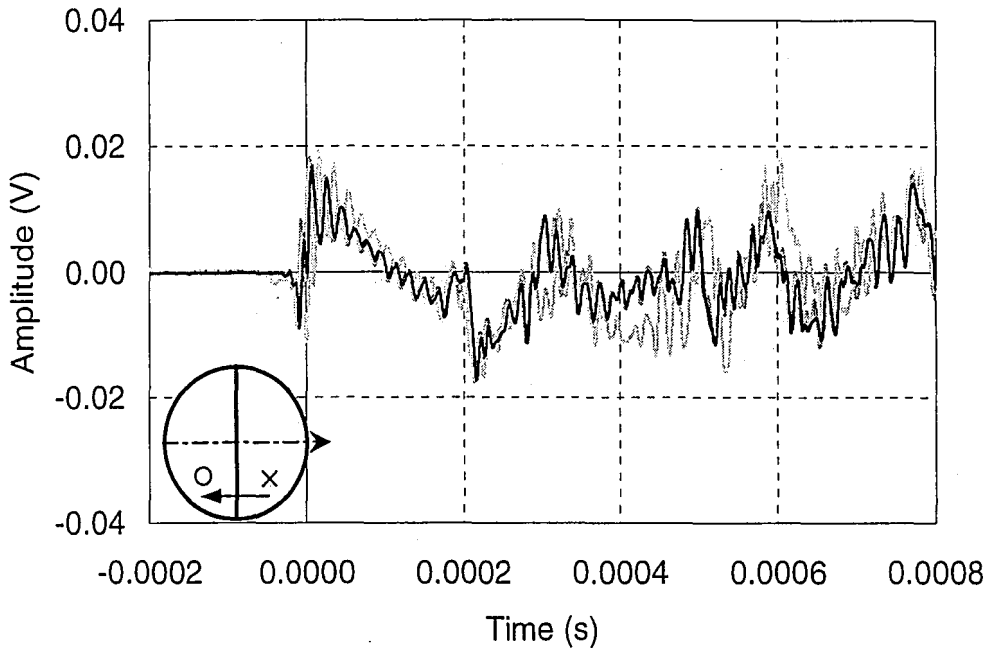

(a)

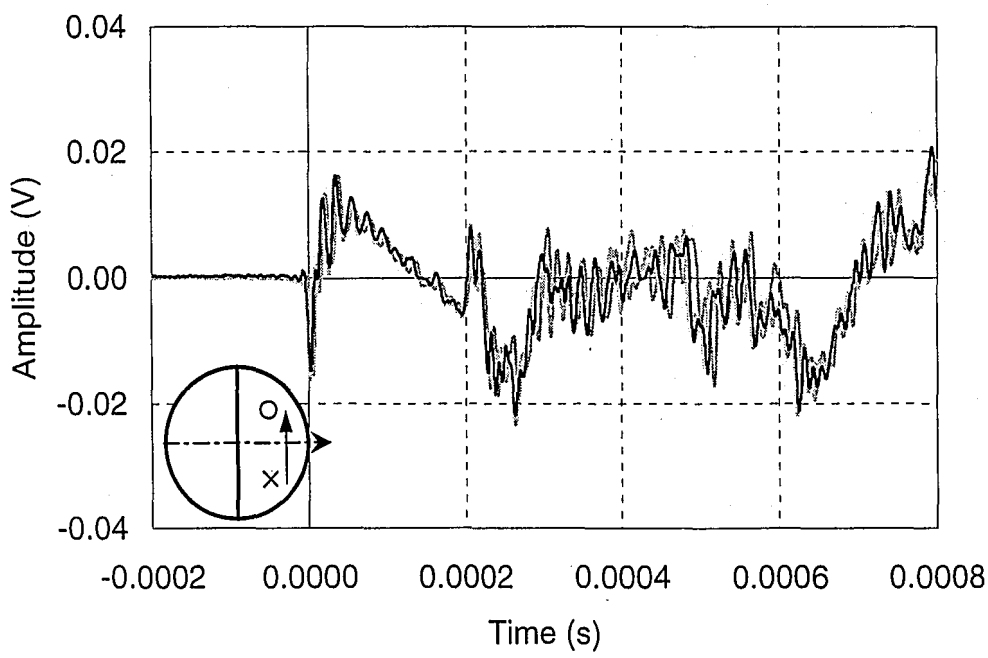

(b)

Figure 5.4 Waveforms for P4 (flange splice): impact in Q2 (a) parallel to the roll direction; and (b) perpendicular to the roll direction;

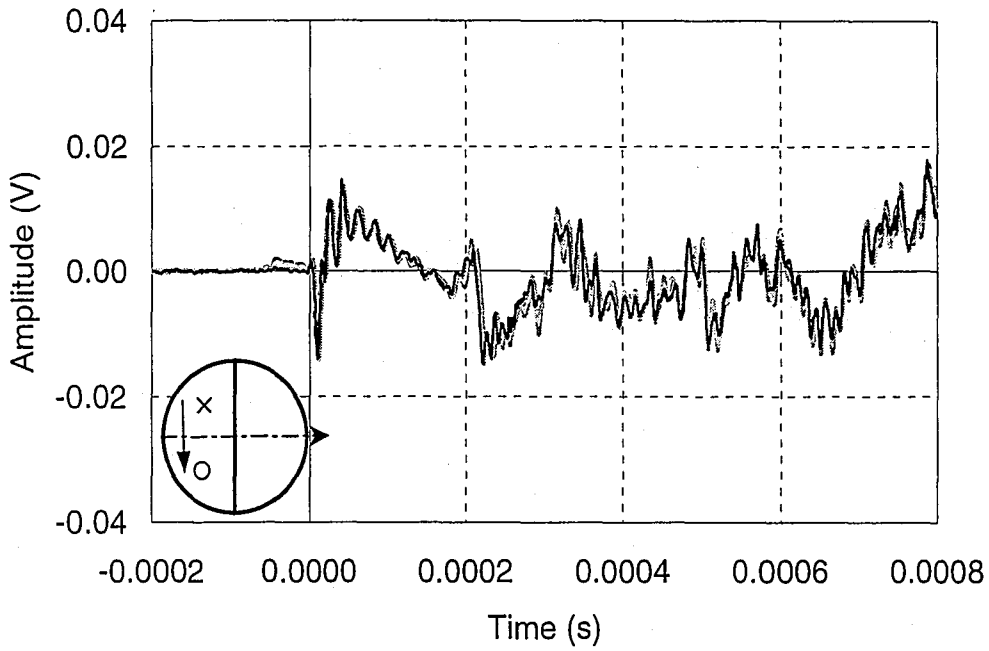

(c)

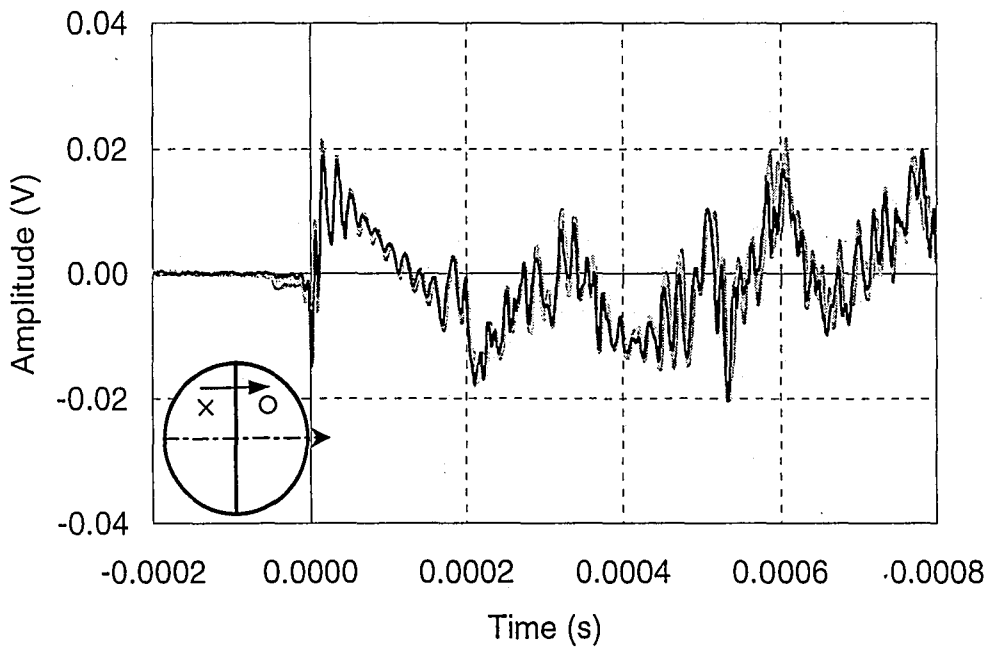

(d)

Figure 5.4 (continued) Waveforms for P4 (flange splice): impact in Q4 (c) perpendicular to the roll direction; and (d) parallel to the roll direction.

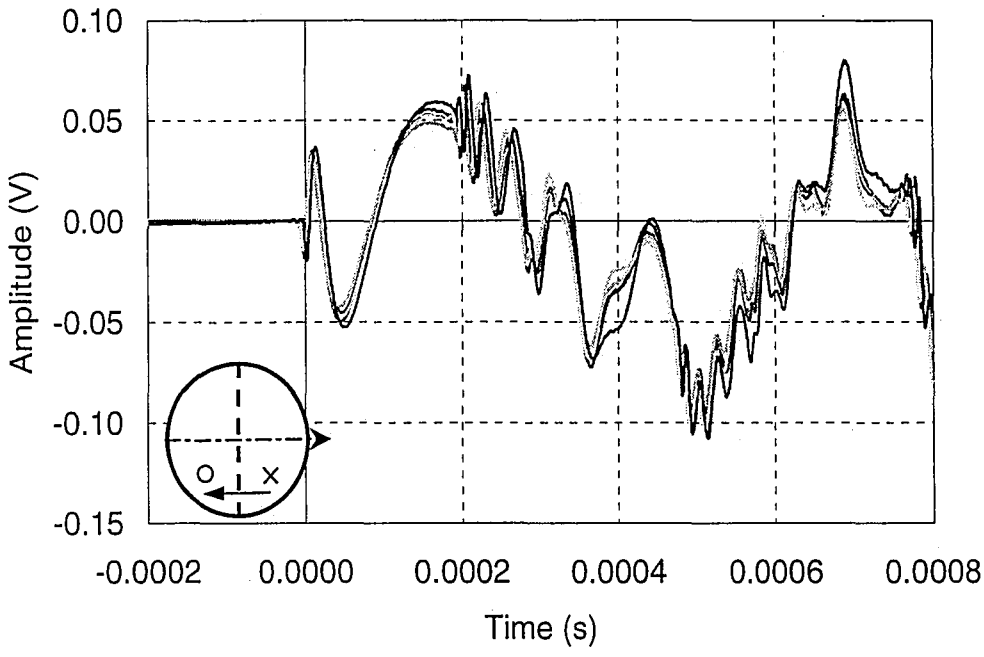

(a)

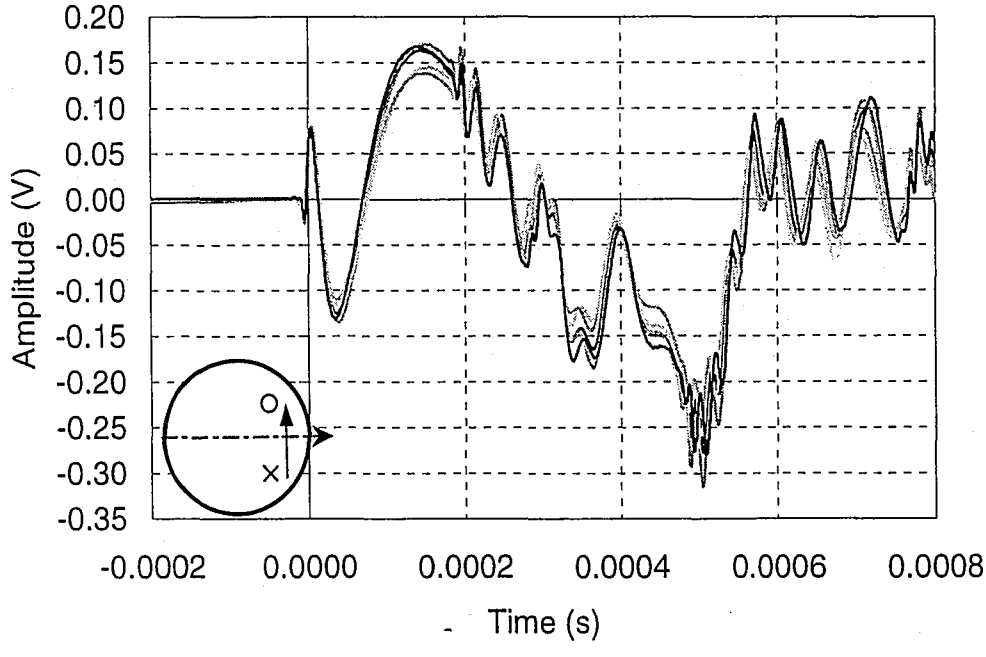

(b)

Figure 5.5 Waveforms for P3' (web splice): impact in Q2 (a) parallel to the roll direction; and (b) perpendicular to the roll direction;

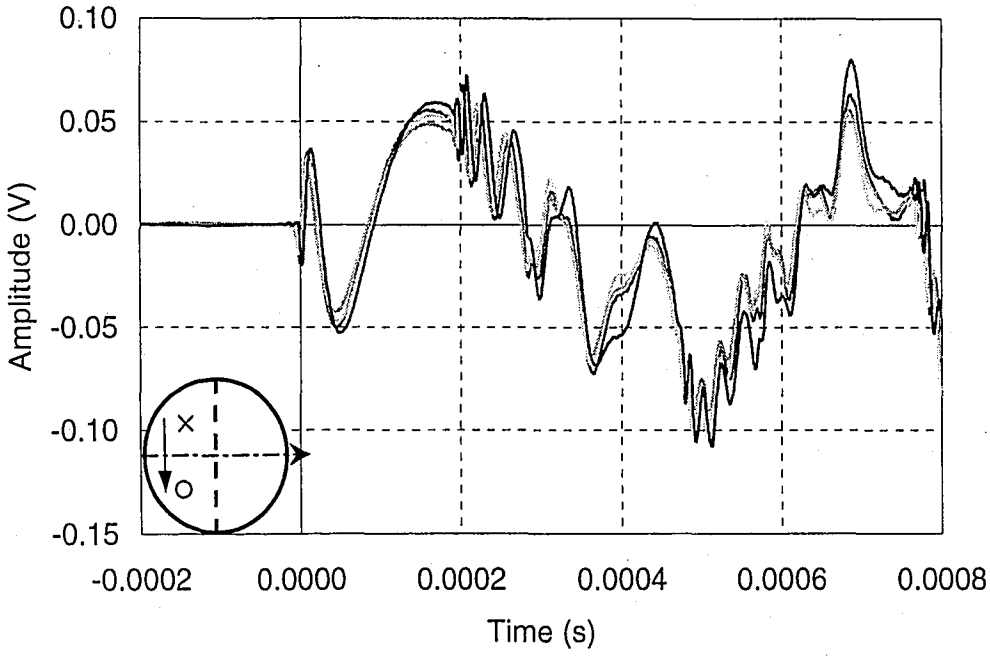

(c)

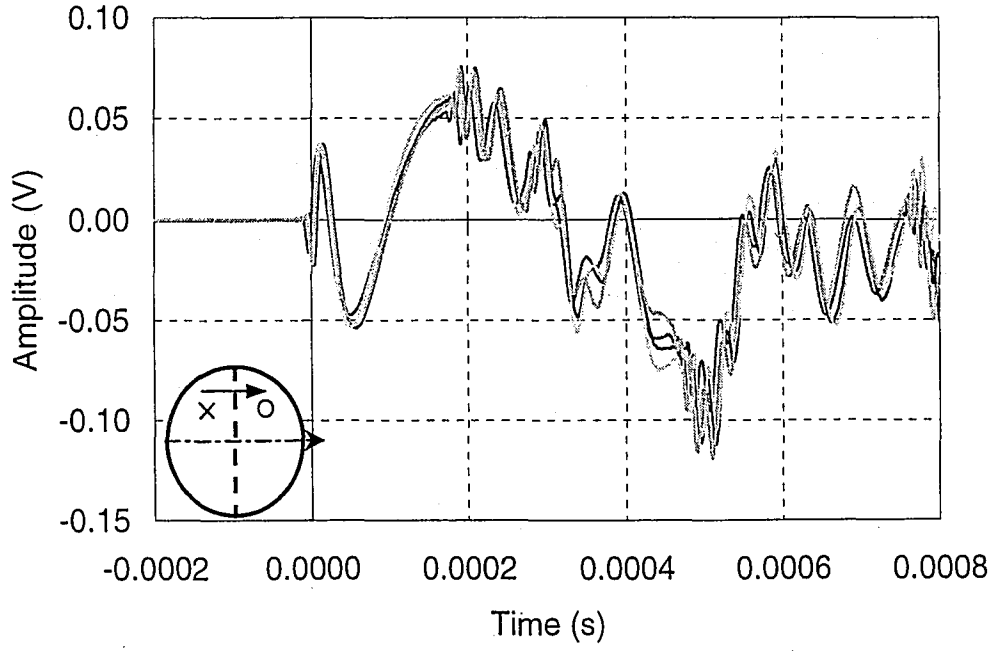

(d)

Figure 5.5 (continued) Waveforms for P3' (web splice): impact in Q4 (c) perpendicular to the roll direction; and (d) parallel to the roll direction.

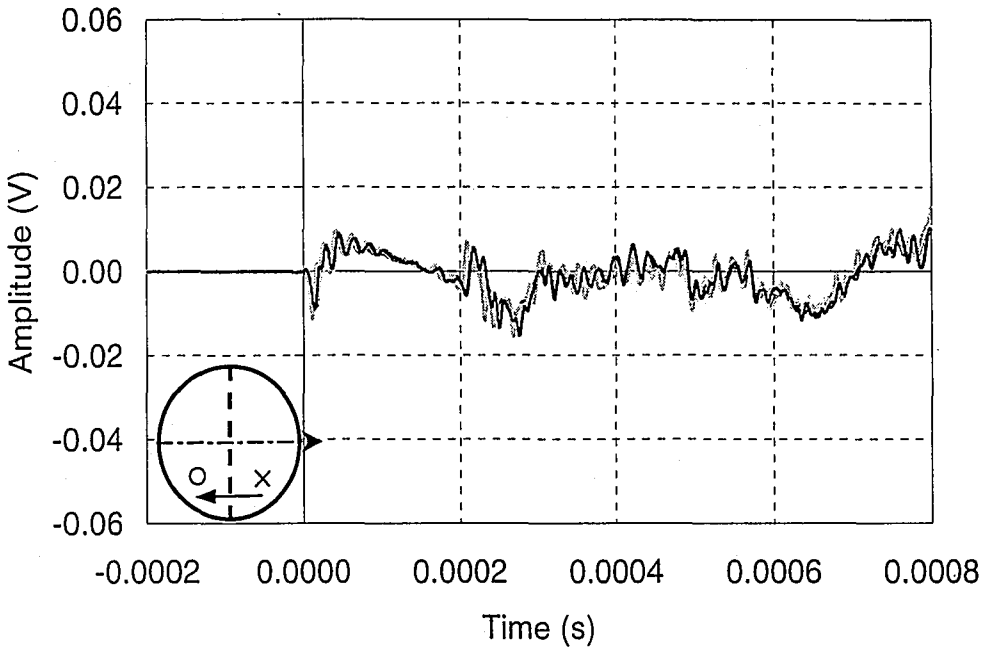

(a)

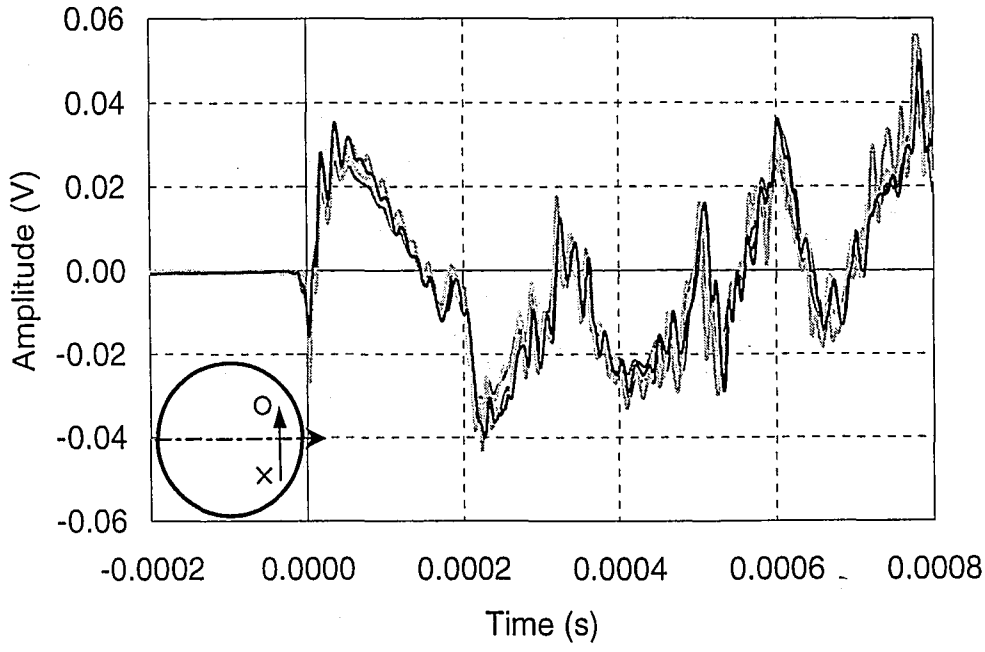

(b)

Figure 5.6 Waveforms for P4' (flange splice): impact in Q2 (a) parallel to the roll direction; and (b) perpendicular to the roll direction;

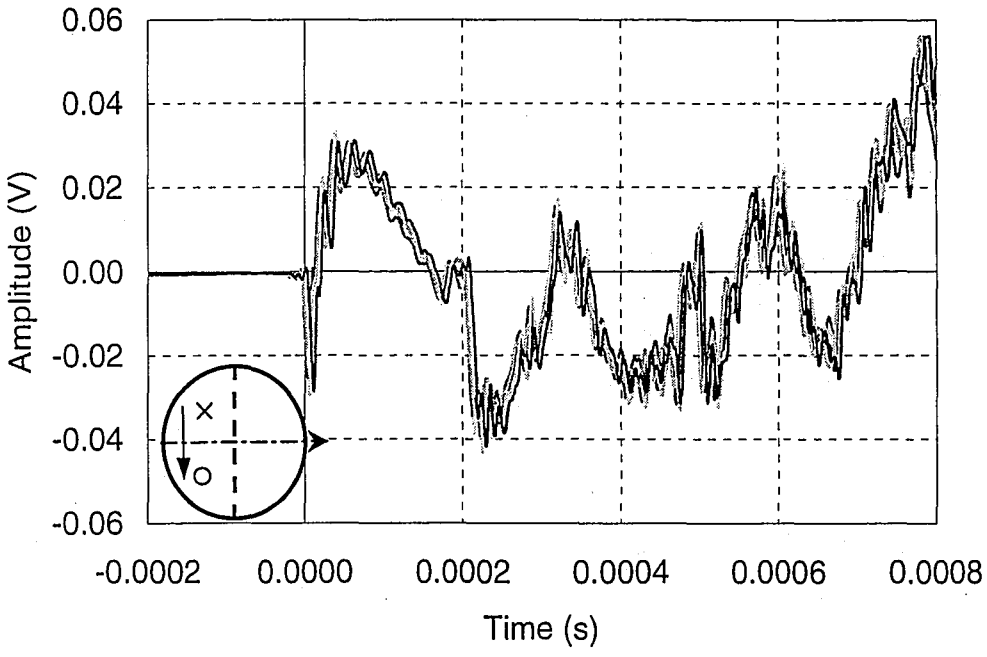

(c)

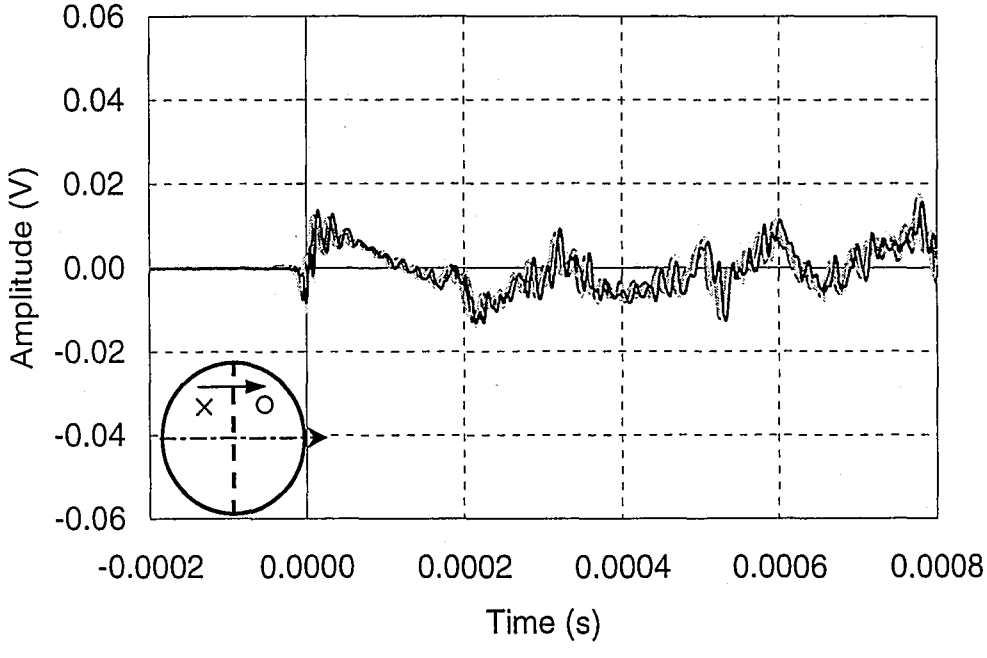

(d)

Figure 5.6 (continued) Waveforms for P4' (flange splice): impact in Q4 (c) perpendicular to the roll direction; and (d) parallel to the roll direction.

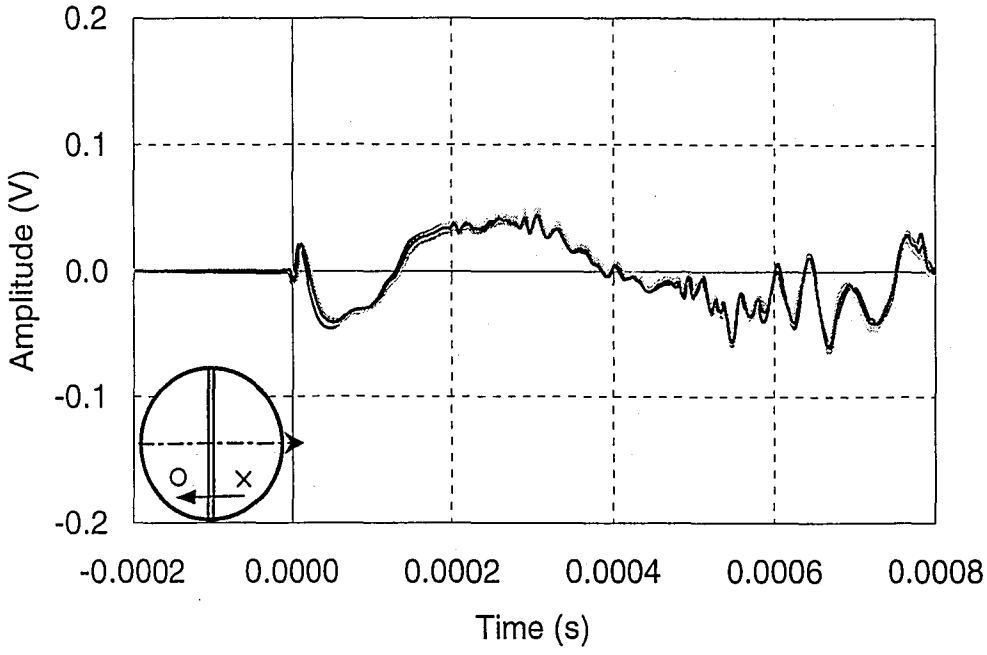

(a)

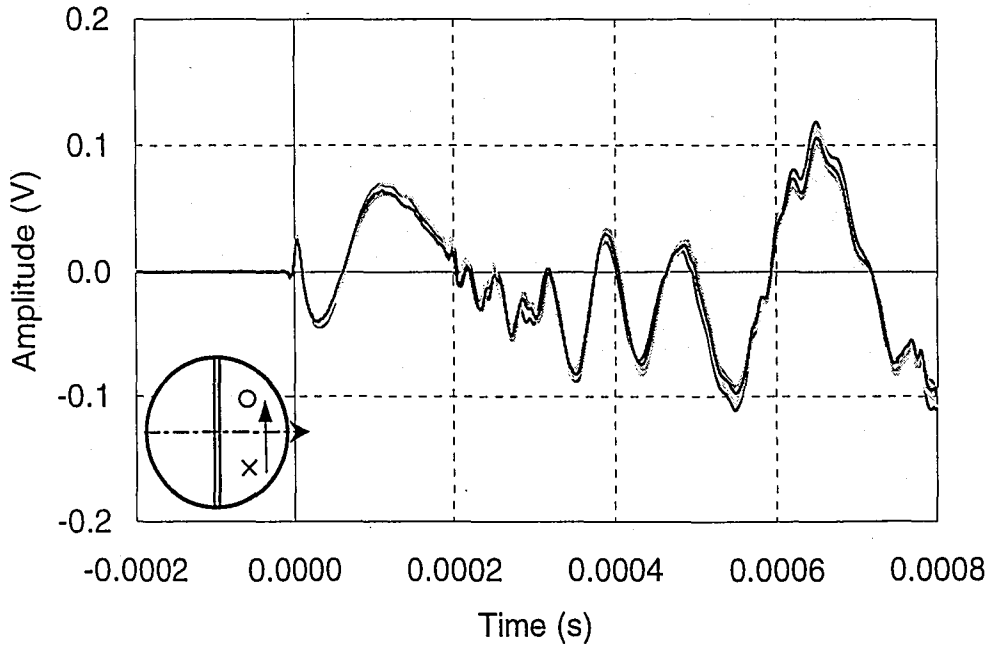

(b)

Figure 5.7 Waveforms for P5 (stiffener-to-web connection): impact in Q2 (a) parallel to the roll direction; and (b) perpendicular to the roll direction;

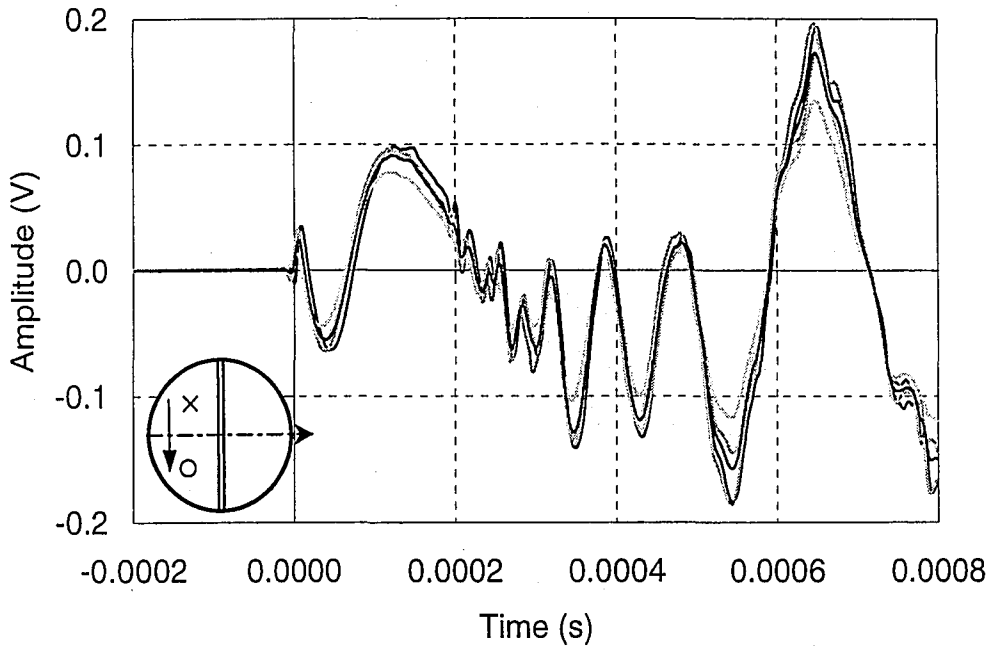

(c)

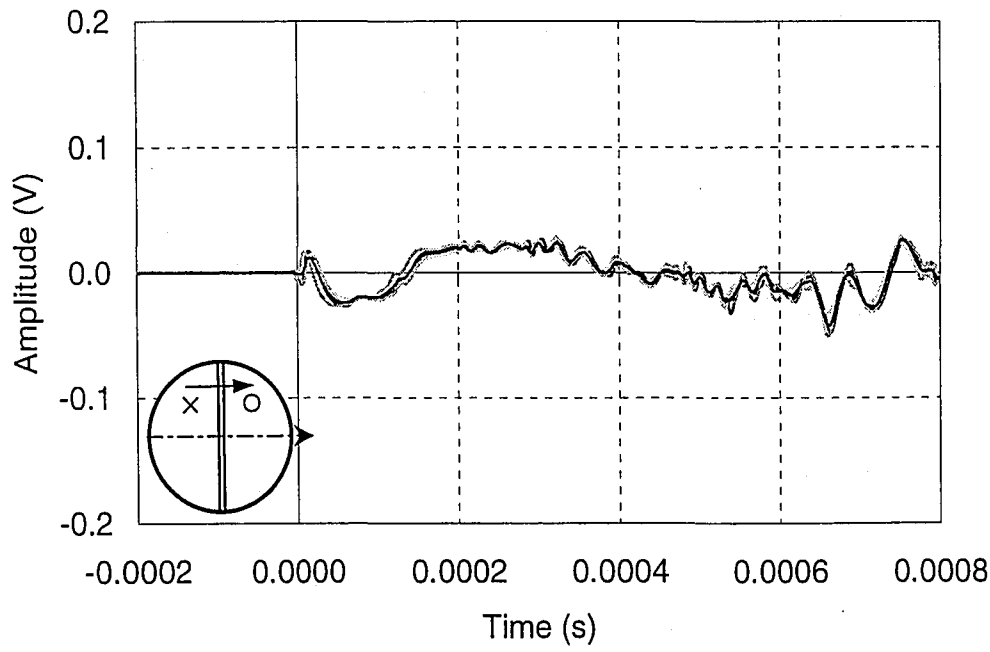

(d)

Figure 5.7 (continued) Waveforms for P5 (stiffener-to-web connection): impact in Q4 (c) perpendicular to the roll direction; and (d) parallel to the roll direction.

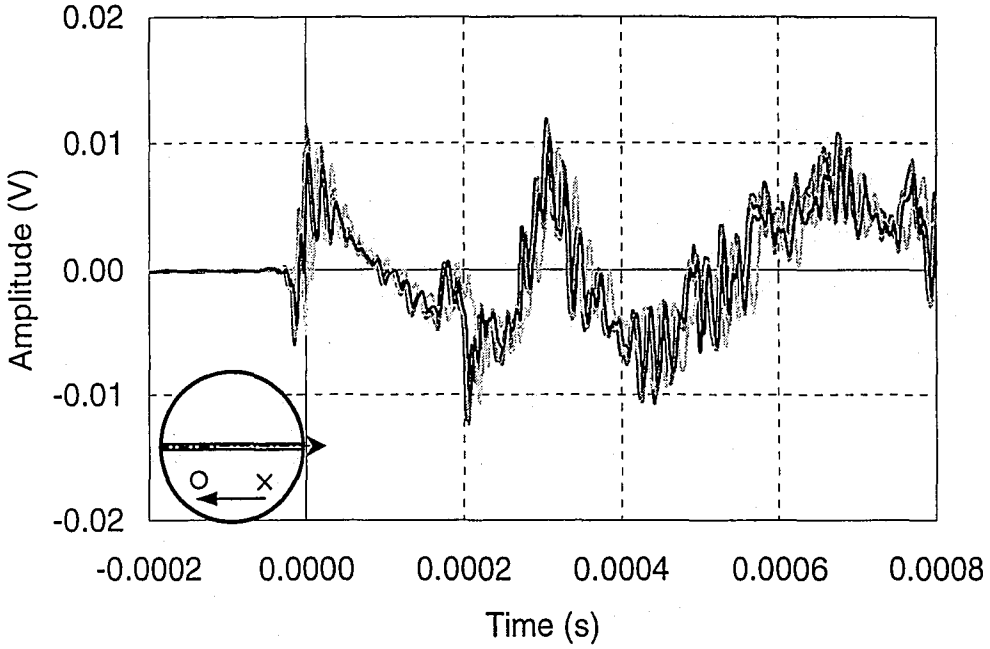

(a)

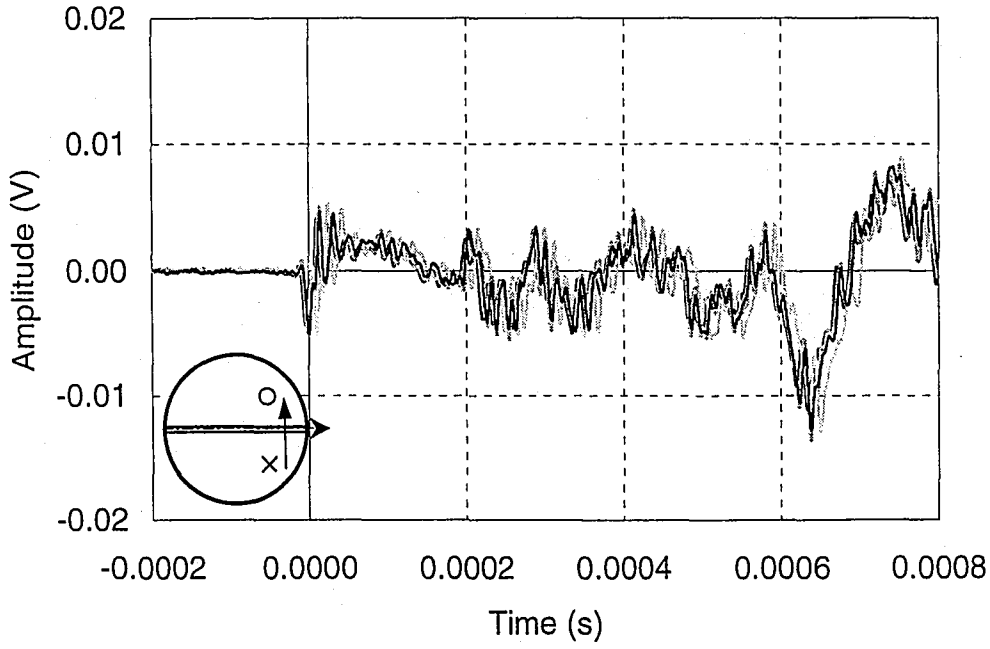

(b)

Figure 5.8 Waveforms for P6 (web-to-flange connection): impact in Q2 (a) parallel to the roll direction; and (b) perpendicular to the roll direction;

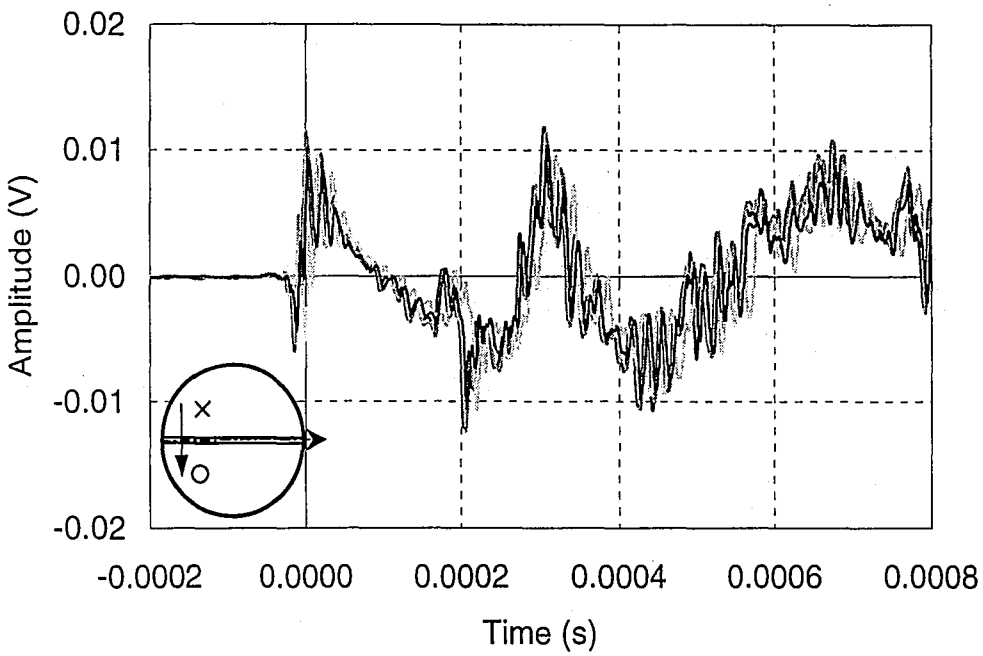

(c)

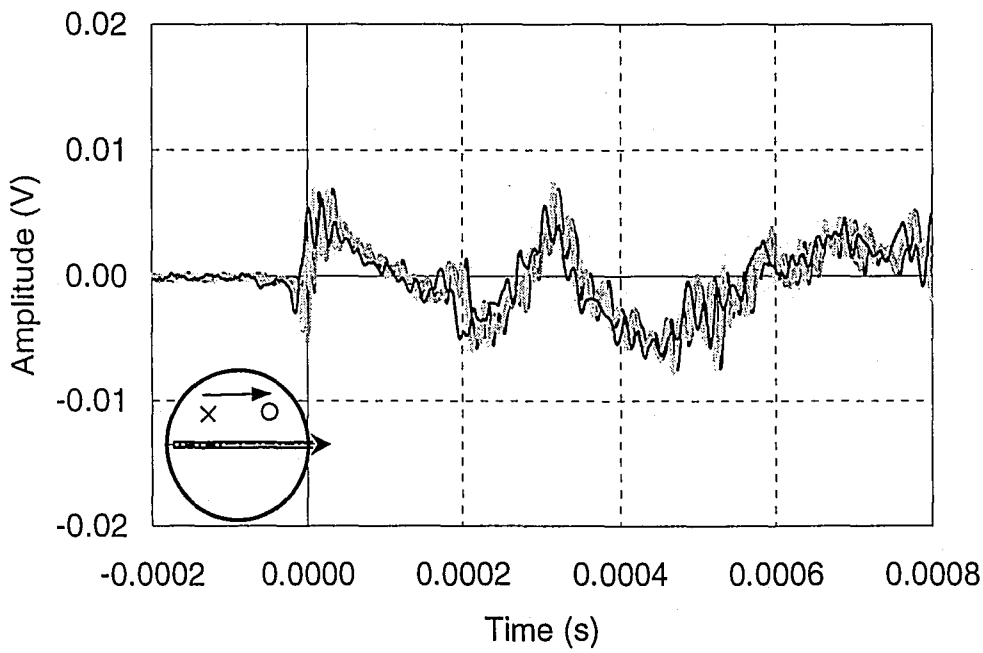

(d)

Figure 5.8 (continued) Waveforms for P6 (web-to-flange connection): impact in Q4 (c) perpendicular to the roll direction; and (d) parallel to the roll direction.

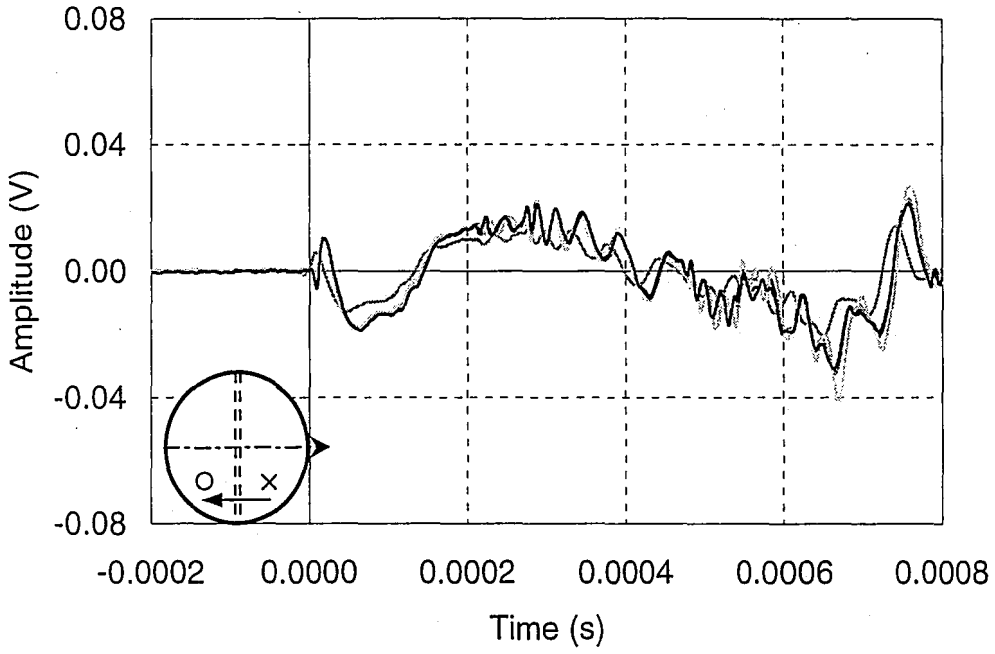

(a)

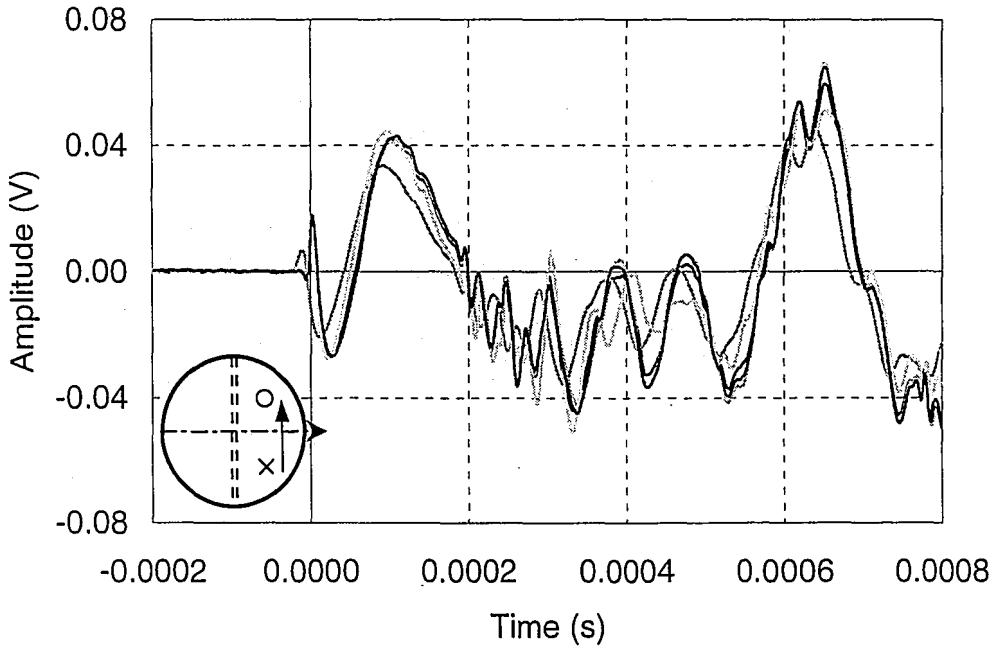

(b)

Figure 5.9 Waveforms for P5' (stiffener-to-web connection on opposite side of plate): impact in Q2 (a) parallel to the roll direction; and (b) perpendicular to the roll direction;

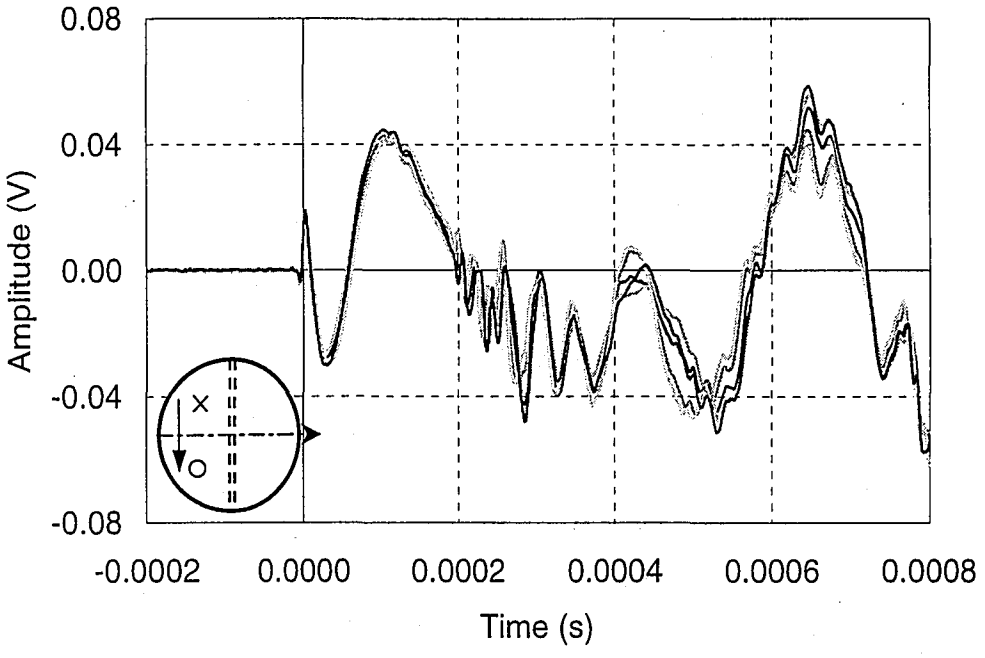

(c)

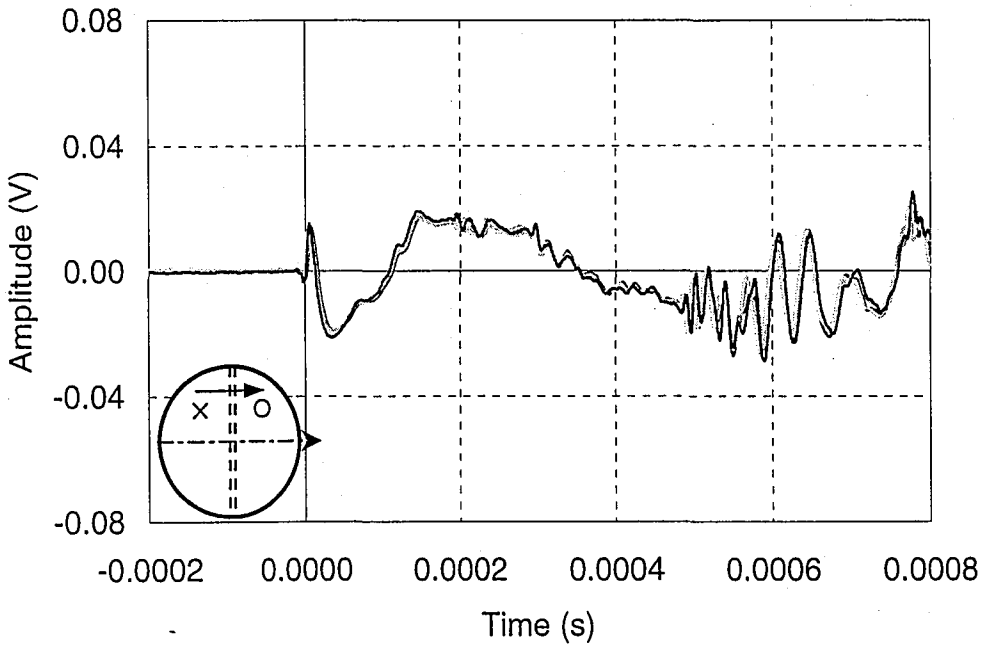

(d)

Figure 5.9 (continued) Waveforms for P5' (stiffener-to-web connection on opposite side of plate): impact in Q4 (c) perpendicular to the roll direction; and (d) parallel to the roll direction.

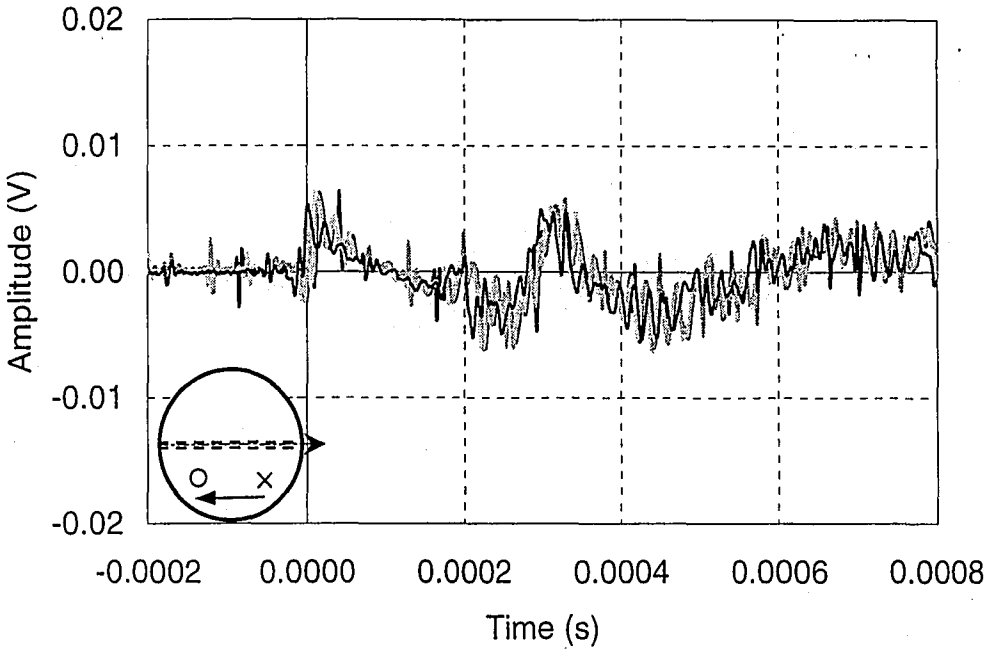

(a)

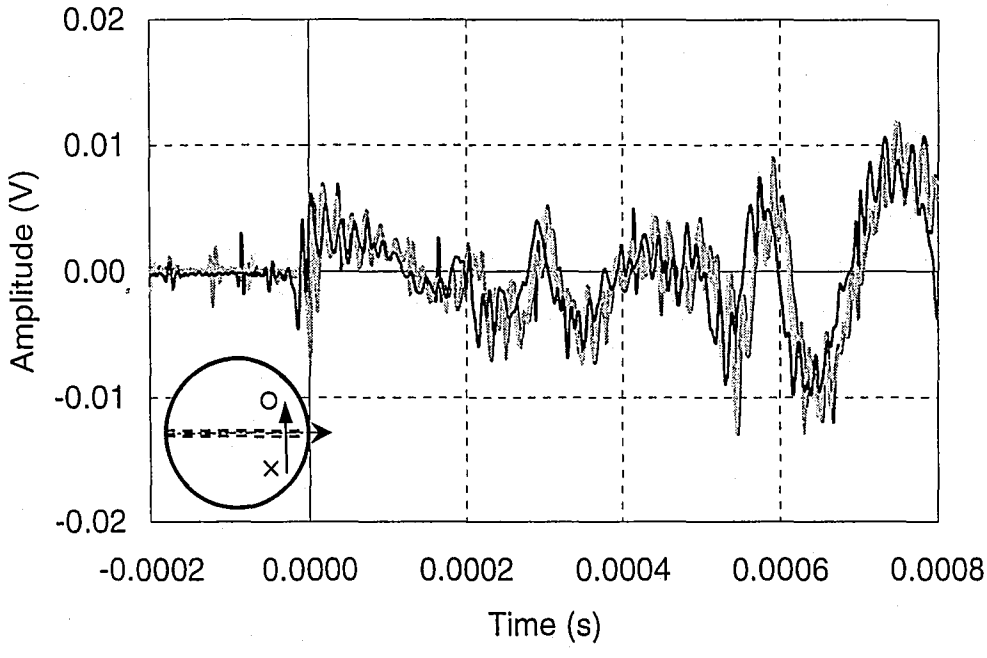

(b)

Figure 5.10 Waveforms for P6' (web-to-flange connection on opposite side of plate): impact in Q2 (a) parallel to the roll direction; and (b) perpendicular to the roll direction;

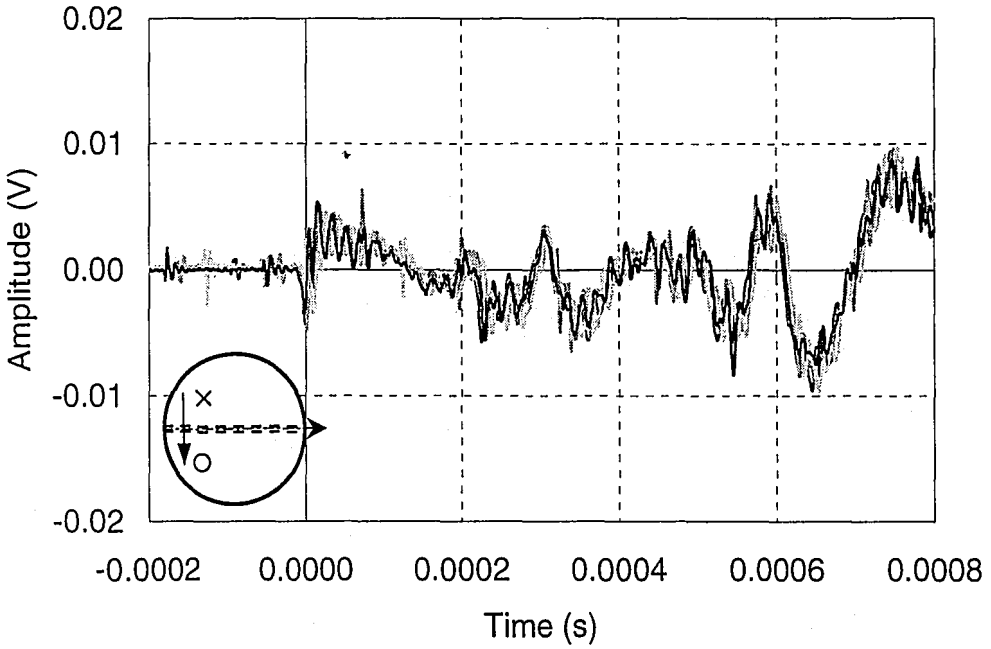

(c)

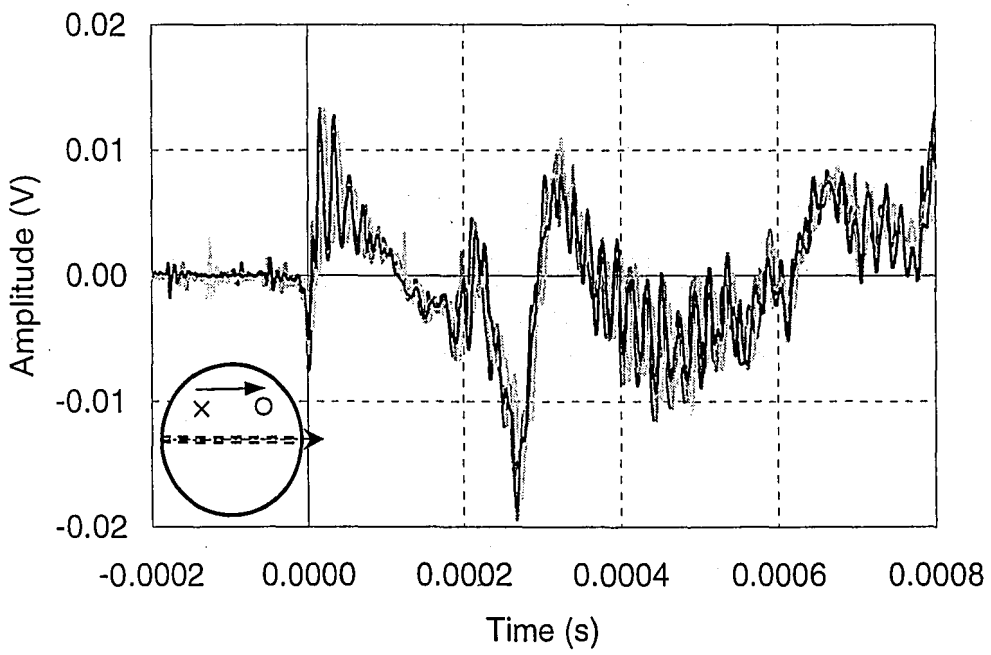

(d)

Figure 5.10 (continued) Waveforms for P6' (web-to-flange connection on opposite side of plate): impact in Q4 (c) perpendicular to the roll direction; and (d) parallel to the roll direction.

CHAPTER 6

DISCUSSION OF RESULTS

6.1 INTRODUCTION

This chapter presents analysis of the results of the experimental program presented in Chapter 5. Section 6.2 discusses the repeatability of the signals generated by impact and Section 6.3 discuses analyzing signals in their average form. The symmetric response of the test setup to impact is discussed in Section 6.4. The remainder of Chapter 6 compares the waveforms of Chapter 5 for each test specimen. Waveforms are compared in their amplitude, shape and the arrival time of peaks in the waveform. Section 6.5 presents a comparison of waveforms for P1 and P2, the plain web and flange plates. It also includes a discussion on the effect of plate thickness on the response generated by impact. The effects of the presence of a web splice or flange splice are presented in Sections 6.6 and 6.7 respectively. To determine if the orientation of the bevel weld used for the plate splices impacts the waveforms, Sections 6.8 and 6.9 investigate the effect of the plate splice with the bevel on the opposite side for the web splice plate (P3′) and the flange splice plate (P4′). The effect of the stiffener-to-web connection in P5 is discussed in Section 6.10 and the effect of the web-to-flange connection is presented in Section 6.11. To determine if the effect of these welded attachments on the waveforms depends on the orientation of the attachment, Sections 6.12 and 6.13 compare the waveforms of P5′ and P6′, the stiff-

ener-to-web and web-to-flange connections with the attachment on the opposite side. A summary of the results is given in Section 6.14.

6.2 REPEATABILITY

As explained in Chapter 4, five impacts were repeated at two separate impact locations for each plate. This section examines the repeatability of the displacement waveforms obtained from repeated impacts at a point.

An average signal can be computed and used in analysis if a repeatable signal can be obtained from the five repeated impacts at each point. Comparison of these waveforms is used to show that the signal produced by the impact of the steel sphere is repeatable. Figure 6.1 shows the five waveforms recorded on P1 with an impact in Q2 and the transducer in Q1. The waveforms produced in this setup travel perpendicular to the roll direction. The collection of five waveforms is labeled "unmodified signals" since they are presented exactly as captured with the oscilloscope. This plot shows little variance in the waveforms and therefore good repeatability for the setup.

Closer examination of the "unmodified signals" shown in Figure 6.1 shows that although the signals are repeatable they are shifted slightly with respect to one another along the time axis. Also shown in Figure 6.1 are the same five waveforms, with the signals shifted to alight the first positive peak of each of the five trials with the peak in trial 1. These shifted waveforms are labeled "aligned signals" in Figure 6.1. This figure shows that aligning the signals does further

improve the agreement between repeated trials early in the waveforms, but no clear improvement is noted later in the waveforms. From the results presented in Figure 6.1 it is concluded that the waveforms that result from successive impacts are highly repeatable.

6.3 WAVEFORM AVERAGING

Figure 6.2 shows the average displacement waveforms of the five "unmodified signals" and five "aligned signals" shown in Figure 6.1. This figure shows that the differences between the average waveforms are small. Comparisons presented in later sections of this chapter will be made using the averages of the unmodified waveforms.

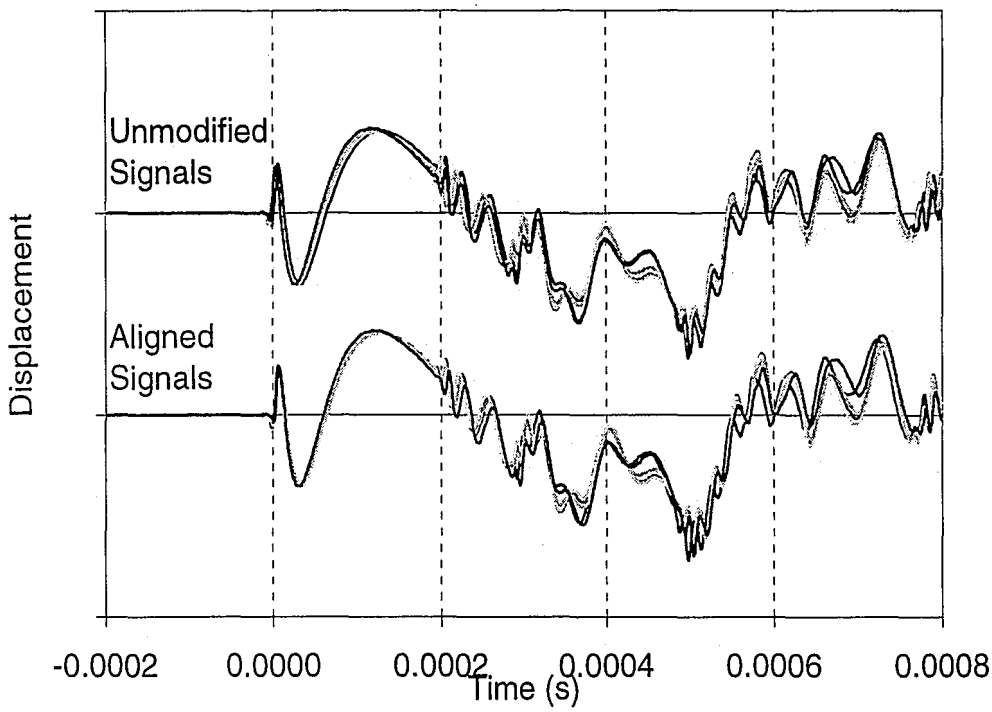

Figure 6.1 Repeatability of surface displacement waveforms.

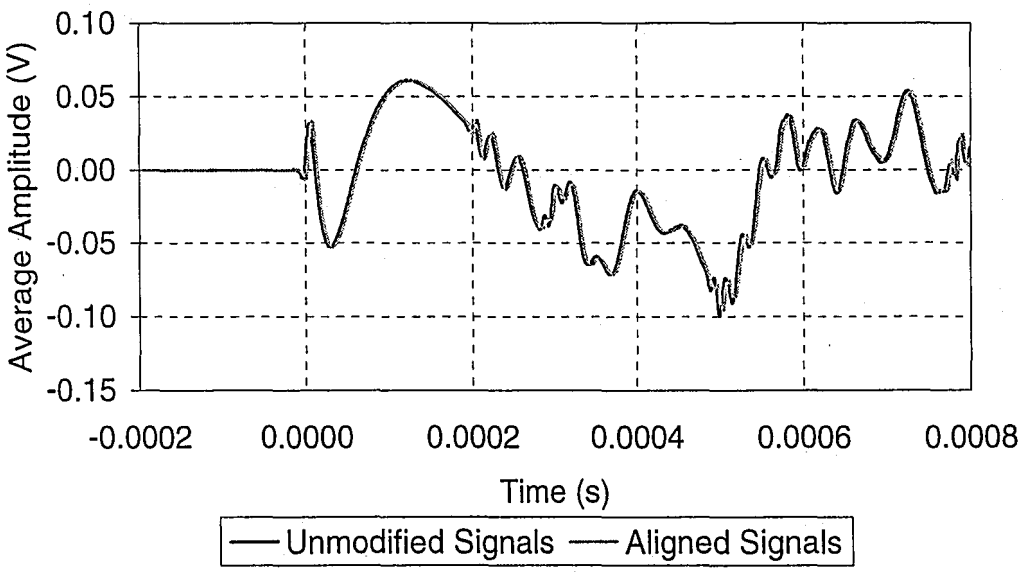

Figure 6.2 Averages of unmodified and aligned displacement waveform signals.

6.4 SYMMETRIC RESPONSE OF THE TEST SETUP

In this research, the assumption is made that a symmetric transducer and impact setup will yield identical behavior regardless if the impact occurs in Q2 or Q4. If this assumption is true, an impact in Q2 should produce a response in Q3 identical to that produced in Q1 from an impact in Q4. Figure 6.3 (a) shows the average waveforms generated in P1 parallel to the roll direction. These waveforms result in Q3 from an impact in Q2 and in Q1 from an impact in Q4. In this and subsequent figures, shaded arrows in the sketch of the specimen correspond to the grayscale colors used to plot the waveforms. Figure 6.4 (a) shows these same waveforms normalized by the first positive peak value to remove the effects of transducer coupling. Nearly identical normalized waveforms are produced by the impacts. The analogous case, the comparison of waveforms perpendicular to the roll direction, is presented in Figure 6.3 (b) and the normalized signals are presented in Figure 6.4 (b). Again, the normalized waveforms are nearly identical. It is concluded that the test setup yields a symmetric response, especially early in the displacement waveform before reflections are obtained from the plate boundaries, and that difference in waveforms may be attributed to variable introduced along the path length (i.e. the presence of welds and welded attachments).

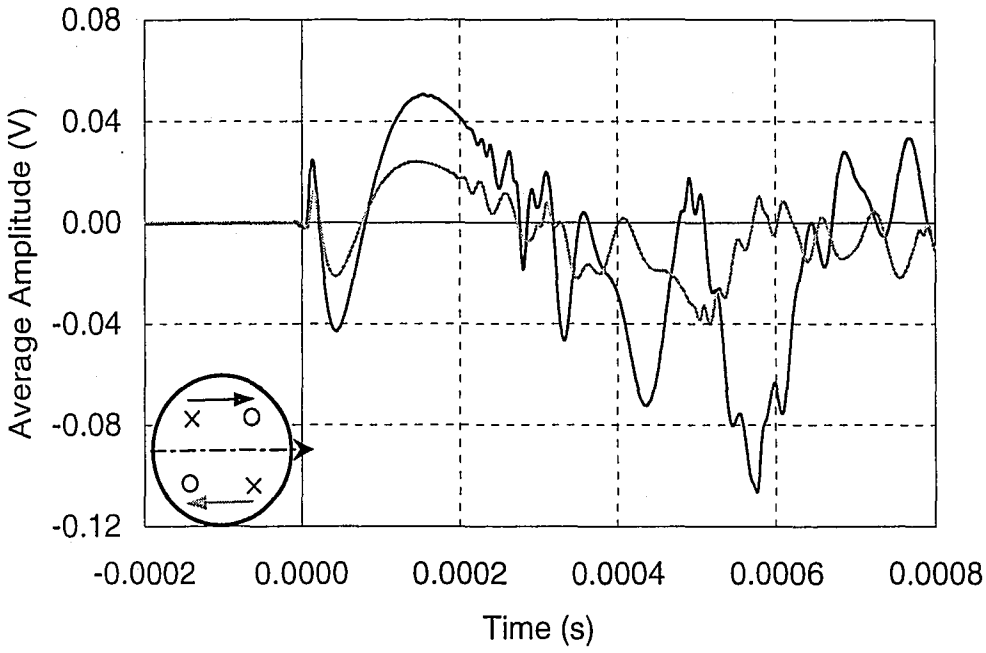

(a)

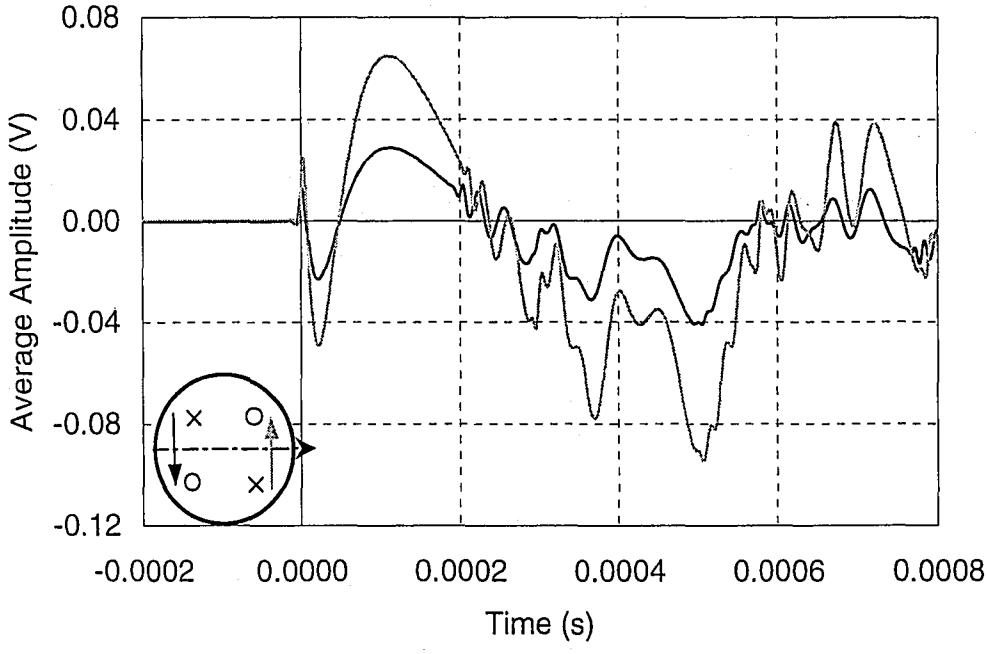

(b)

Figure 6.3 Examination of symmetric response of the test setup: (a) signals parallel to the roll direction; (b) signals perpendicular to the roll direction.

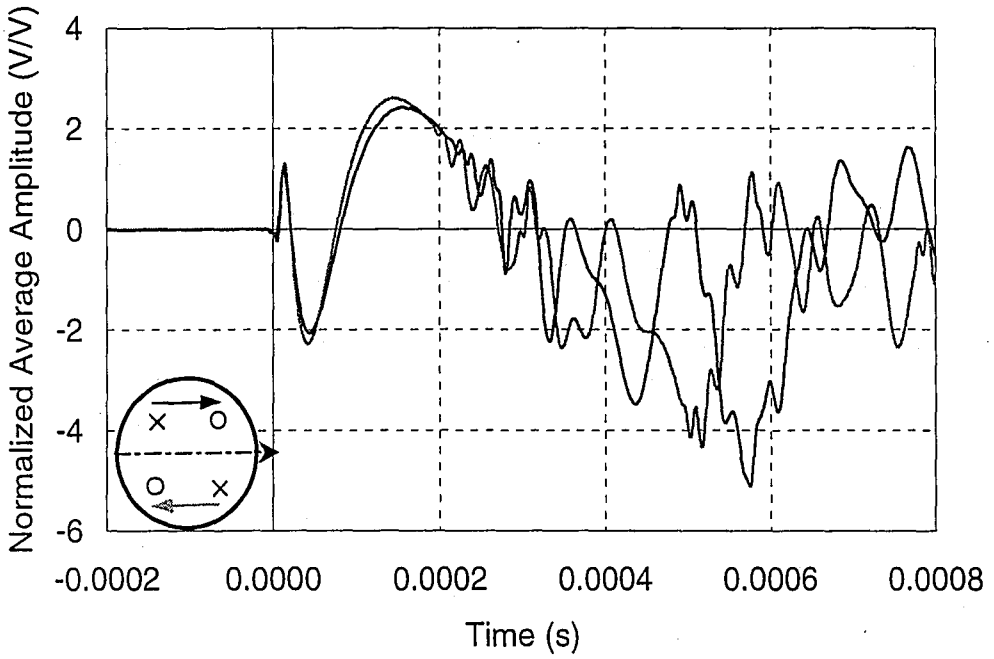

(a)

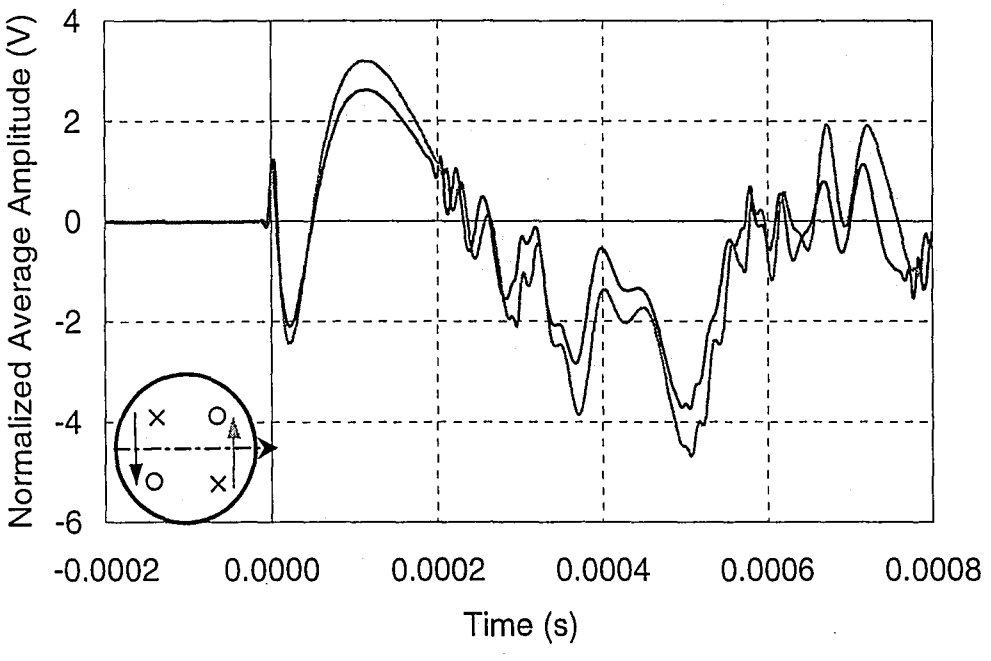

(b)

Figure 6.4 Using normalization to remove transducer coupling effects: (1) signals parallel to the roll direction; (b) signals perependicular to the roll direction.

6.5 EFFECT OF ROLL DIRECTION IN WEB AND FLANGE PLATES

In order to determine the influence of the presence of a weld or welded attachment on an acoustic emission signal, the effect of the direction of roll must first be determined. Because P1 and P2 have no welded detail, it is possible to observe the effects of the roll direction on the waveform without interference of a weld or welded attachment.

Figure 6.5 shows the effects of roll direction on the acoustic emission signal in P1, the 13 mm thick web plate. Figure 6.5 (a) shows results for a test setup with transducers in Q1 and Q3 for an impact in Q2. The impact produces stress waves that propagate parallel to the roll direction to the transducer in Q3, and perpendicular to the roll direction to the transducer in Q1. Figure 6.5 (b) shows results for a test setup with transducers in Q1 and Q3 and an impact in Q4. The impact in Q4 produces stress waves that propagate parallel to the roll direction to the transducer in Q1, and perpendicular to the roll direction to the transducer in Q3. Shown in Figure 6.5 are average waveforms (average of five impacts at each impact location).

Each waveform begins with a small positive peak followed by a large negative peak, attributed to the arrival of the R-wave. The waveform then has a large positive peak of long duration for both signals. At approximately 0.0002 seconds, small amplitude high frequency oscillations appear in the signal. Until 0.0003 seconds, the two waveforms shown in Figure 6.5 (a) are similar in shape. After this time, the shape of the signals begins to differ. Figure 6.5 (a) shows the

waveform propagating parallel to the roll direction, to the transducer in Q3, has a higher amplitude than that traveling perpendicular to the roll direction to the transducer in Q1. The signal perpendicular to the roll direction arrives at the transducer location before the signal traveling parallel to the roll direction.

The waveforms of Figure 6.5 (b) are geometrically similar throughout the duration of the recorded signal. The waveform propagating perpendicular to the roll direction to the transducer in Q3 has higher amplitude than the waveform traveling parallel to the roll direction. The waveform traveling perpendicular to the roll direction arrives at the transducer location prior to the waveform traveling parallel to the roll direction.

For both impact locations, a larger amplitude response is obtained with the transducer positioned in Q3. This shows that the coupling between the transducer and the plate is not equal for both transducers. As discussed in Section 3.5.4, differences in the coupling of the transducer can be removed through normalization of the waveforms. Figure 6.6 shows the normalized waveforms for P1. The waveforms are normalized by the amplitude of the first positive peak, as described in Section 6.4. Figure 6.6 (a) shows the normalized average waveforms resulting from impact in Q2, and Figure 6.6 (b) shows normalized average waveforms resulting from impact in Q4. The normalized waveforms have consistent amplitudes, particularly in the first 0.0003 seconds of the record. Thus, the amplitude variation appears to be cause by transducer coupling rather than by the influence of roll direction.

For both impact positions, displacements that are similar in both waveforms appear first in the transducer placed perpendicular to the roll direction. Figure 6.7 shows a small difference in arrival time between the signals parallel and perpendicular to the roll direction. Common peaks within the signal are denoted a, a′, b, b′, c and c′. Points accented with a prime correspond to waveforms perpendicular to the roll direction. The lag of the signal at the three peak locations denoted on the waveforms of Figure 6.7 is given in Table 6.1. The time between peaks, Δt, is listed for each signal (Δt_{ab}, Δt_{bc}, Δt_{ac}, $\Delta t_{a'b'}$, $\Delta t_{b'c'}$, $\Delta t_{a'c'}$) for both an impact in Q2 and in Q4. The time lag between the signals is also given in Table 6.1 ($\Delta t_{aa'}$, $\Delta t_{bb'}$, $\Delta t_{cc'}$).

The Δt values are consistent for impact in Q2 and Q4. The time between peaks of the waveform perpendicular to the roll direction can be compared with the time between peaks for the waveform parallel to the roll direction. The time between peaks is consistently larger for the signal parallel to the roll direction than for waveforms perpendicular to the roll direction. The time between corresponding peaks in the waveforms parallel and perpendicular to the roll direction are also presented in Table 6.1. $\Delta t_{aa'}$ is the time difference between the first positive peak of the waveform parallel to the roll direction and the waveform perpendicular to the roll direction. Table 6.1 shows that the time between corresponding peaks of the waveforms increases for each peak.

To determine if the lag is a function of irregularity in the shape of the test setup, the change in distance, Δa, between the transducer and the source loca-

tion necessary for the lag is calculated for both P- and R- waves. Focusing on the lag, $\Delta t_{aa'}$, of the first positive peak of the signal, a value of Δa of 70 mm is necessary to produce the given lag if the arrival is assumed to be that of a P-wave. Δa equals 48 mm if the first positive peak is assumed to be caused by the arrival of an R-wave. A misplacement of the transducer and/or impact is unlikely to cause a change in travel length to the extent necessary to cause the lag seen in the signals.

Examining the average signals resulting from an impact in Q2 and Q4, it can be seen that the signal traveling parallel to the roll direction appears to lag behind that traveling perpendicular to the roll direction. This is attributed to steel being a dispersive medium. The similar shape and amplitude of the signals parallel and perpendicular to the roll direction seen in Figures 6.6 (a) and (b) indicate that the roll direction of the plate has no effect on the shape or amplitude of the signal. Only the time lag distinguishes the signals during the initial 0.0003 seconds of the response. Any discrepancy in the signal shape after the first 0.000261 seconds of the response is attributed to the reflection of stress waves from the boundaries of the plate. The discrepancies in the waveforms can also be due to the plate vibrating in mode shapes which have three nodal diameters separated by 60°. This causes the displacements due to these nodes to be opposite in sign at the transducer locations.

Figure 6.8 shows the average waveforms generated from impact in P2, the 51 mm thick flange plate. The waveforms of Figure 6.8 (a) result from an im-

pact in Q2. The waveforms of Figure 6.8 (b) result from impact in Q4. Figure 6.8 (a) shows the waveforms received in Q1 that travel perpendicular to the roll direction and the waveforms received in Q3 travel parallel to the roll direction. Figure 6.8 (b) shows the average waveform parallel to the roll direction, received in Q1 and the average waveform propagating perpendicular to the roll direction to Q3.

The waveforms presented in Figure 6.8 begin with a negative peak followed by a positive peak. The waveforms consist of a low frequency oscillation and a high frequency low amplitude oscillation. The high frequency oscillations begin almost immediately after the arrival of the signal. Figure 6.8 (a) shows the wave traveling perpendicular to the roll direction to TB in Q1 having higher amplitude than the waveform recorded by TA in Q3. Figure 6.8 (b) shows a higher amplitude for the wave traveling parallel to the roll direction to TB located in Q1 than for the wave traveling perpendicular to the roll direction to TA located in Q3.

The waveforms seen in Figure 6.8 are, in general, geometrically similar throughout the duration of the response. For both impact positions, a larger amplitude response is obtained with TA positioned in Q1. The change in amplitude can be removed through normalization of the signal. Figure 6.9 shows the waveforms of Figure 6.9 normalized by the amplitude of the first positive peak. The normalization removes the amplitude variation between the signals.

The waveforms created in P2 are in general geometrically similar. A difference in amplitude is attributed to the transducer coupling and not to the influence of the roll direction.

The signals generated in P1 and P2 differ in amplitude and shape. Figure 6.5 and Figure 6.8 show that the amplitude of the waveforms recorded from P1 are larger than the amplitude of the waveforms recorded from P2. The reduced amplitude may be attributed to attenuation of the signal by dispersion of energy in the large volume of material of P2 (Section 2.3.2). The waves in P1 contain a relatively large amplitude and length positive peak after the arrival of the R-wave. After this peak, a high frequency low amplitude oscillation is present. The waves generated in P2 do not include this long sweeping portion of the signal and the high frequency oscillations begin immediately.

The change of wave shape for the signals of P2 can be attributed to the strength of the reflected P- and S-waves in comparison with those of P1. Section 2.4 gives general information on stress wave propagation and amplitude. In P1 (t=13 mm), the 2P- and 2S-waves that are reflected from the opposite surface of the plate travel at an angle of 80° with respect to the impact. The amplitude of both P- and S-waves at this angle is relatively low. In P2 (t=51 mm), the reflected 2P- and 2S-waves that are reflected from the opposite surface of the plate travel at an angle of 54° with the impact. At this angle, the amplitude of the S-wave is near maximum, and the amplitude of the P-wave is approximately half of

its maximum amplitude. In P2 the amplitude of the P- and S-waves is stronger, and therefore more prevalent in the waveform.

Time Lag	Impact	
	Q2	Q4
Δt_{ab}	35 μs	22 μs
Δt_{bc}	109 μs	116 μs
Δt_{ac}	144 μs	138 μs
$\Delta t_{a'b'}$	25 μs	22 μs
$\Delta t_{b'c'}$	91 μs	93 μs
$\Delta t_{a'c'}$	116 μs	115 μs
$\Delta t_{aa'}$	12 μs	14 μs
$\Delta t_{bb'}$	22 μs	13 μs
$\Delta_{cc'}$	40 μs	37 μs

Table 6.1 Lag time of initial peaks of waveforms from 13 mm web plate (P1).

Time Lag	Impact	
	Q2	Q4
Δt_{ab}	33 μs	42 μs
Δt_{bc}	111 μs	119 μs
Δt_{ac}	144 μs	161 μs
$\Delta t_{a'b'}$	25 μs	27 μs
$\Delta t_{b'c'}$	88 μs	107 μs
$\Delta t_{a'c'}$	113 μs	134 μs
$\Delta t_{aa'}$	5 μs	19 μs
$\Delta t_{bb'}$	13 μs	34 μs
$\Delta_{cc'}$	36 μs	46 μs

Table 6.2 Lag time of initial peaks of waveforms from 13 mm spliced web plate (P3).

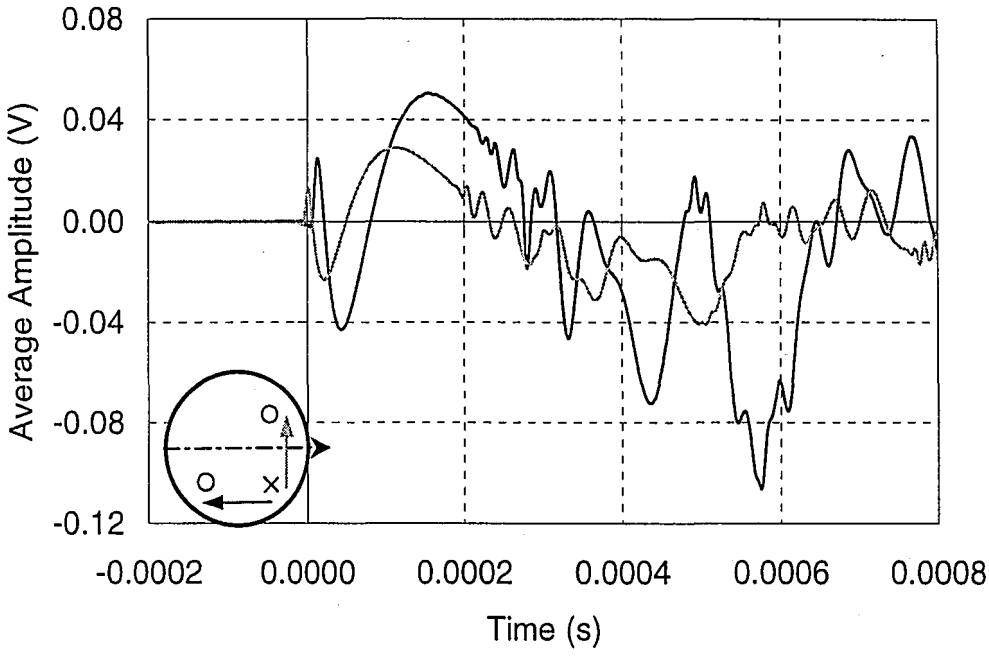

(a)

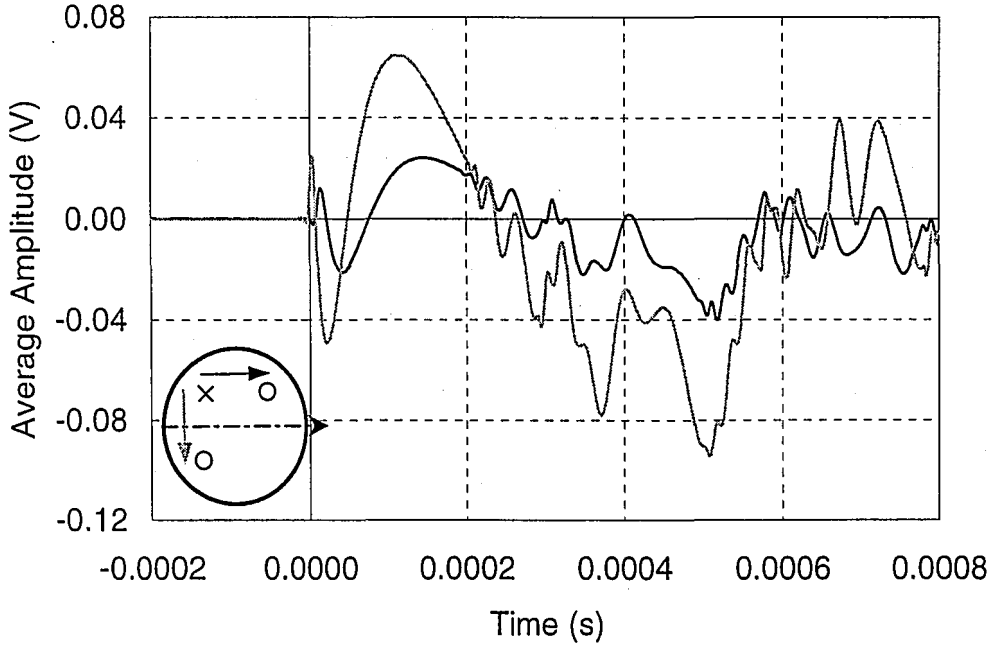

(b)

Figure 6.5 Effect of the roll direction in the 13 mm plate (P1): (a) resulting from impact in Q2; (b) resulting from impact in Q4.

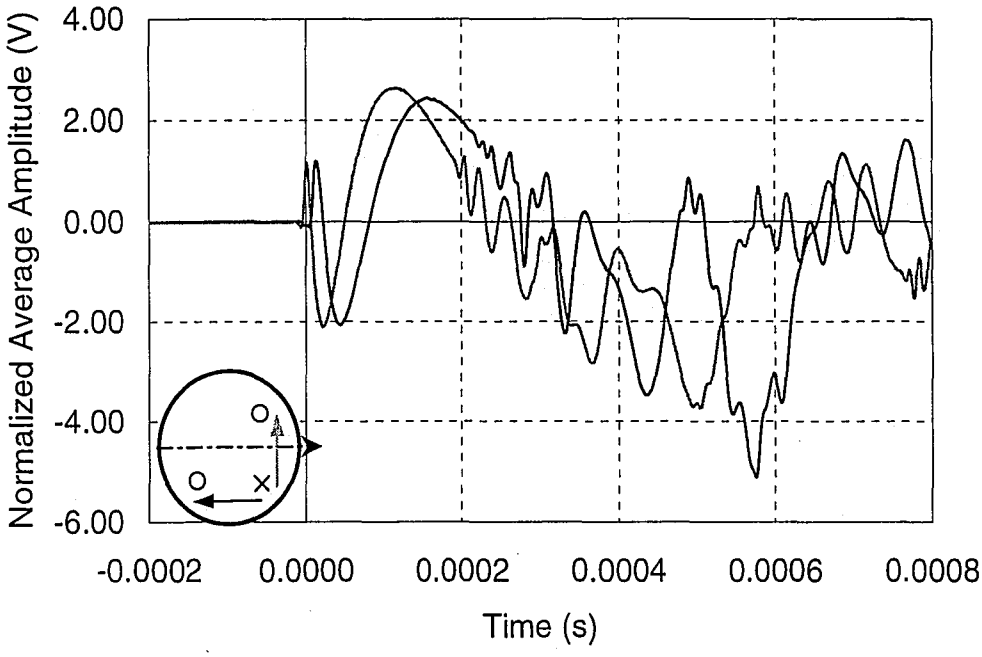

(a)

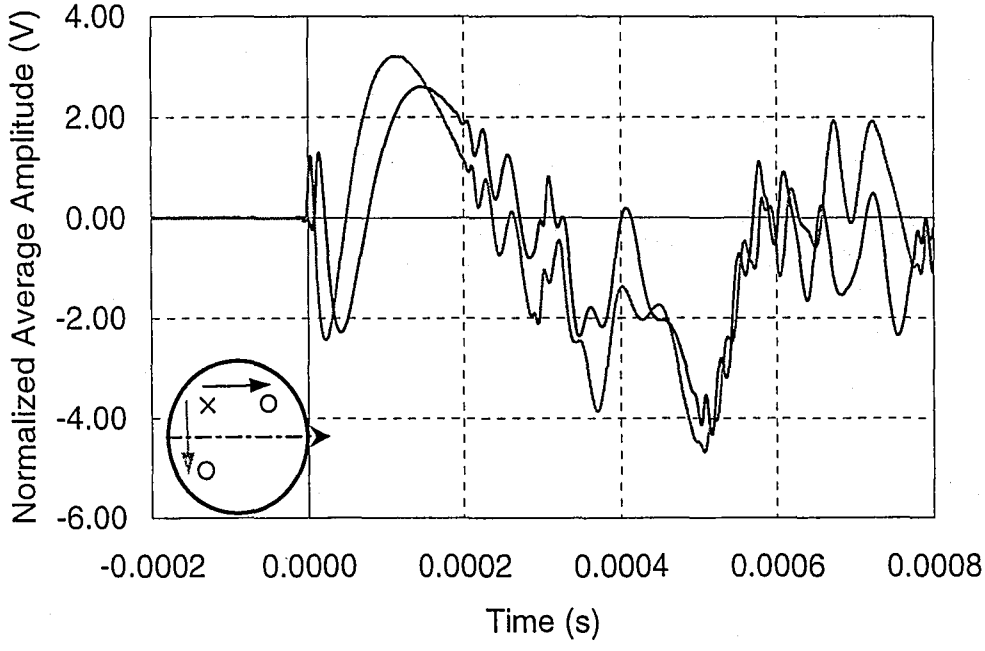

(b)

Figure 6.6 Effect of the roll direction in the 13 mm plate (P1), normalized to remove coupling effects: (a) resulting from impact in Q2; (b) resulting from impact in Q4.

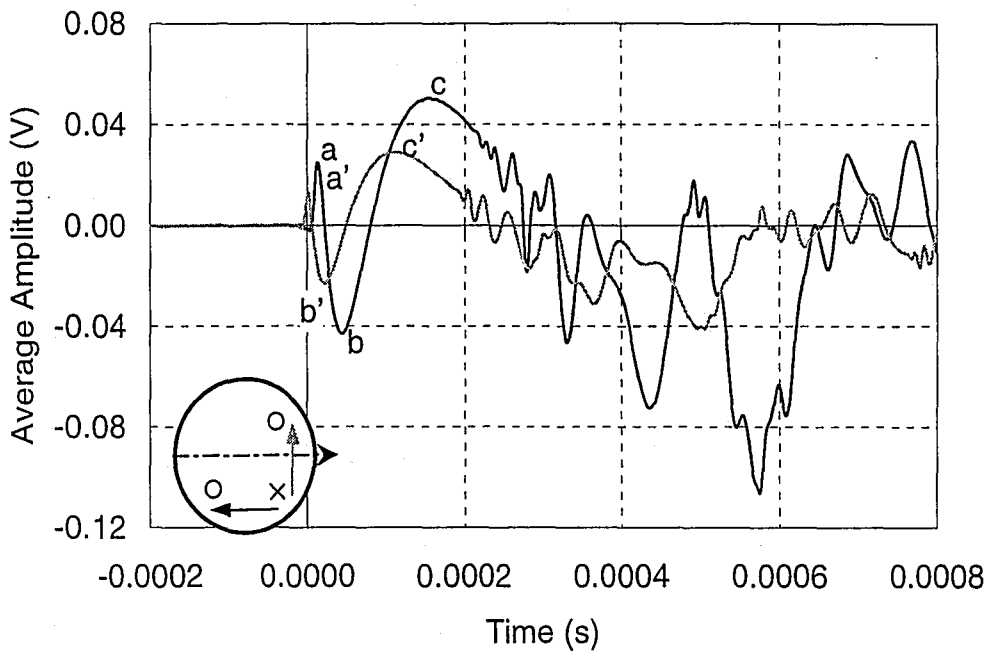

(a)

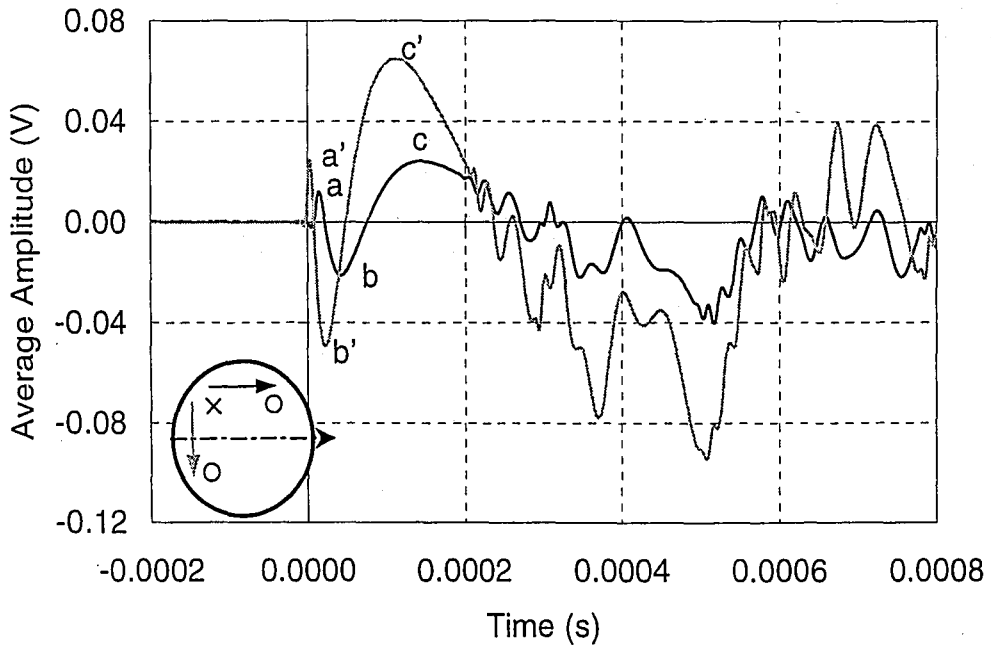

(b)

Figure 6.7 The lag in arrival time due to the roll direction of the 13 mm plate (P1).

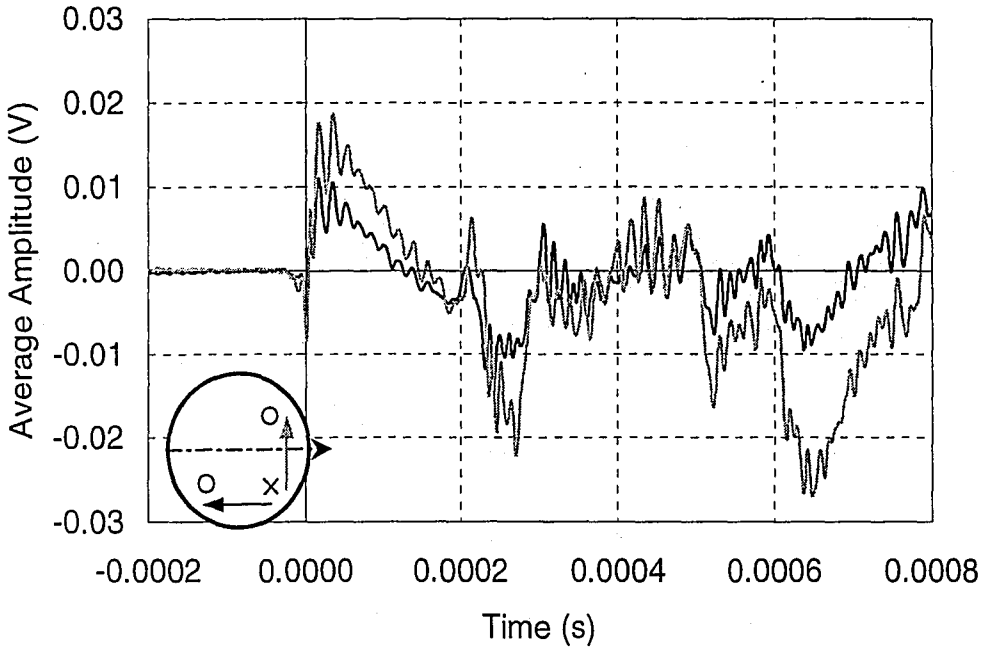

(a)

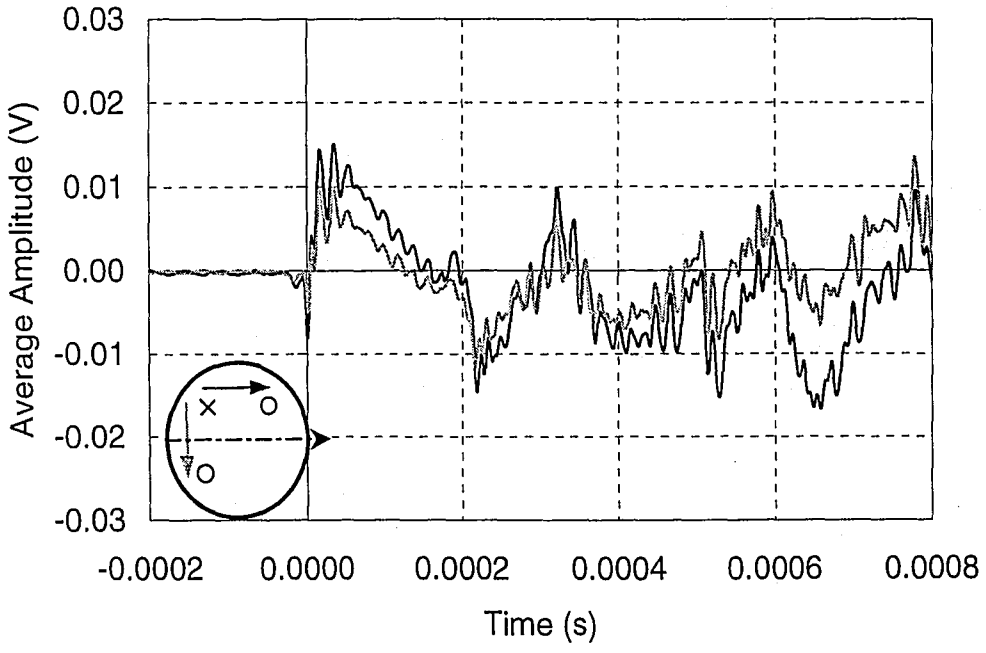

(b)

Figure 6.8 Effect of the roll direction in the 51 mm plate (P2): (a) resulting from impact in Q2; (b) resulting from impact in Q4.

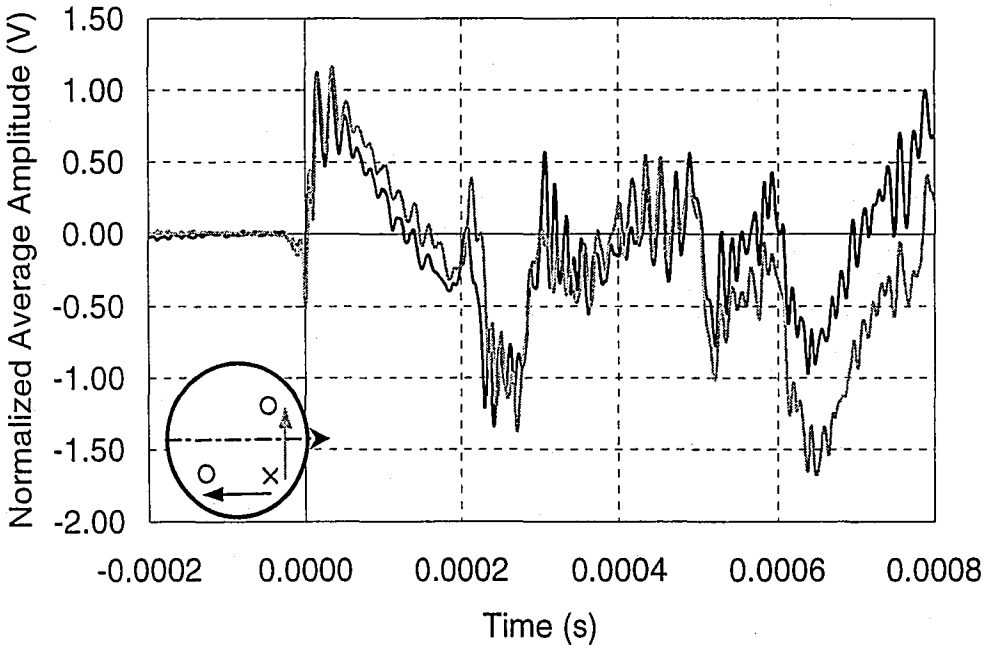

(a)

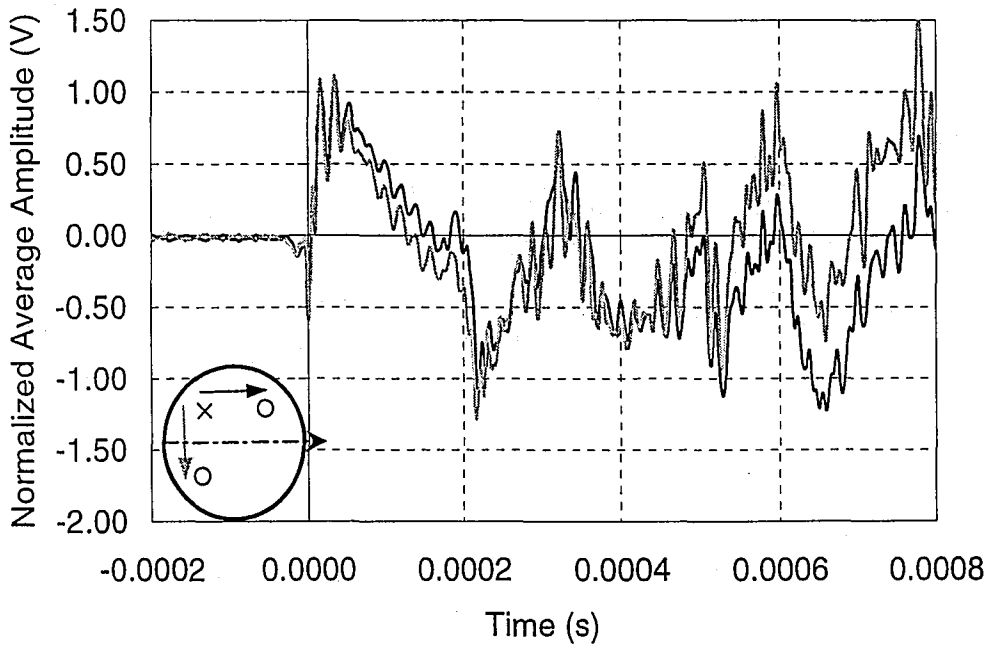

(b)

Figure 6.9 Effect of the roll direction in the 51 mm plate (P2), normalized to remove coupling effects: (a) resulting from impact in Q2; (b) resulting from impact in Q4.

6.6 EFFECT OF WEB SPLICE

The first type of welded detail investigated in this study is a plate splice. A splice can occur between the acoustic source and the receiver in the form of a web splice (P3) or flange splice (P4). The splices are orientated perpendicular to the direction of roll. Figure 6.10 shows the average waveforms for the 13 mm spliced plate, P3. Figure 6.10 (a) shows waveforms generated from an impact in Q2 and Figure 6.10 (b) shows waveforms generated from an impact in Q4. An impact in Q2 will cause a wave to travel parallel to the roll direction obstructed by the weld, to a transducer in Q3. A wave will also travel perpendicular to the roll direction unobstructed by the splice, to a transducer in Q1.

Each waveform begins with a small positive peak followed by a large negative peak, caused by the arrival of the R-wave. The waveform then has a large positive peak of long duration for both signals. At approximately 0.0002 seconds, small amplitude high frequency oscillations appear in the signal. The waveforms are geometrically similar throughout the duration of the record, especially during the initial 0.0003 seconds. Figure 6.10 (a) shows the waveform propagating parallel to the roll direction, to the transducer in Q3, has a higher amplitude than that traveling perpendicular to the roll direction to the transducer in Q1. The waveform propagating perpendicular to the roll direction to the transducer in Q3 has higher amplitude than the waveform traveling parallel to the roll direction. In both Figure 6.10 (a) and Figure 6.10 (b), the signal perpendicular to the roll direction arrives at the transducer location before the signal traveling par-

allel to the roll direction. The high frequency oscillations of the waveform begin at 0.0002 seconds regardless of the lag in the signal.

Figure 6.11 shows the waveforms of Figure 6.10, with the arrival of key peaks of the waveforms parallel to the roll direction denoted a, b, and c, and the corresponding peaks of the waveform propagating perpendicular to the roll direction denoted a′, b′, and c′. Table 6.2 shows the time differences between peaks in the signals. The peaks for waveforms traveling parallel to the roll direction arrive consistently later than the peak for the waveforms traveling parallel the roll direction. The lag times recorded for impact in Q2 and Q4 are equivalent. As the waveform progresses, the lag time between corresponding peaks in the signals increases.

The variation in amplitude between signals is removed through normalization of the waveforms by the amplitude of the first positive peak. Figure 6.12 shows the normalized waveforms corresponding to the waveforms of Figure 6.10. Normalization removes the difference in amplitude between the signals.

The waveforms of the web splice plate,P3, can be compared with the waveforms of the plain web plate, P1. Figure 6.13 shows normalized waveforms of P1 and P3. The black waveforms originate in P1, while the gray waveforms originate in P3. The waveforms are normalized to remove any variation in the transducer coupling. Figure 6.13 (a) shows average waveforms of P1 parallel to the roll direction and the average waveform of P3 parallel to the roll direction, obstructed by the weld. The waveforms presented in Figure 6.13 (a) are

generated by an impact in Q2 and received by a transducer in Q3. Figure 6.13 (b) shows the average waveform of P1 perpendicular to the roll direction and the average waveform of P3 perpendicular to the roll direction and unobstructed by the weld. The waveforms of Figure 6.13 (b) are generated by an impact in Q2 and received by a transducer in Q1. The only difference in path length of the stress waves as they propagate is the presence of the single V groove weld.

Figure 6.13 (a) shows that the waveforms parallel to the roll direction in P1 and P3 are similar in shape and amplitude, especially during the first 0.0003 seconds of the signal. The obstruction of the waveform by the weld in P3 has no effect on the signal. Figure 6.13 (b) shows that the waveforms perpendicular to the roll direction in P1 and P3 are also similar in shape and amplitude. Comparing Tables 6.1 and 6.2, there is not a significant increase or decrease in lag times when the single V groove weld is introduced in P3. The lag can, therefore, be attributed to the roll direction as concluded in Section 6.5. Thus any reflection of the stress wave off the weld does not effect the waveform as it travels parallel to the weld.

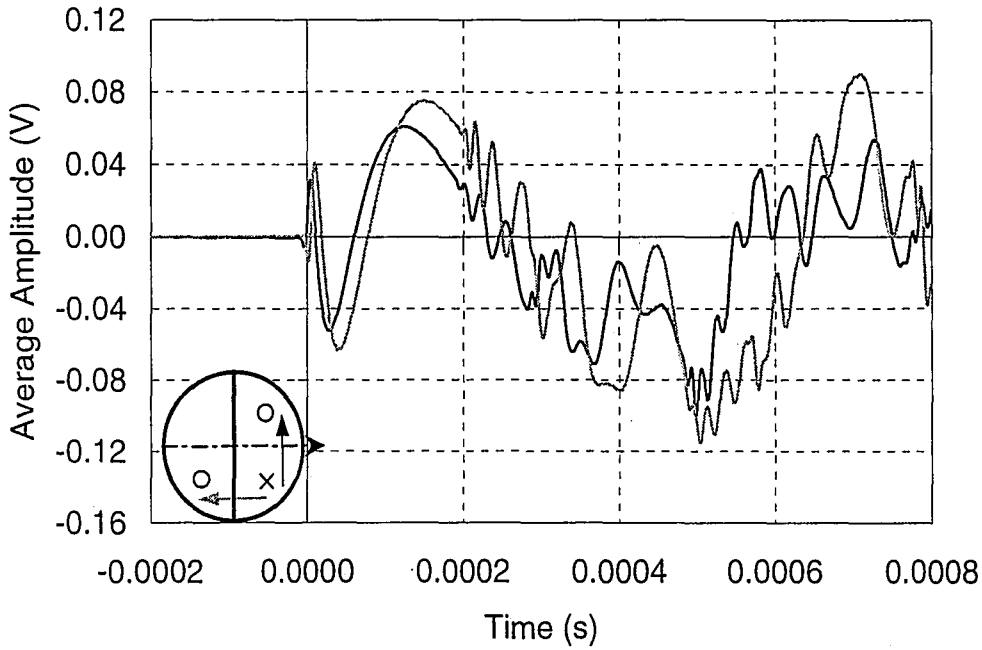

(a)

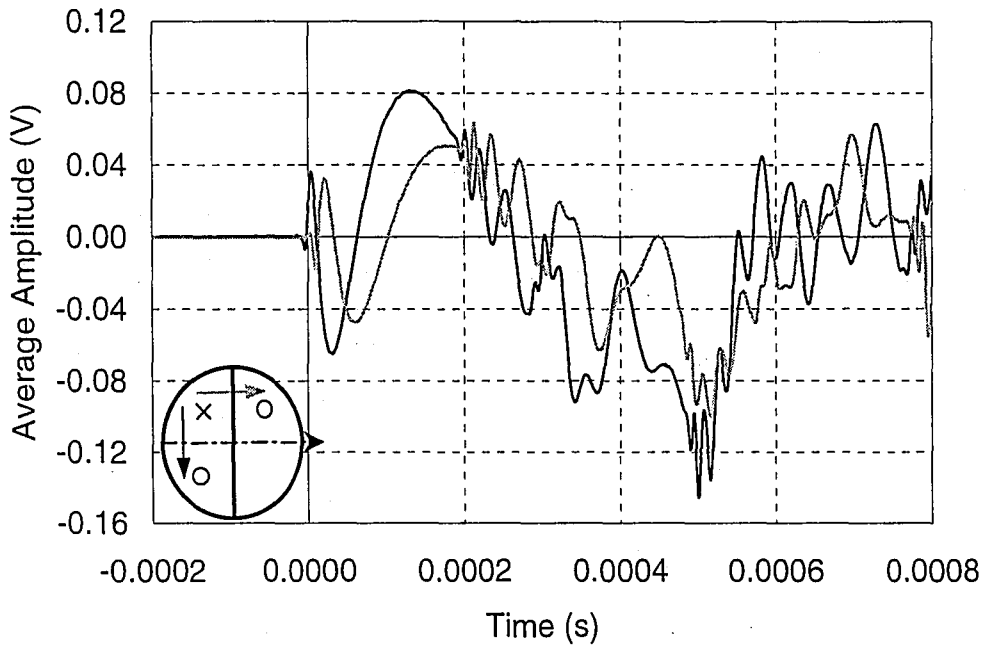

(b)

Figure 6.10 Effect of the single V groove weld in the 13 mm splice plate (P3): (a) resulting from impact in Q2; (b) resulting from impact in Q4.

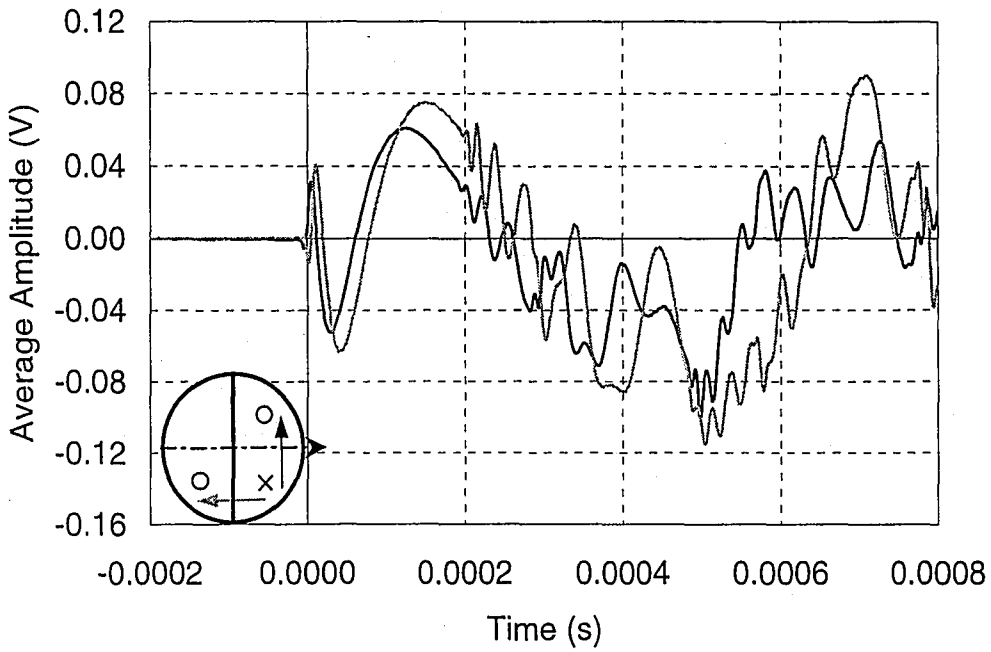

(a)

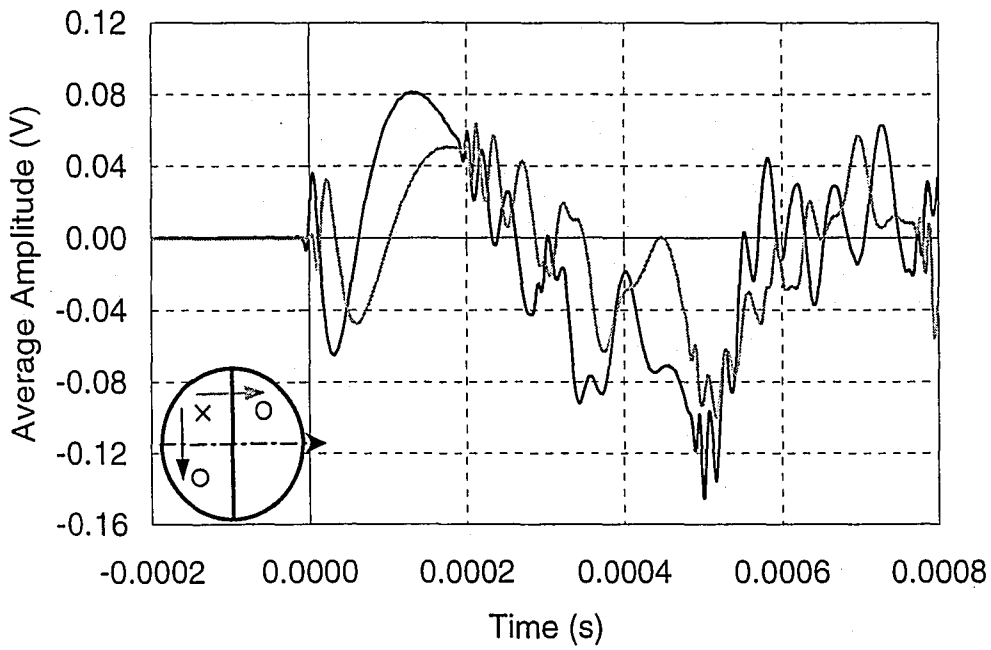

(b)

Figure 6.10 Effect of the single V groove weld in the 13 mm splice plate (P3): (a) resulting from impact in Q2; (b) resulting from impact in Q4.

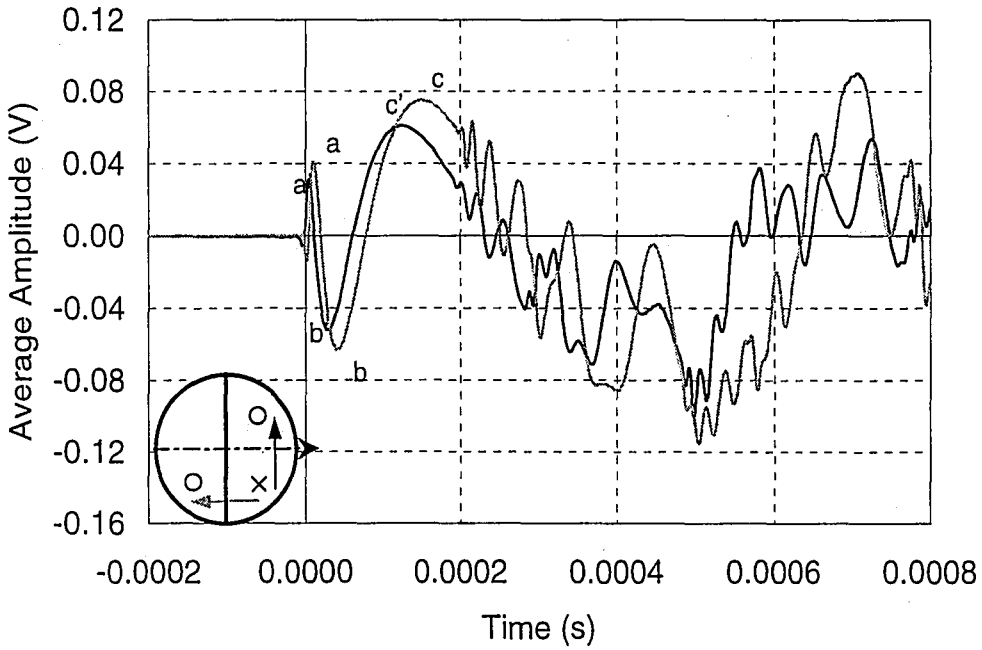

(a)

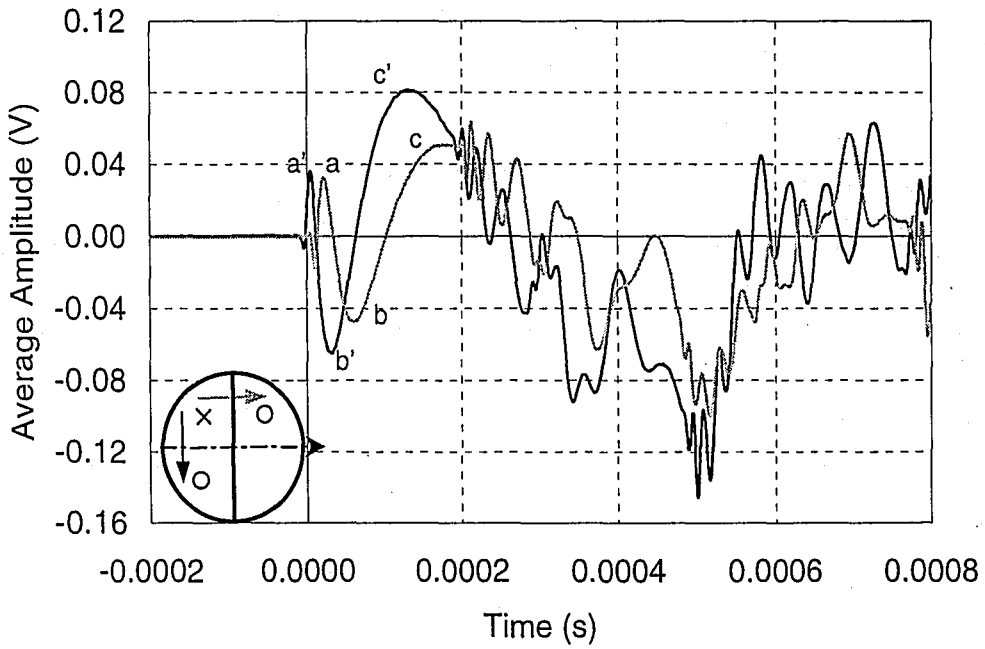

(b)

Figure 6.11 The lag in arrival time due to the roll direction of the 13 mm splice plate (P3).

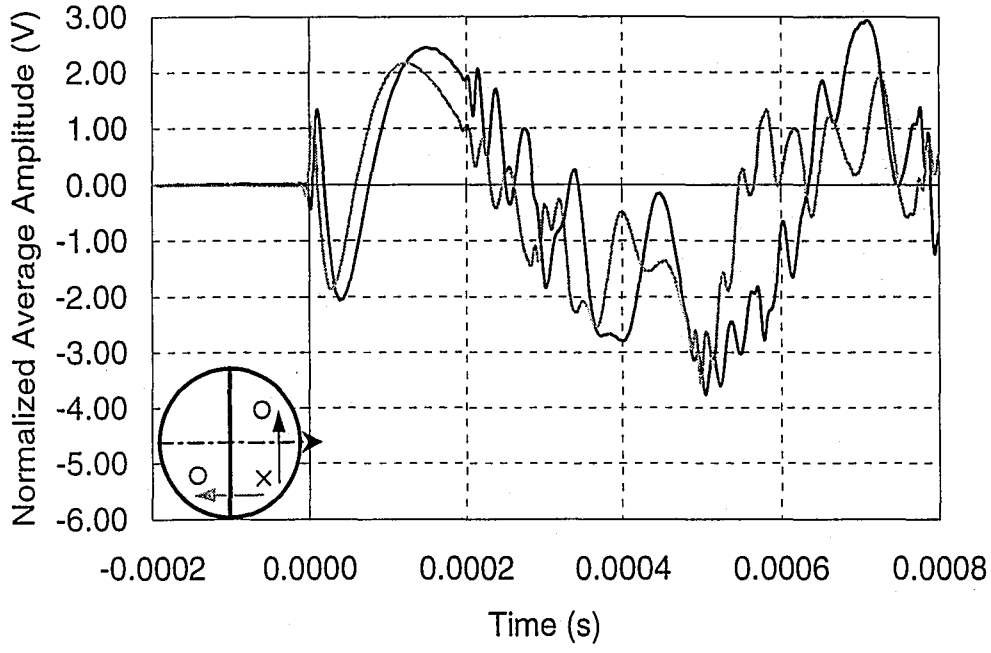

(a)

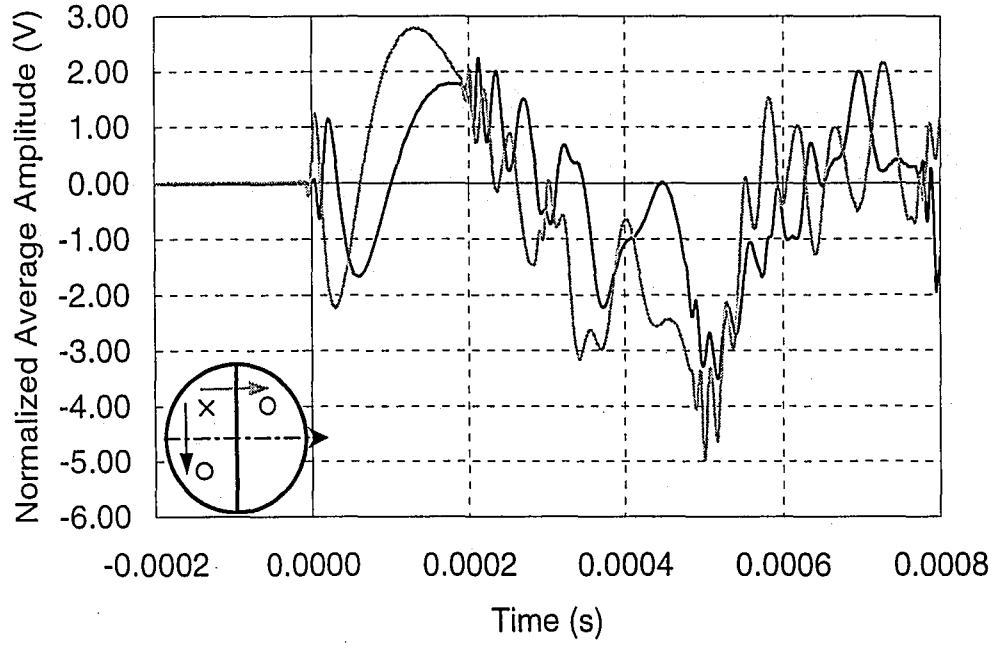

(b)

Figure 6.12 Effect of the single V groove weld in the 13 mm splice plate (P3), normalized to remove coupling effects: (a) resulting from impact in Q2; (b) resulting from impact in Q4.

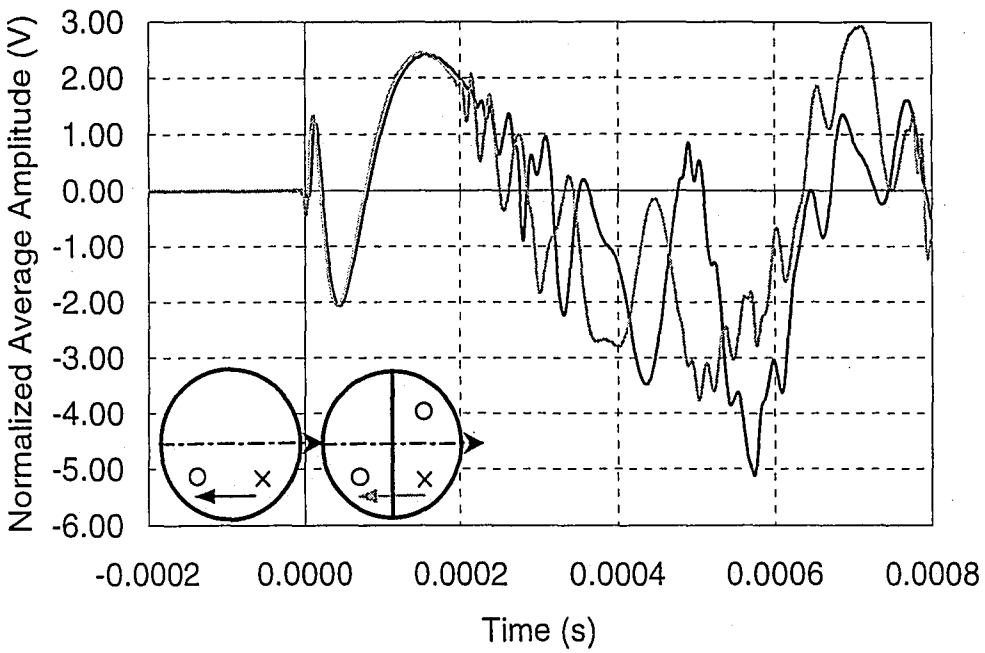

(a)

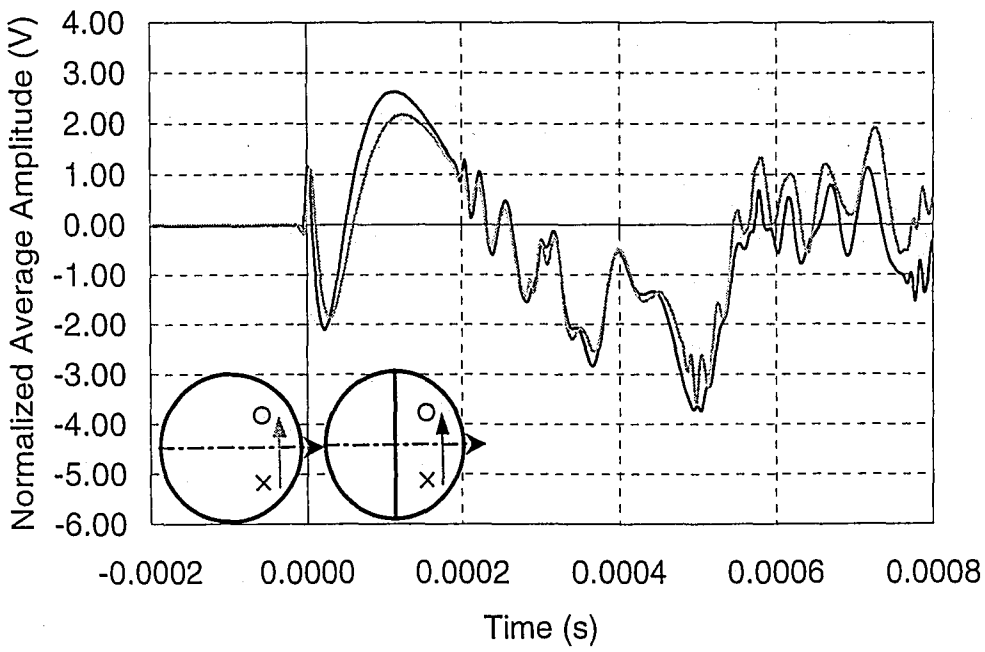

(b)

Figure 6.13 Effect of the presnece of a single V groove weld for an impact in Q2: (a) signals parallel to the roll direction; (b) signals perpendicular to the roll direction.

6.7 EFFECT OF FLANGE SPLICE

Figure 6.14 shows waveforms for the flange splice plate, P4. Figure 6.14 (a) shows waves generated by impact in Q2. Waves travel parallel to the roll direction obstructed by the flange splice to a transducer in Q3, and perpendicular to the roll direction unobstructed by the weld to a transducer in Q1. Figure 6.14 (b) shows the corresponding waves resulting from an impact in Q4.

The waveforms of Figure 6.14 begin with a sharp negative peak followed by a positive peak. A low frequency oscillation begins at the positive peak and continues throughout the signal. Immediately following the negative peak, a high frequency surface displacement begins and continues for the duration of the signal. The waveforms of Figure 6.14 (a) agree in shape and amplitude for the first 0.002 seconds following the impact. The waveforms of Figure 6.14 (b) agree in shape and amplitude for the duration of the record.

Because the waveforms agree in shape and amplitude in their unaltered state, no normalization is performed on the signals. Any time lag present between peaks of the waveforms is small and deemed negligible. The single V groove weld has no effect on the waveforms.

Figure 6.15 shows a comparison between waveforms generated on P2 and P4 by impacts in Q2. This comparison will show if the presence of the groove weld effects the waveforms by attenuating as the waveform passes through, or by causing reflection or refraction of the signal as it travels parallel to the weld. Waveforms shown in black originate from P2. Waveforms shown in

gray originate from P4. Figure 6.15 (a) shows the waveforms that travel from the impact parallel to the roll direction. The waveform for P4 is parallel to the roll direction, obstructed by the weld. Figure 6.15 (b) shows the waveforms that travel perpendicular to the roll direction. The waveform for P4 is perpendicular to the roll direction unobstructed by the weld.

The waveforms of Figure 6.15 (a) and Figure 6.15 (b) are similar in shape and amplitude. The presence of the weld in the 51 mm flange plate has no effect on the waveform as it propagates either parallel or perpendicular to the single V groove weld.

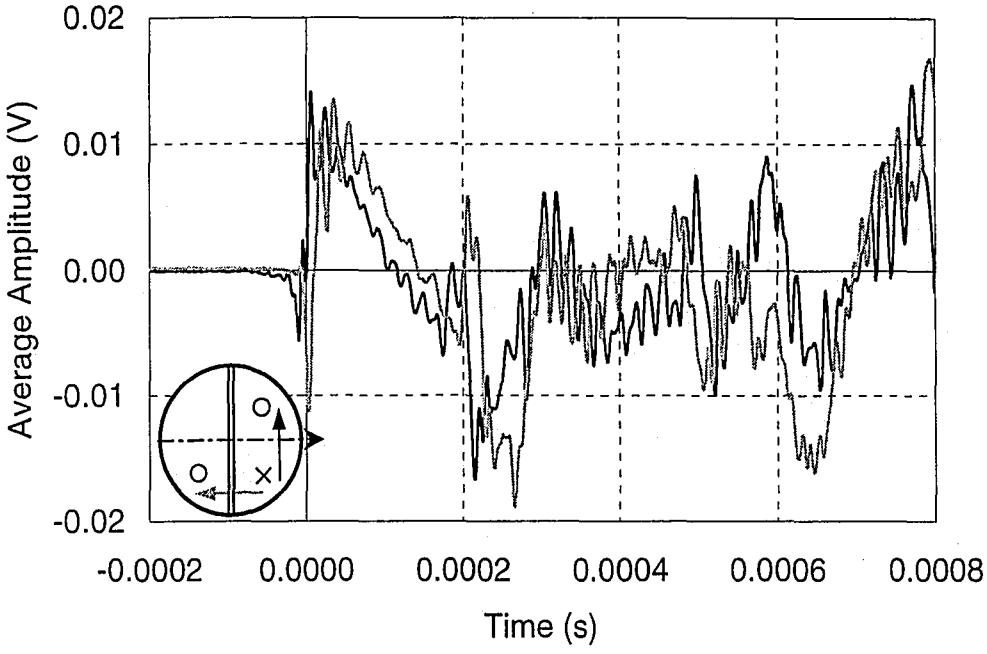

(a)

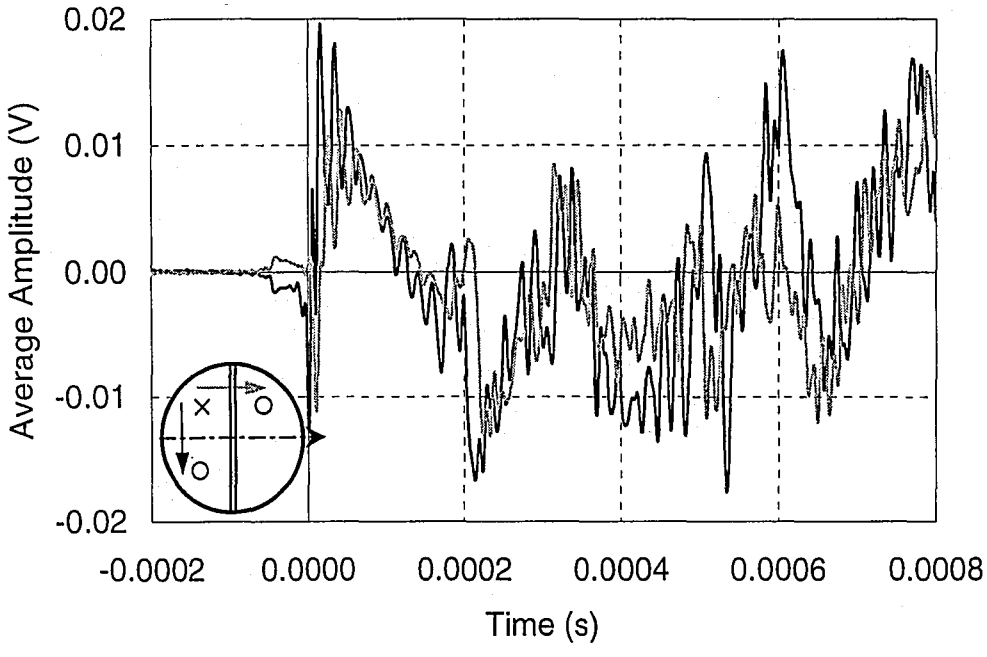

(b)

Figure 6.14 Effect of the single V groove weld in the 51 mm plate (P4): (a) resulting from impact in Q2; (b) resulting from impact in Q4.

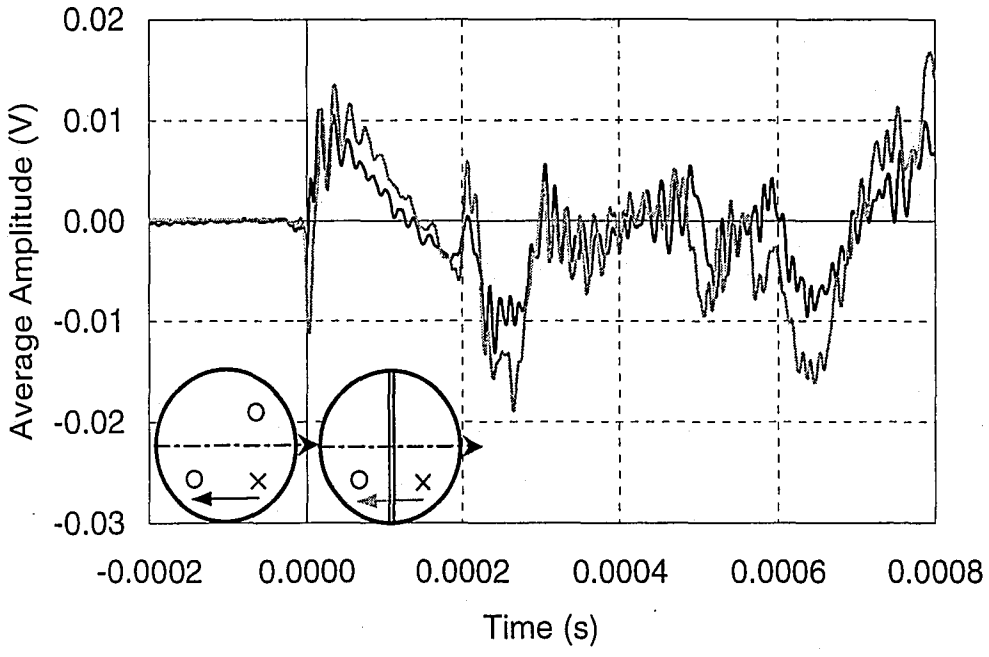

(a)

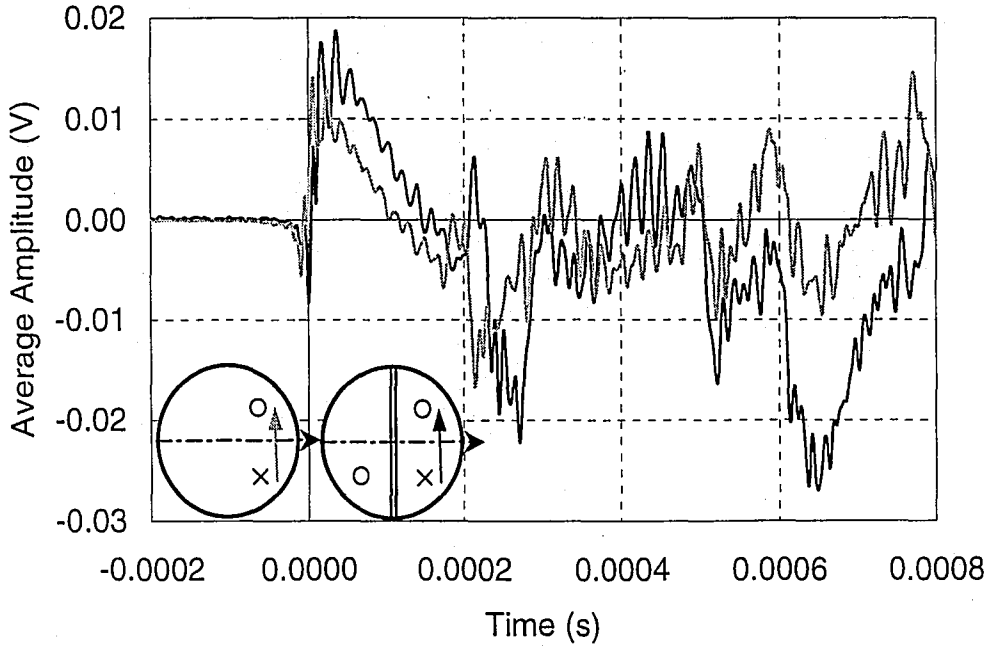

(b)

Figure 6.15 Effect of the presence of a single V groove weld in the 51 mm flange plate (P4): (a) parallel to the roll direction; (b) perpendicular to the roll direction.

6.8 EFFECT OF WEB SPLICE WITH BEVEL WELD ON OPPOSITE SIDE

Figure 6.16 shows waveforms generated in P3′, the spliced web plate with the bevel of the weld on the opposite side of the plate. Figure 6.16 (a) shows average waveforms generated by impact in Q2 and Figure 6.16 (b) shows average waveforms generate by impact in Q4.

Figure 6.16 shows the waveforms are similar in shape but not amplitude. The waveform received by the transducer in Q1 is consistently higher in Figure 6.16 (a) and (b). To remove the effect of the transducer coupling, the signals of Figure 6.16 are normalized and presented in Figure 6.17. The waveforms of Figure 6.17 are the same in amplitude and shape. Therefore the amplitude differences can be attributed to unequal coupling of the transducer, and are not a function of the plate shape. This indicates that the bevel weld with the bevel on the opposite side has no effect on the waveform as it propagates though the plate.

Figure 6.18 compares the normalized average waveforms of P3′ with those of P3 to determine whether the orientation of the bevel weld in the splice effects the stress waves as they propagate parallel to or through the weld. Figure 6.18 (a) shows the signals from P3 and P3′ originating from an impact in Q2 propagating parallel to the roll direction obstructed by the weld. The waveforms generated in P3′ are shown in black, while the waveforms of P3 are shown in gray. Figure 6.18 (b) shows the signals from the web splice plates originating from an impact in Q2, propagating perpendicular to the roll direction unobstructed

by the weld. The waveforms for P3 and P3′ are similar in shape and amplitude. Therefore, the orientation of the weld in the web splice has no effect on the signals.

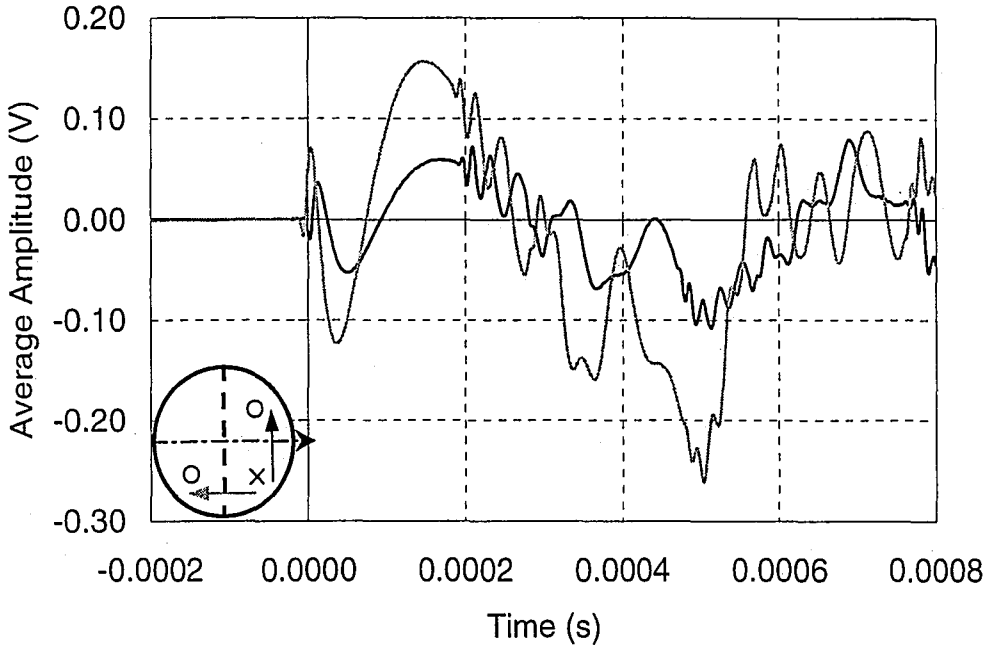

(a)

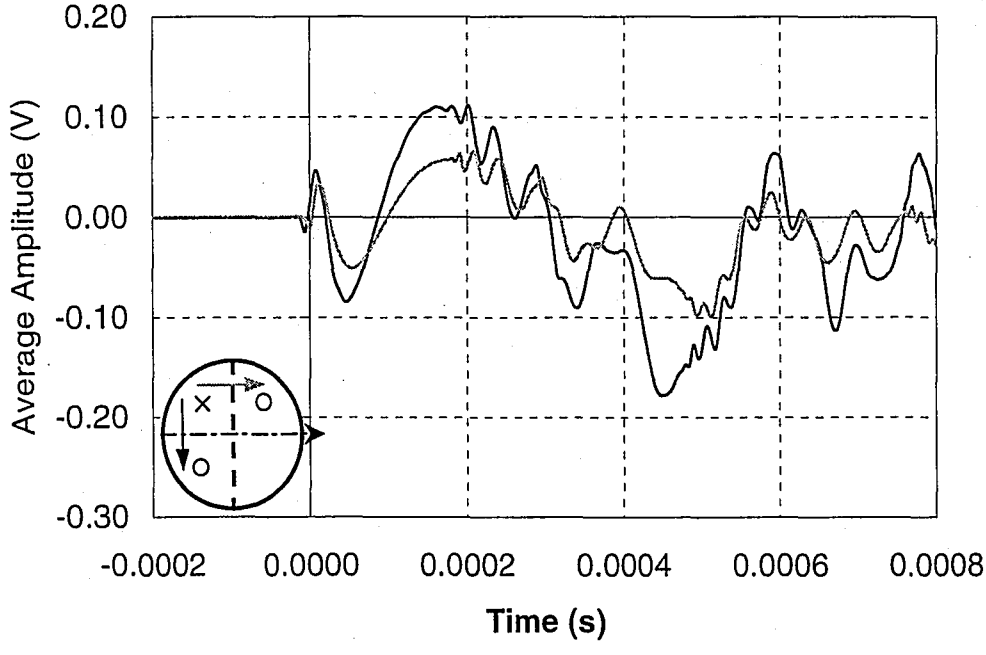

(b)

Figure 6.16 Effect of the web splice with the bevel on the opposite side of the plate (P3'): (a) resulting from impact in Q2; (b) resulting from impact in Q4.

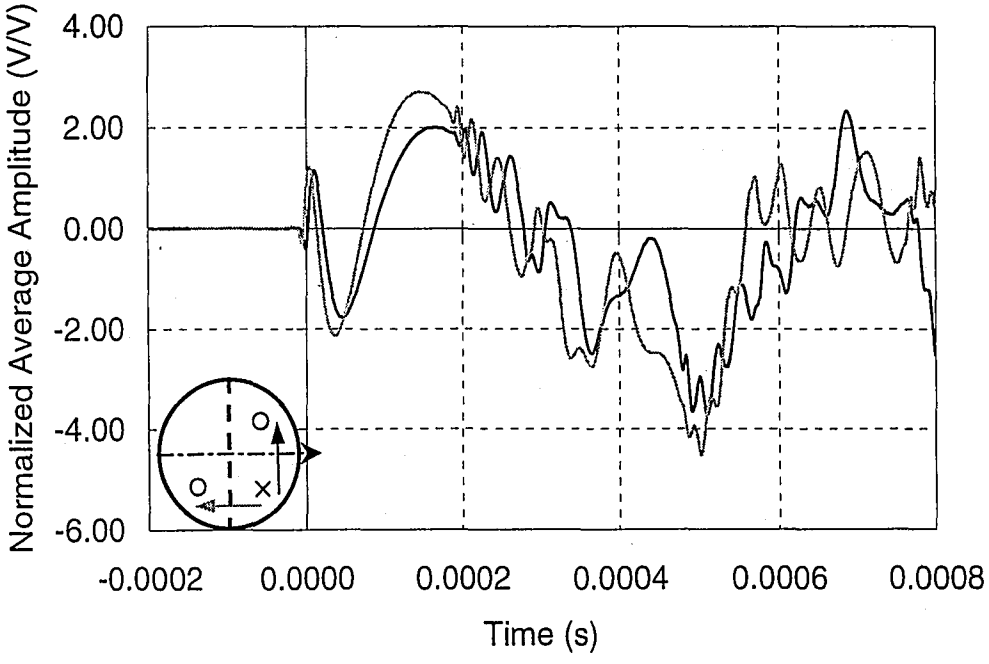

(a)

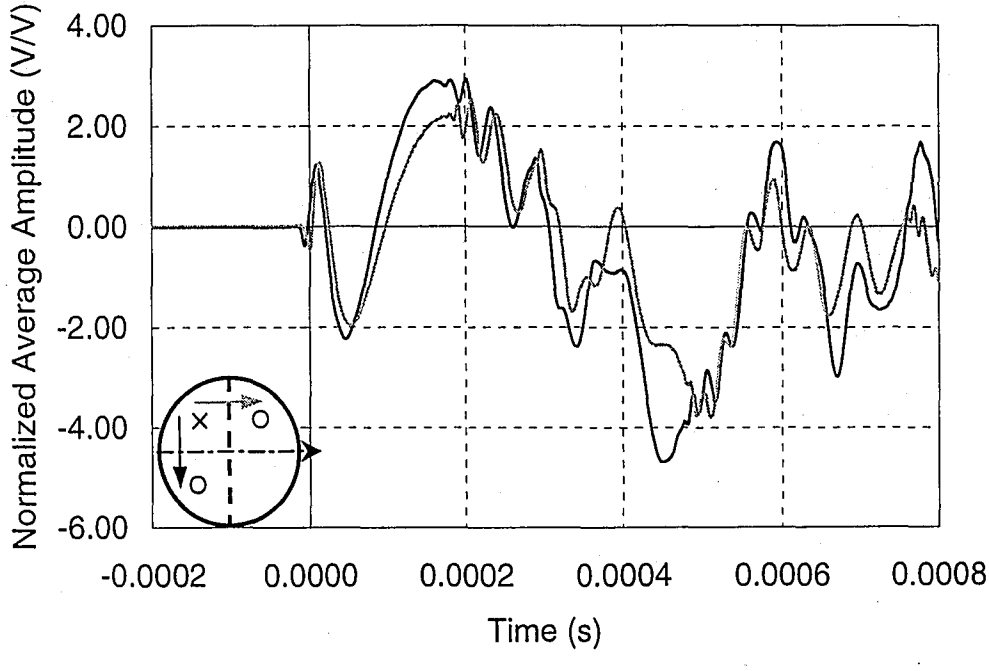

(b)

Figure 6.17 Effect of the web splice in P3', normalized to remove coupling effects: (a) resulting from impact in Q2; (b) resulting from impact in Q3.

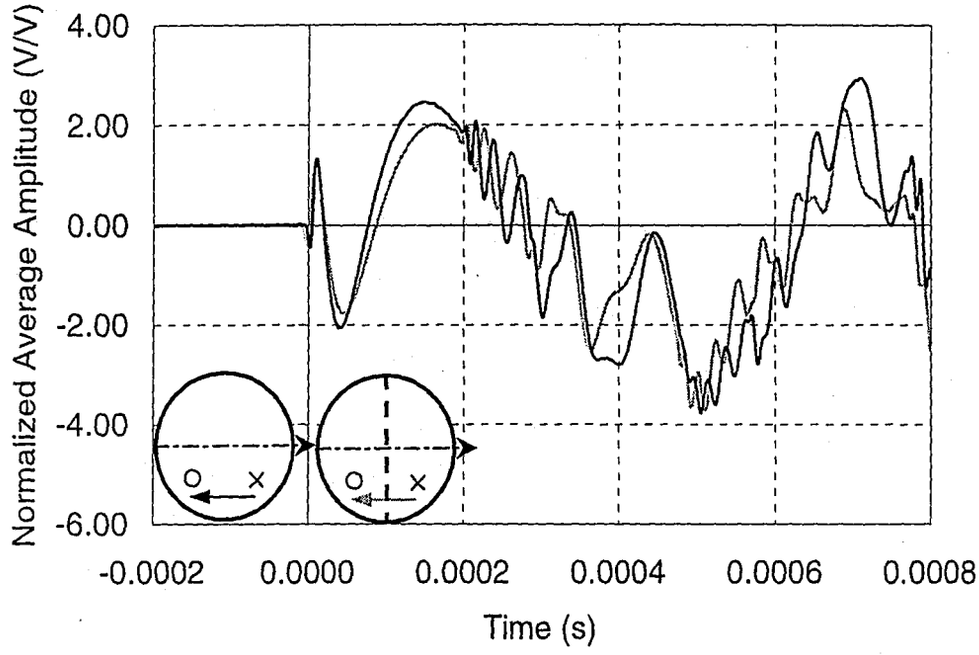

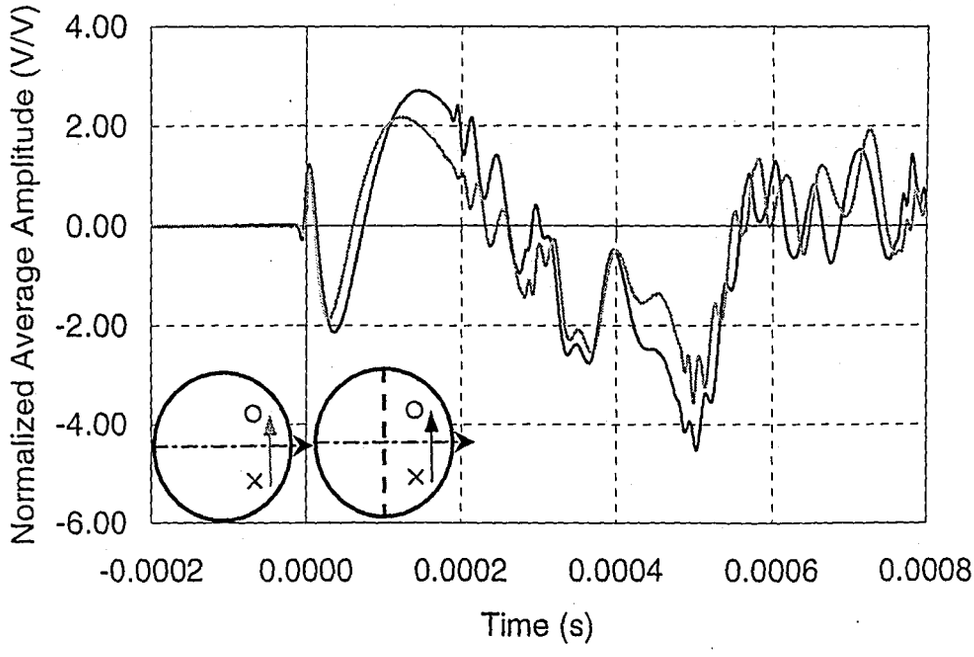

Figure 6.18 Effect of the orientation of a weld splice in the 13 mm web plate (P3 and P3').

6.9 EFFECT OF FLANGE SPLICE WITH BEVEL WELD ON OPPOSITE SIDE

Figure 6.19 shows the average waveforms generated in P4′, the spliced flange plate with bevel of the groove weld on the opposite side. Figure 6.19 (a) shows average waveforms generated by impact in Q2 and Figure 6.19 (b) shows average waveforms generate by impact in Q4.

The amplitudes of the average waveforms in Figure 6.19 are very different. Figure 6.20 shows the average waveforms of Figure 6.19 normalized by the amplitude of the first positive peak. The waveforms of Figure 6.20 are similar in both shape and amplitude. This indicates that the bevel weld with the bevel on the opposite side has no effect on the waveform as it propagates though the plate.

Figure 6.21 compares the waveforms of P4′ with those of P4 to determine whether the orientation of the double bevel weld in the splice effects the stress waves as they propagate parallel to or through the weld. Figure 6.21 (a) shows the signals from P4 and P4′ originating from an impact in Q2, propagating parallel to the roll direction obstructed by the weld. Figure 6.21 (b) shows the signals from the web splice plates originating from an impact in Q2, propagating perpendicular to the roll direction unobstructed by the weld. The waveforms for P4 and P4′ are similar in shape and amplitude for both cases. Therefore, the orientation of the weld in the flange splice has no effect on the signals.

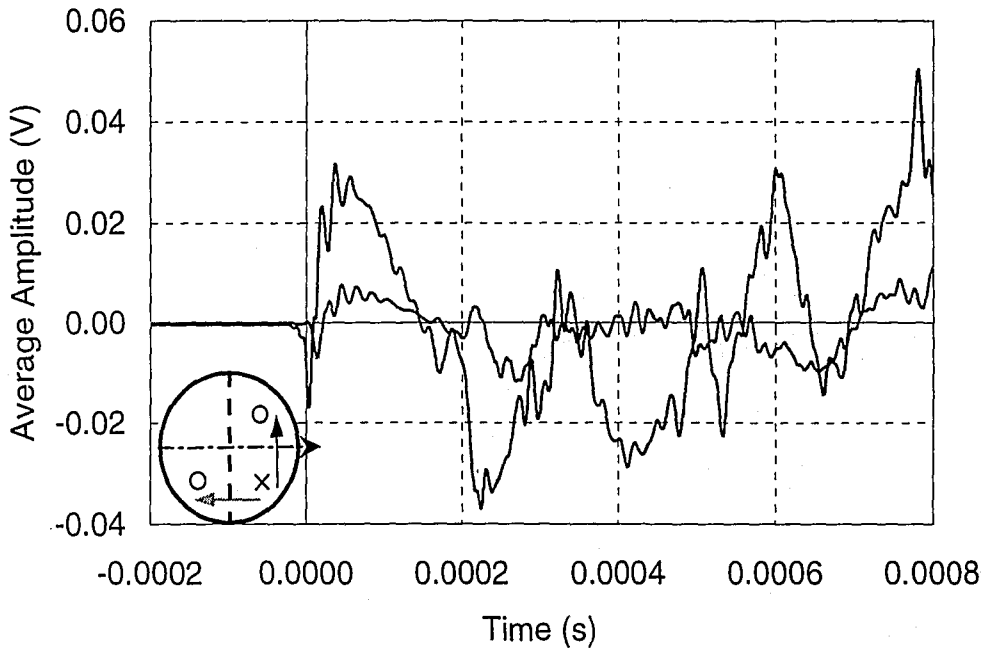

(a)

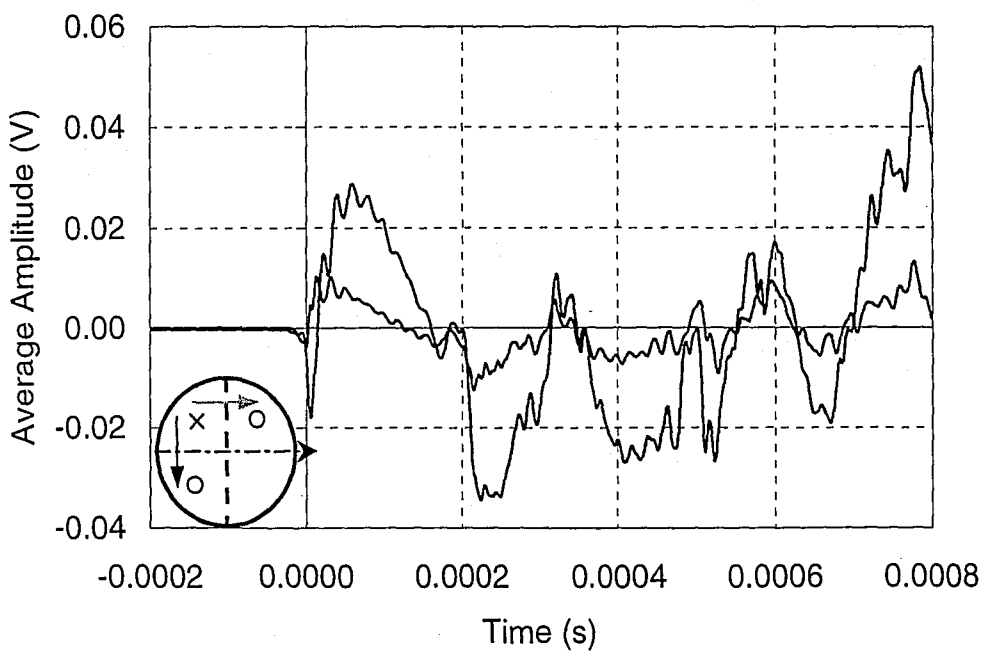

(b)

Figure 6.19 Effect of the flange splice with the bevel on the opposite side of the plate (P4'): (a) resulting from impact in Q2; (b) resulting from impact in Q4.

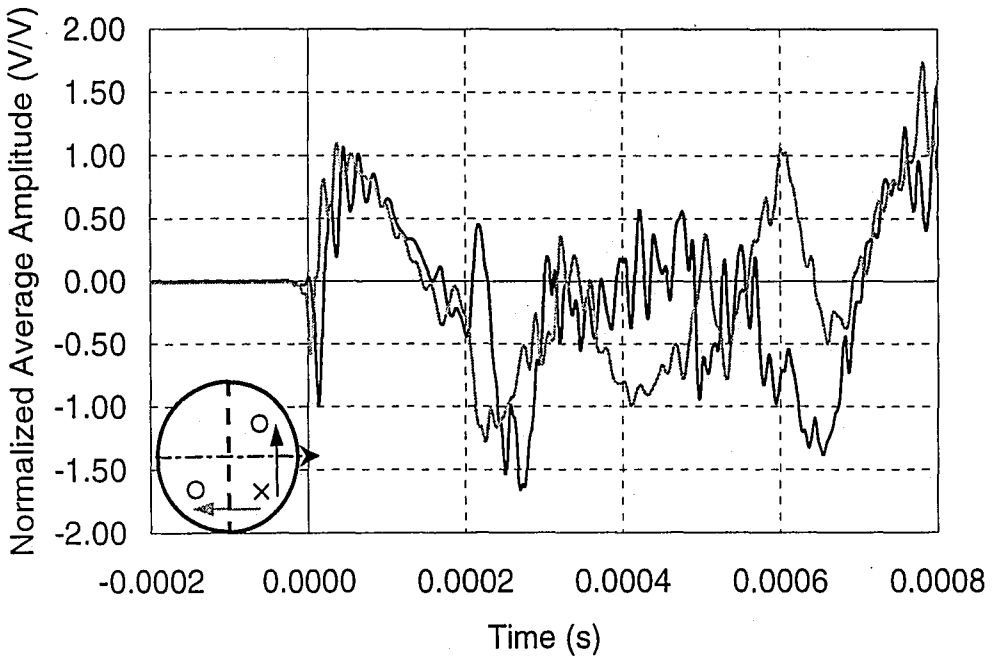

(a)

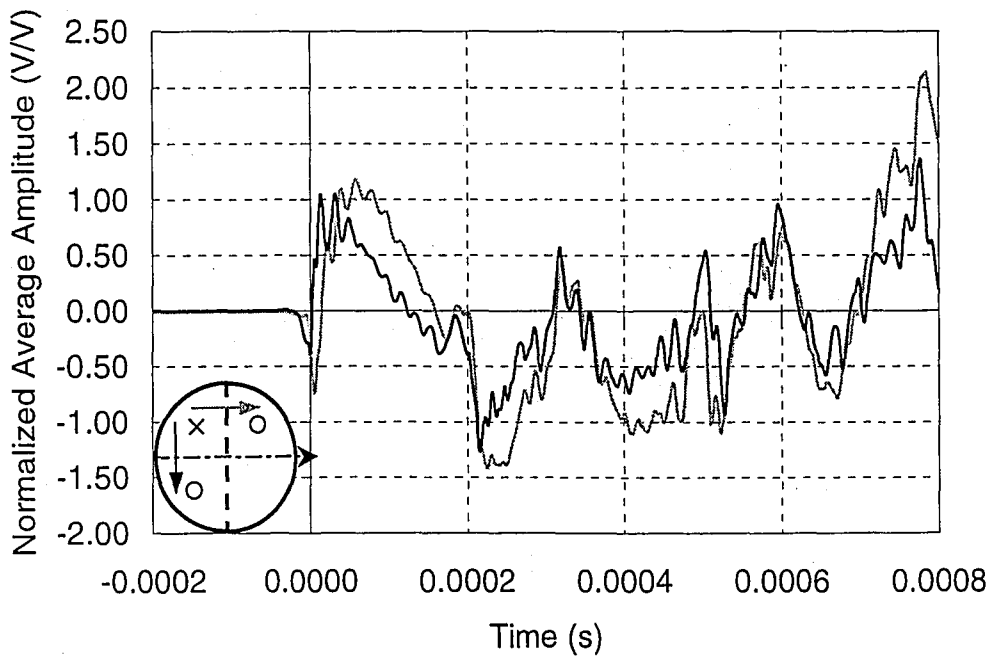

(b)

Figure 6.20 Effect of the flange splice in P4', normalized to remove coupling effects: (a) resulting from impact in Q2; (b) resulting from impact in Q3.

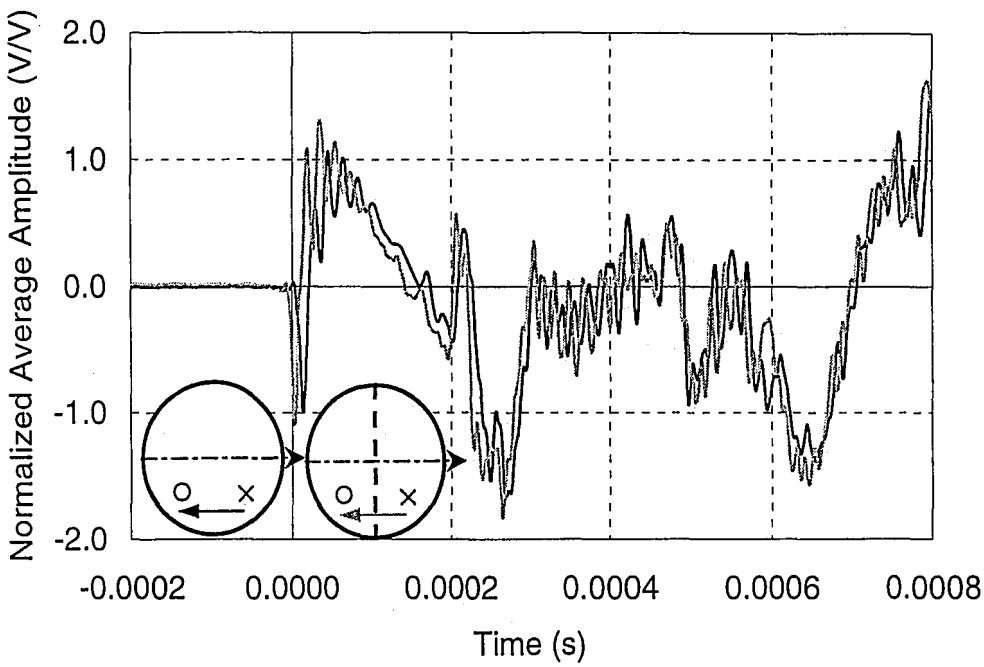

(a)

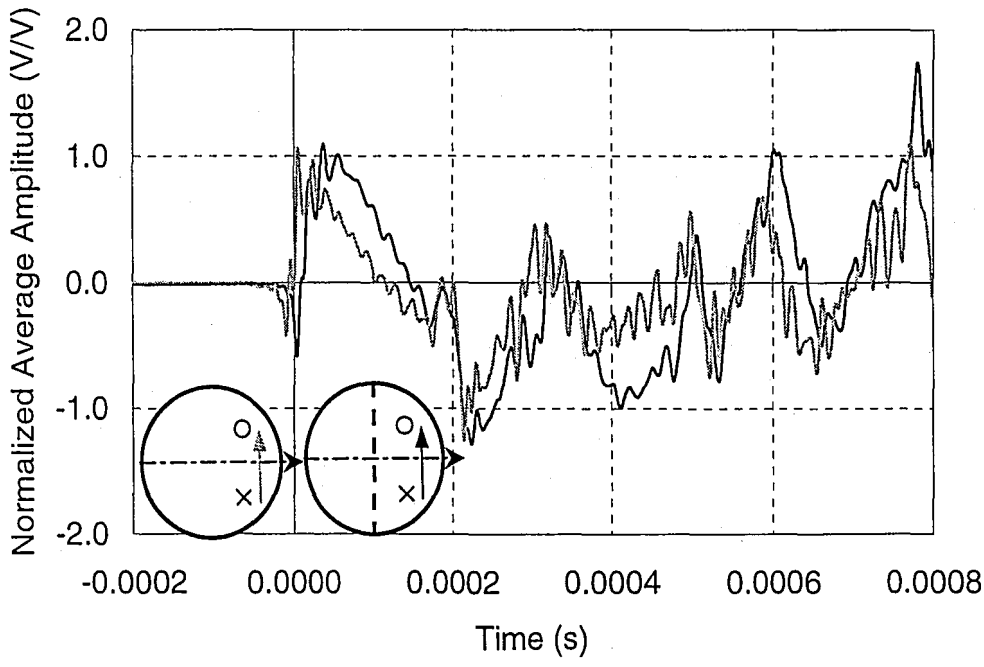

(b)

Figure 6.21 Effect of the orientation of a weld splice in the 51 mm web plate (P4 and P4').

6.10 EFFECT OF STIFFENER-TO-WEB CONNECTION ON THE TRANSDUCER SIDE

The second type of welded obstruction studied in this report is the presence of a welded attachment. Two welded attachments are treated, a stiffener-to-web connection and a web-to-flange connection. Figure 6.22 shows waveforms generated in P5, the stiffener-to-web connection with the attachment on the transducer side. Figure 6.22 (a) shows waveforms generated for impact in Q2, and Figure 6.22 (b) shows waveforms generated for impact in Q4.

Waveforms propagating perpendicular to the roll direction, unobstructed by the stiffener, begin with a small positive peak followed by a negative peak and a positive peak, as did the waveforms of the plain web plate (P1). During the second positive peak, high frequency oscillations begin in the signal and continue for the duration of the response. Waveforms propagating parallel to the roll direction obstructed by the stiffener begin with a positive peak. Following the positive peak, the waveform has no more high amplitude displacements. High frequency oscillations can be seen beginning at approximately 0.0007 seconds and continue for the duration of the response.

There are very clear differences in the obstructed waveform as compared to the unobstructed waveform. This is true even at very early times in the response, before arrivals of reflections from the plate boundaries. The waveforms are modified in amplitude and shape as they cross the stiffener. Obstructed signals have lower amplitudes for both the high frequency and low frequency oscillations at both impact locations. The shape of the waveform also changes.

There is no clear common pattern of displacement peaks between the signals. Because the waveforms are so different, it is impossible to compare the lag time of the signals.

Figure 6.23 compares the waveforms of P1 and P5 generated by an impact in Q2. The black waveform represents P1 and the gray waveform represents P5. Figure 6.23 (a) shows the comparison of the waveforms of P1 and P5 parallel to the roll direction with the waveform from P5 being obstructed by the stiffener-to-web connection. Figure 6.23 (b) shows the comparison of the waveforms perpendicular to the roll direction.

The waveforms of Figure 6.23 (a), parallel to the roll direction, are similar in shape and amplitude to only 0.0007 seconds into the response. At this point, the large amplitude oscillations of the signals begin to differ. There appears to be some commonality in the small amplitude, high frequency components of the two signals. The waveforms of Figure 6.23 (b), perpendicular to the roll direction, do not agree in shape or amplitude during the response. Thus, the presence of the web-to-stiffener connection alters the waveforms that travel through and perpendicular to the stiffener.

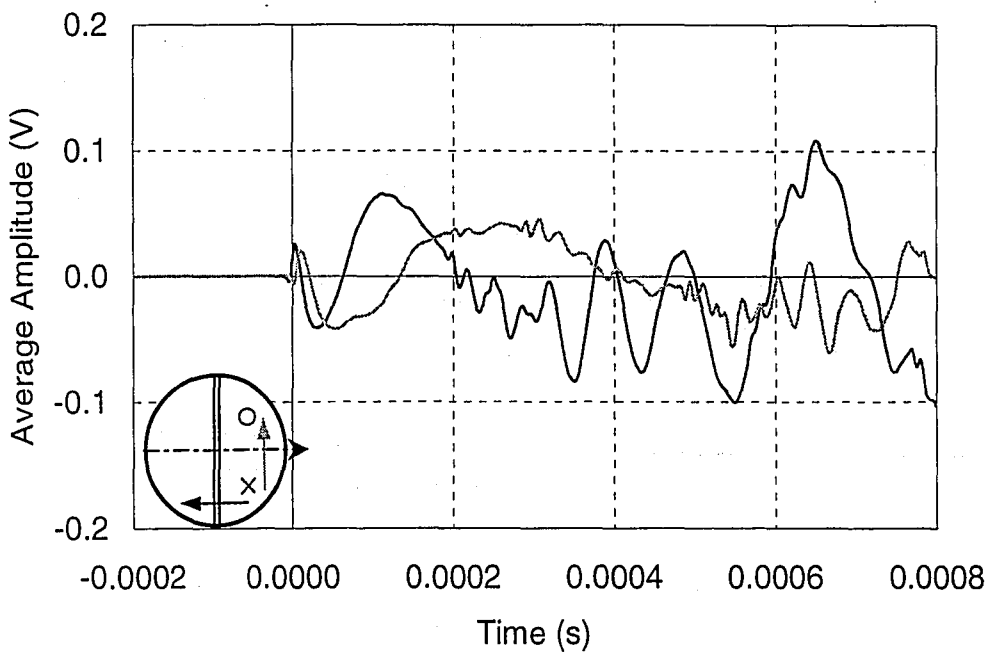

(a)

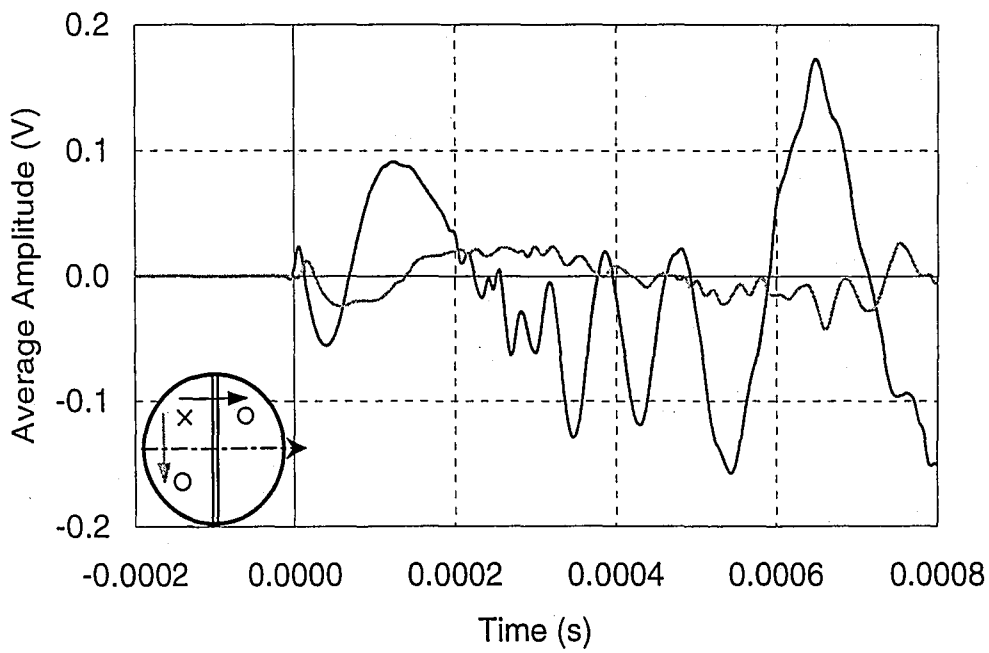

(b)

Figure 6.22 Effect of the stiffener-to-web connection on the transducer side of the plate (P5): (a) resulting from impact in Q2; (b) resulting from impact in Q4.

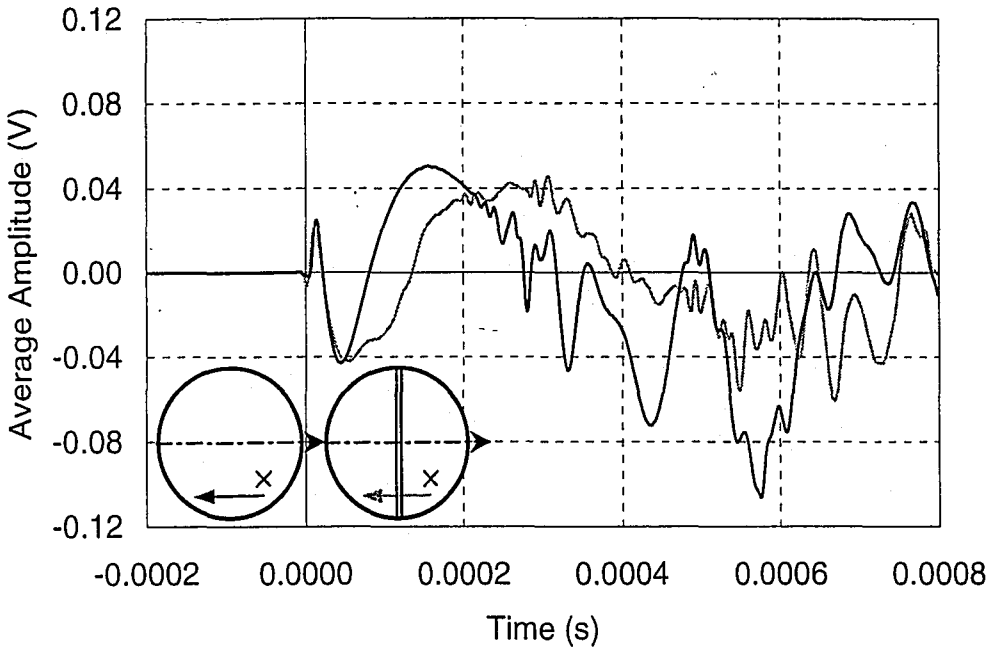

(a)

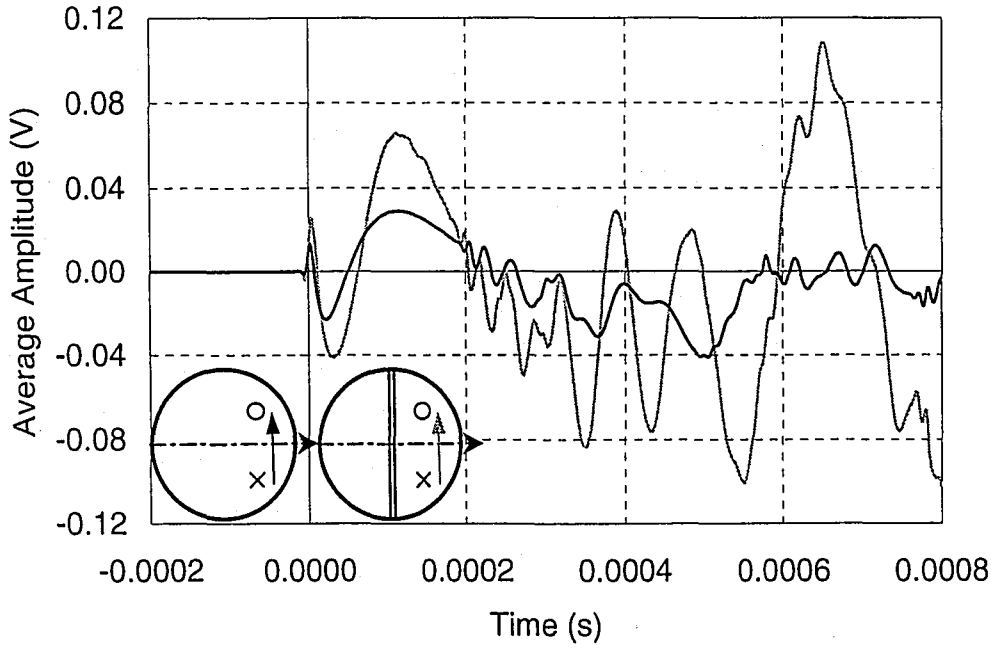

(b)

Figure 6.23 Effect of the presence of the stiffener-to-web connection (p5) as compared to the plain web plate (P1): (a) parallel to the roll direction; (b) perpendicular to the roll direction.

6.11 EFFECT OF WEB-TO-FLANGE CONNECTION ON THE TRANSDUCER SIDE

Figure 6.24 shows the average waveforms generated in P6, the web-to-flange connection. Figure 6.24 (a) and Figure 6.24 (b) show the average waveforms resulting from impact in Q2 and Q4 respectively. It is important to note that, as discussed in Chapter 4, the simulated web is attached to the flange plate parallel to the roll direction.

The waveforms of Figure 6.24 (a) are generated from an impact in Q2. The waveform parallel to the roll direction and unobstructed appears to have many features of the corresponding waveform in the plain flange plate (P2). The waveform contains a low frequency oscillation superimposed with a high frequency low amplitude oscillation. The waveform perpendicular to the roll direction and obstructed by the attachment contains a low frequency oscillation that has an amplitude lower than the amplitude of the low frequency oscillation in the waveform parallel to the roll direction and unobstructed. The obstructed signal also contains high frequency oscillations, but the pattern of peaks does not correspond to the peaks in the unobstructed signal.

Figure 6.24 (b) shows waveforms resulting from impact in Q4. Both the wave parallel to the roll direction and unobstructed and the waveform perpendicular to the roll direction and obstructed by the attachment seem similar in both amplitude and shape. This is different from the observations for an impact in Q2 seen in Figure 6.24 (a).

The waveforms of the web-to-flange connection can be compared with the waveforms of the plain flange plate. Figure 6.25 shows waveforms generated from an impact in Q2 for plates P2 and P6. Figure 6.25 (a) shows waveforms parallel to the roll direction. Figure 6.25 (b) shows waveforms perpendicular to the roll directions with the P6 waveform obstructed by the attachment.

The waveform parallel to the roll direction have the same geometric pattern of peaks and troughs with similar amplitude for the first 0.0002 seconds of the response. After this point, the large amplitude oscillations of the two stress waves become out of phase. It appears as if the small amplitude peaks still correspond between the waveforms. This indicates that the presence of the welded attachment does not affect the waveforms traveling parallel to it.

Waveforms perpendicular to the roll direction (and obstructed by the welded attachment in the case of P6) are different in amplitude and shape throughout the duration of the signal. The differences in these signals are similar to the differences between the obstructed and unobstructed signals in P6 alone.

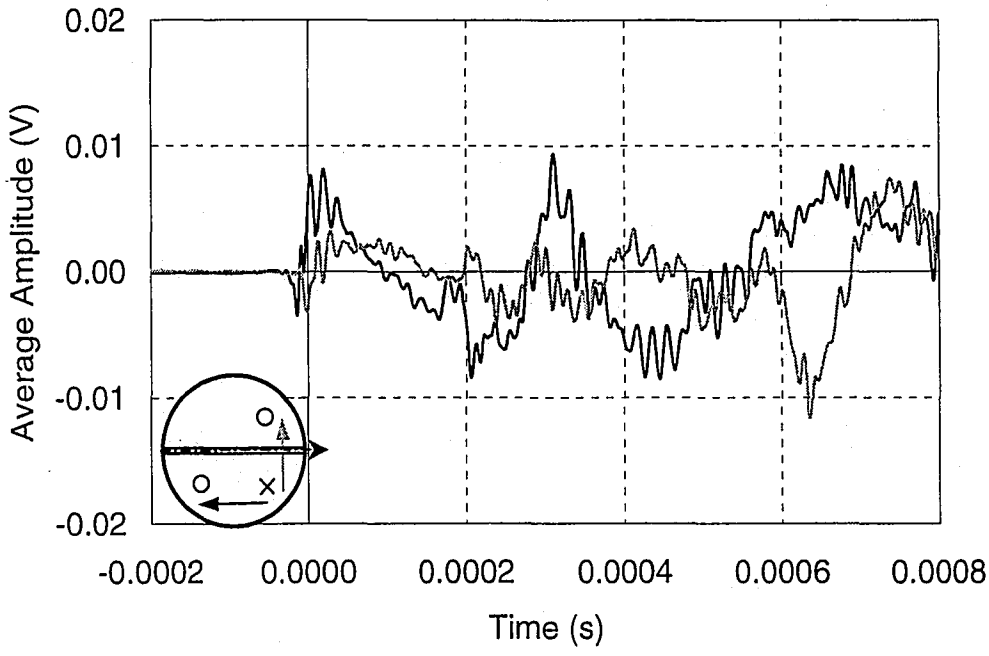

(a)

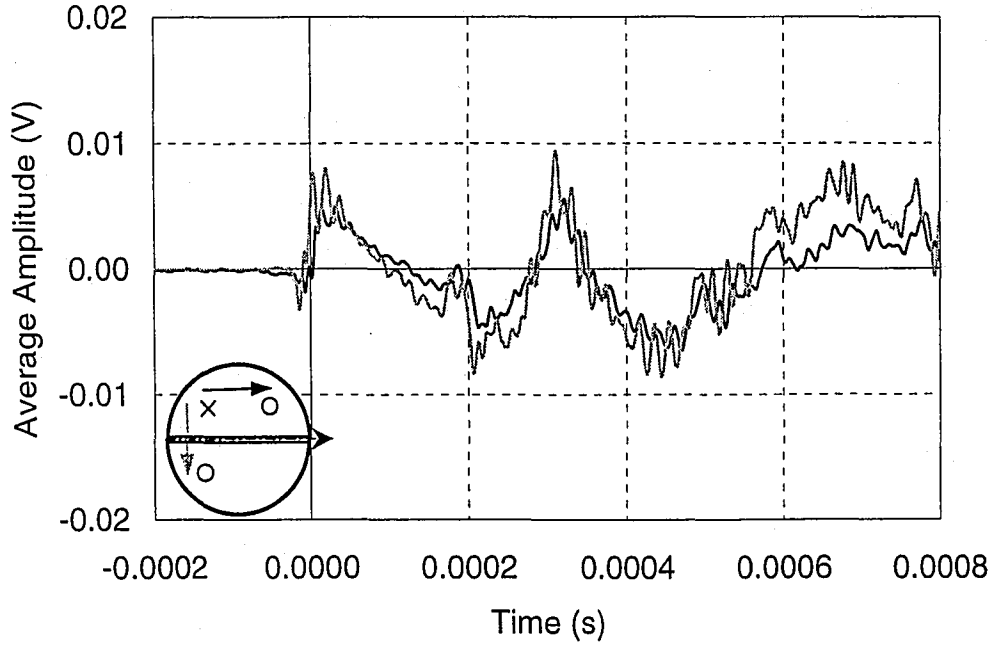

(b)

Figure 6.24 Effect of the web-to-flange connection on the transducer side of the plate (P6): (a) resulting from impact in Q2; (b) resulting from impact in Q4.

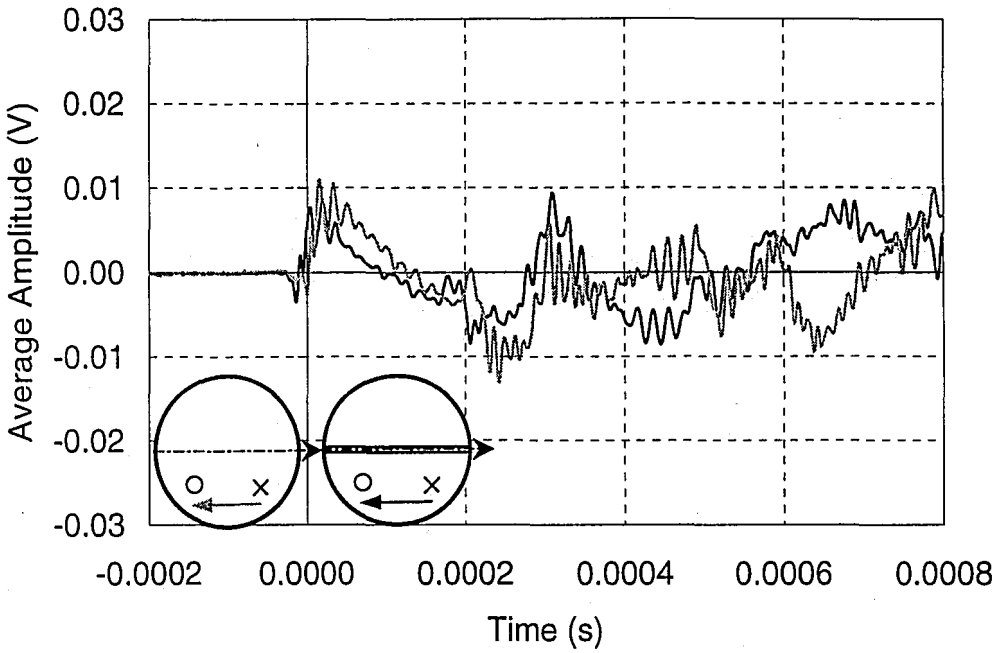

(a)

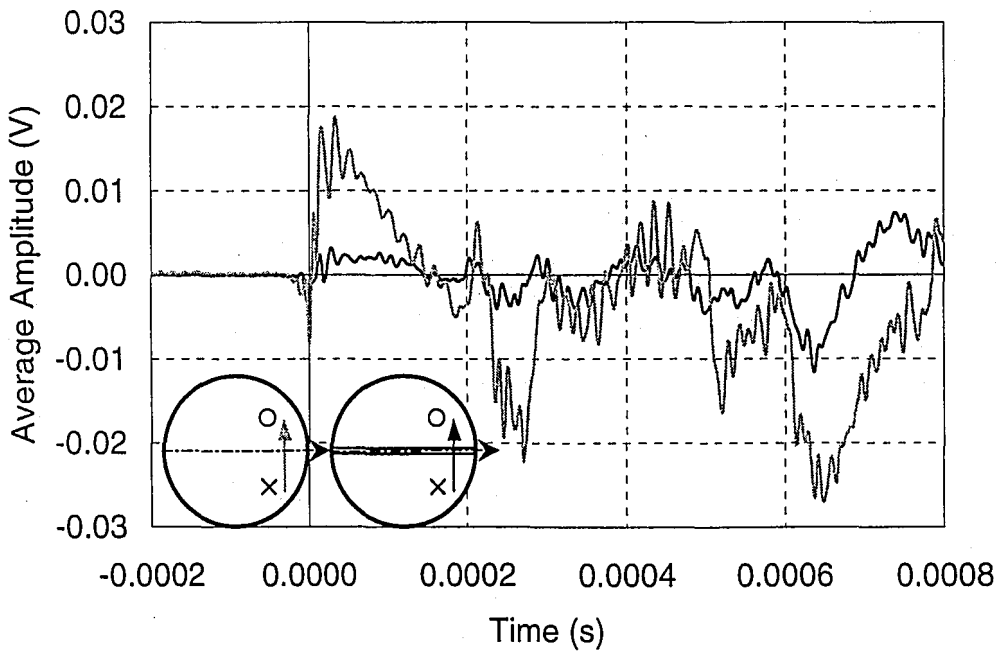

(b)

Figure 6.25 Effect of the presence of the web-to-flange welded attachment (P6) compared to the plain plate (P2): (a) parallel to the roll direction; (b) perpendicular to the roll direction.

6.12 EFFECT OF STIFFENER-TO-WEB CONNECTION ON THE OPPOSITE SIDE OF THE PLATE

A welded attachment on the opposite side of the plate as the transducers and impact effects the acoustic emission signal in a similar manner to the attachment on the same side. Figures 6.26 shows the average waveforms for P5′, the simulated stiffener-to-web connection with the attachment on the opposite side. Figure 6.26 (a) shows the average waveforms generated by impact in Q2, and Figure 6.26 (b) shows the average waveforms generated by impact in Q4.

As in the case when the attachment is located on the same side as the transducer and impact, waveforms in P5′ are modified in amplitude and shape when obstructed by a fillet welded attachment. The waveform parallel to the roll direction and unobstructed by the attachment has the characteristics of the waveforms in the plain web plate. The low frequency oscillations characteristic of the unobstructed signals do not occur in the obstructed signals.

Figure 6.27 compares the waveforms of the plain web plate to the waveform of P5′. The signal perpendicular to the roll direction unobstructed by the attachment in P5′ can be compared with the signal perpendicular to the roll direction in P1 in Figure 6.27 (a). The initial peaks of the waveforms are comparable in amplitude and duration. Approximately 0.0003 seconds after the arrival of the R-wave, the signals begin to differ in shape and amplitude. This shows that the presence of the stiffener-to-web connection had little effect on the stress waves traveling parallel to it. Figure 6.27 (b) shows the waveforms parallel to the

roll direction. The waveform obstructed by the stiffener in P5 is different from the corresponding waveform in P1 in amplitude and shape. The presence of the stiffener attachment does effect the stress waves that propagate through it.

Waveforms obstructed by the welded attachment in P5′ appear to have similar characteristics to the obstructed signal of P5. Figure 6.28 compares the waveforms generated by impact in Q2 for P5 and P5′. Waveforms generated on P5′ are black and waveforms of P5 are gray. Figure 6.28 (a) shows waveforms perpendicular to the roll direction unobstructed by the welded attachment and Figure 6.28 (b) shows waveforms parallel to the roll direction obstructed by the welded attachment. The waveforms of Figure 6.28 (a) have a similar wave pattern. Each peak in the signal of P5 corresponds to a peak in the waveform for P5′. The amplitudes of the peaks vary, with the waveform of P5 having consistently higher amplitude. This suggests a coupling difference between the transducer and the plates. The waveforms obstructed by the welded attachment (Figure 6.28 (b)) are also similar in their shape. Both exhibit the characteristic long negative trough after the arrival of the wave, and small amplitude low frequency oscillation. Again, the waveform of P5 has consistently higher amplitude than that of P5′, suggesting coupling problems.

The similarity in waveforms between P5′ and P5 shows that the orientation of the attachment has little affect on the behavior of the plate.

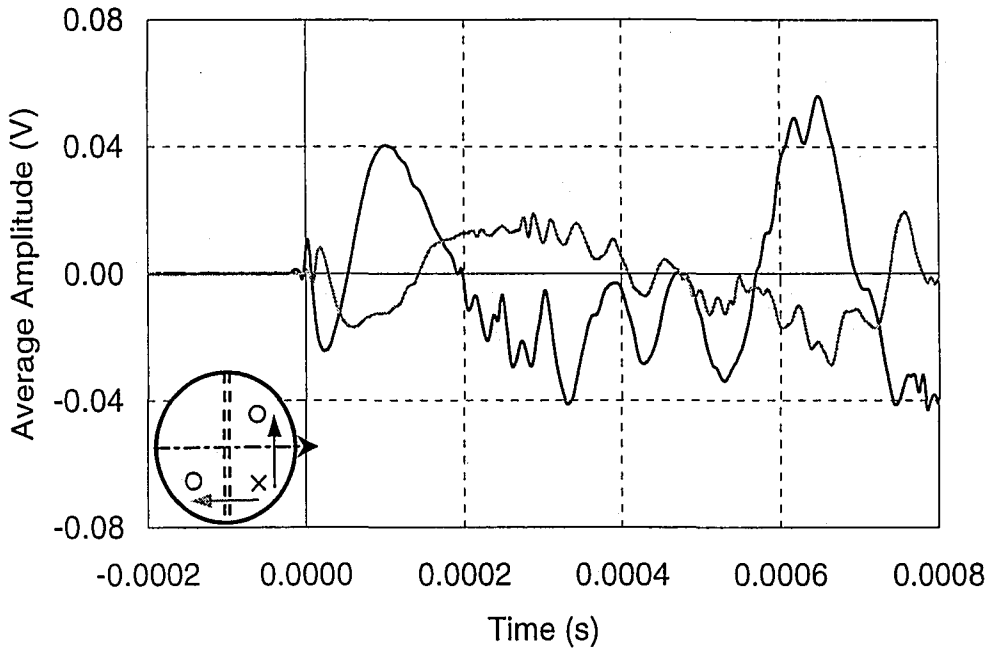

(a)

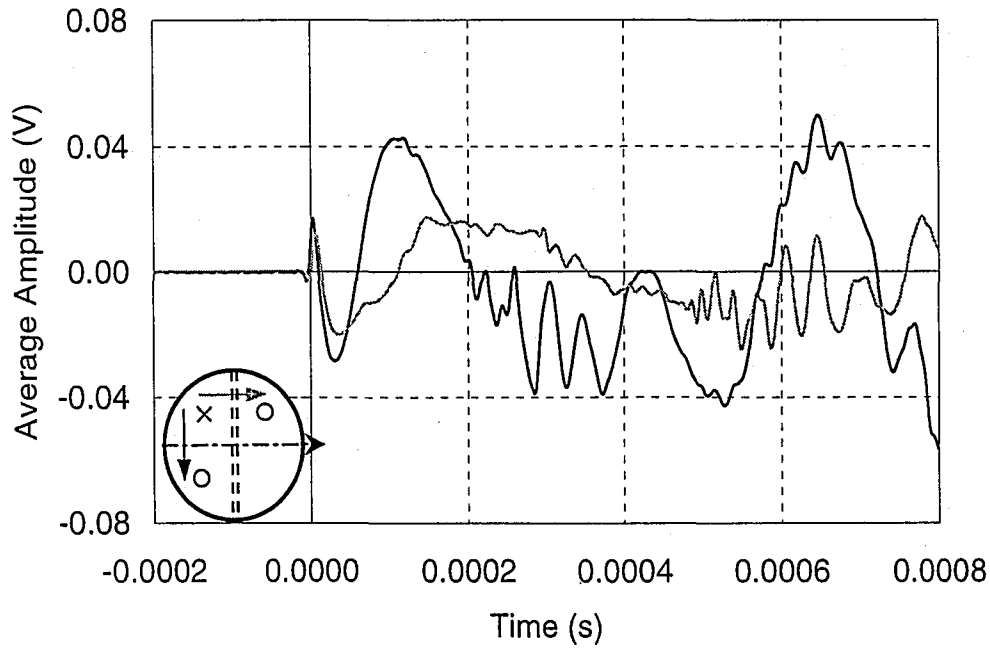

(b)

Figure 6.26 Effect of the stiffener-to-web connection on the opposite side of the plate (P5'): (a) resulting from impact in Q2; (b) resulting from impact in Q4.

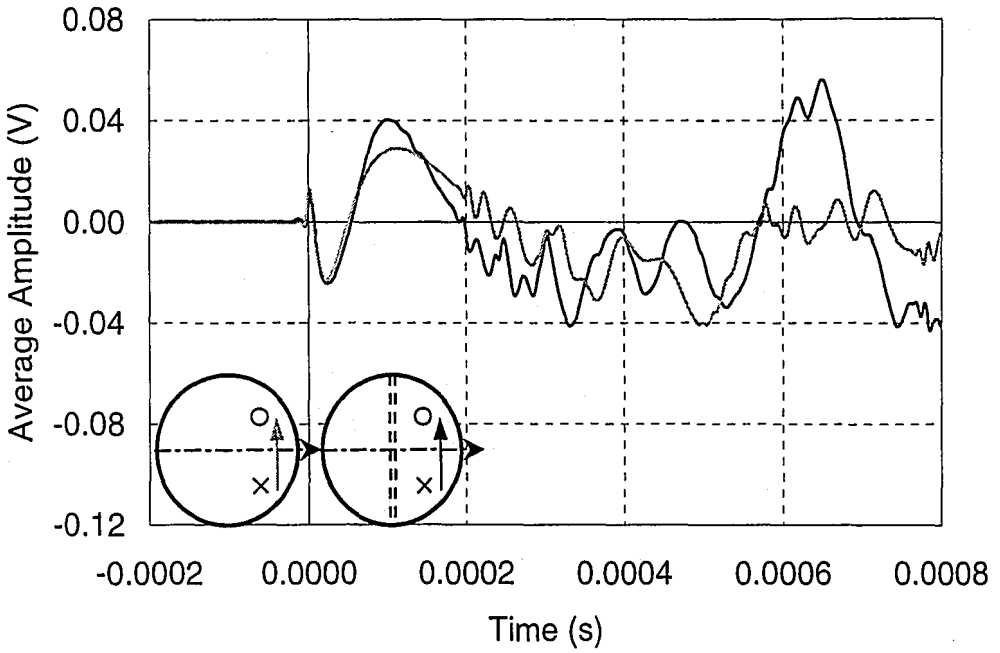

(a)

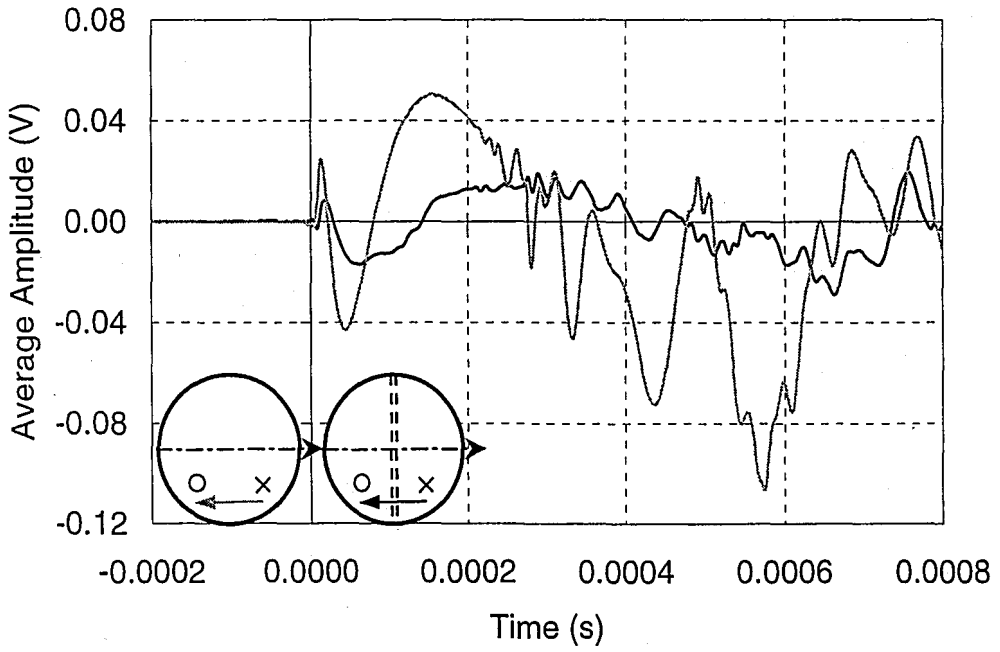

(b)

Figure 6.27 Effect of the presence of the stiffener-to-web welded attachment on the opposite side (P5') compared to the plain plate (P1): (a) perpendicular to the roll direction; (b) parallel to the roll direction.

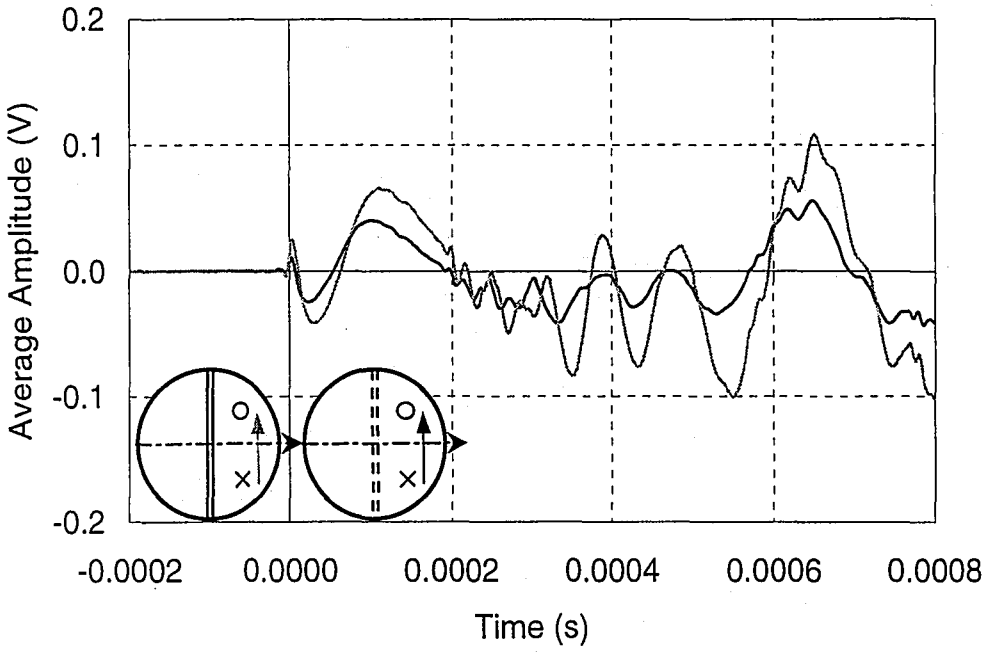

(a)

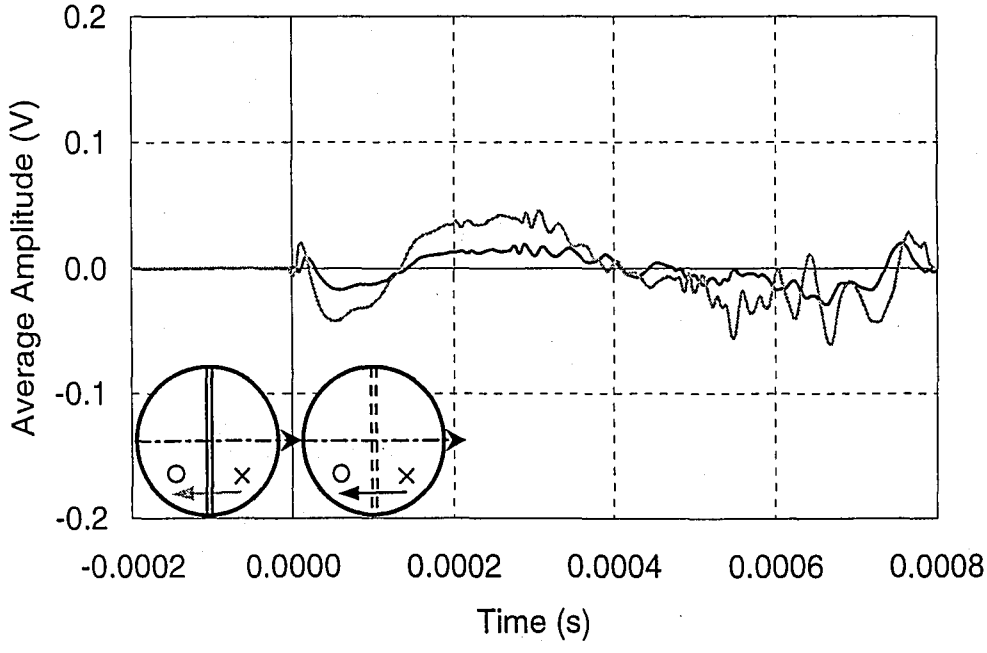

(b)

Figure 6.28 Effect of the orientation of the stiffener-to-web welded attachment (P5 versus P5'): (a) perpendicular to the roll direction; (b) parallel to the roll direction.

6.13 EFFECT OF WEB-TO-FLANGE CONNECTION ON OPPOSITE SIDE OF PLATE

Figure 6.29 presents waveforms generated in P6′, the web-to-flange connection on the opposite side of the plate. The waveforms in Figure 6.29 (a) result from impact in Q2; the waveforms in Figure 6.29 (b) result from impact in Q4. The response consists of a large amount of high frequency oscillations. The arrivals of the peaks of the high frequency oscillation occur simultaneously for the signals parallel and perpendicular to the roll direction. This agreement continues for the entire duration of the record.

Figure 6.29 (a) shows that the low frequency, large amplitude oscillations of the waveforms show general agreement for 0.0003 seconds of response. The response appears to be in phase. After this, the large amplitude oscillations become out of phase. Figure 6.29 (b) has general agreement of the low frequency, large amplitude signal until 0.0003 seconds of response. However, at approximately 0.0002 seconds, the amplitude of the signal parallel to the roll direction unobstructed by the welded attachment becomes significantly larger than the amplitude of the signals obstructed by the welded attachment.

The behavior of the low frequency oscillation of the signals presented in Figure 6.29 is common to both impact locations. Signals obstructed by the welded attachment are much flatter at the first peak, whereas the signal unobstructed by the weld decreases rapidly from the first peak. Due to coupling differences, the effect of the attachment on the amplitude is difficult to determine.

Figure 6.30 presents the average waveforms of Figure 6.29 separated by receiver location. Figure 6.30 (a) shows waveforms parallel and perpendicular to the roll direction received by a transducer in Q1. Because the coupling for the transducer is equal (because the transducer is stationary), the amplitudes of the signals can be accurately compared. Figure 6.30 (b) shows the waveforms received by a transducer in Q3. Again, both sets of waveforms show agreement until 0.0003 seconds in both high frequency and low frequency oscillations. In both figures, the amplitude of the waveform propagating parallel to the roll direction, unobstructed by the welded attachment has an amplitude higher than the waveform propagating perpendicular to the roll direction obstructed by the weld.

The waveforms of the plate with the web-to-flange connection on the opposite side (P6′) are compared with the waveforms for the plain flange plate (P2) in Figure 6.31. Waveforms generated by impact in Q2 are compared, and Figure 6.31 (a) contains waveforms propagating parallel to the roll direction and Figure 6.31 (b) contains waveforms propagating perpendicular to the roll direction. The figure shows that the waveforms parallel to the roll direction and unobstructed by the welded attachment are similar in shape, with a variation in amplitude resulting from coupling of the transducers. The waveforms perpendicular to the roll direction have a similar pattern of high frequency oscillations. Differences occur in the signals low frequency, high amplitude oscillations, particularly in the first positive peak. The waveform from P2 has a much sharper positive peak, with a large

amplitude oscillation that descends rapidly. The waveform of P6′ tends to flatten at the top of this first positive peak.

Other comparisons can be made between the waveforms of P6′ and P6, to determine the effect of the orientation of the web-to-flange connection. Figure 6.31 shows the waveforms generated from an impact in Q2 for these two plates (P6′ and P6). In both Figure 6.31 (a) (waveforms parallel to the roll direction and unobstructed by the welded attachment) and Figure 6.31 (b) (waveforms perpendicular to the roll direction and obstructed by the attachment), the waveforms of P6′ and P6 agree in amplitude and shape for the duration of the record. This indicates that the orientation of the web-to-flange connection with respect to the impact and transducer locations (i.e. same or opposite side) does not effect the stress waves as they propagate through the plate.

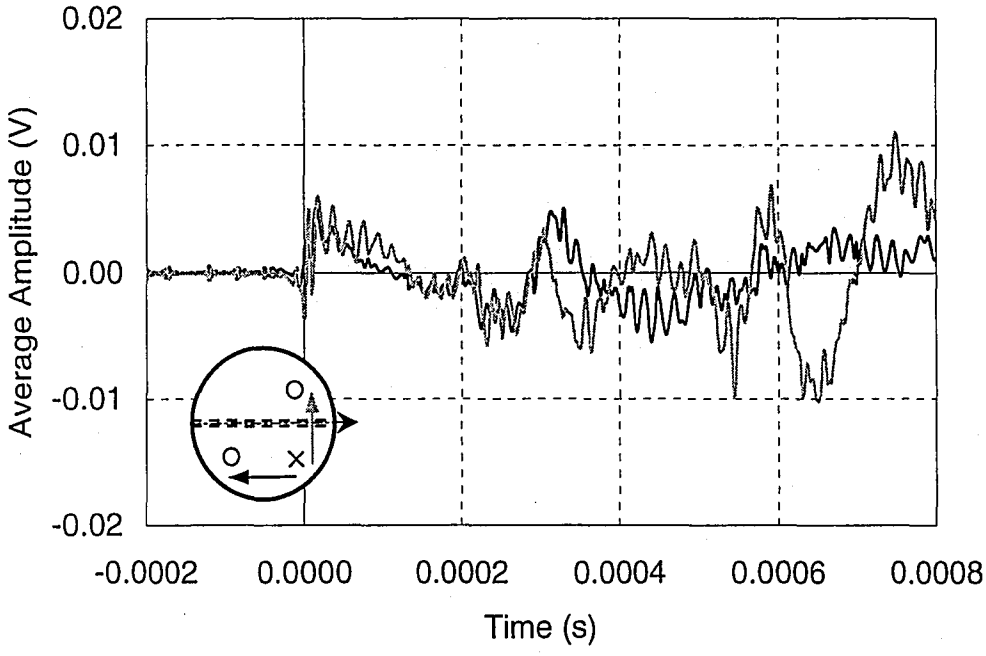

(a)

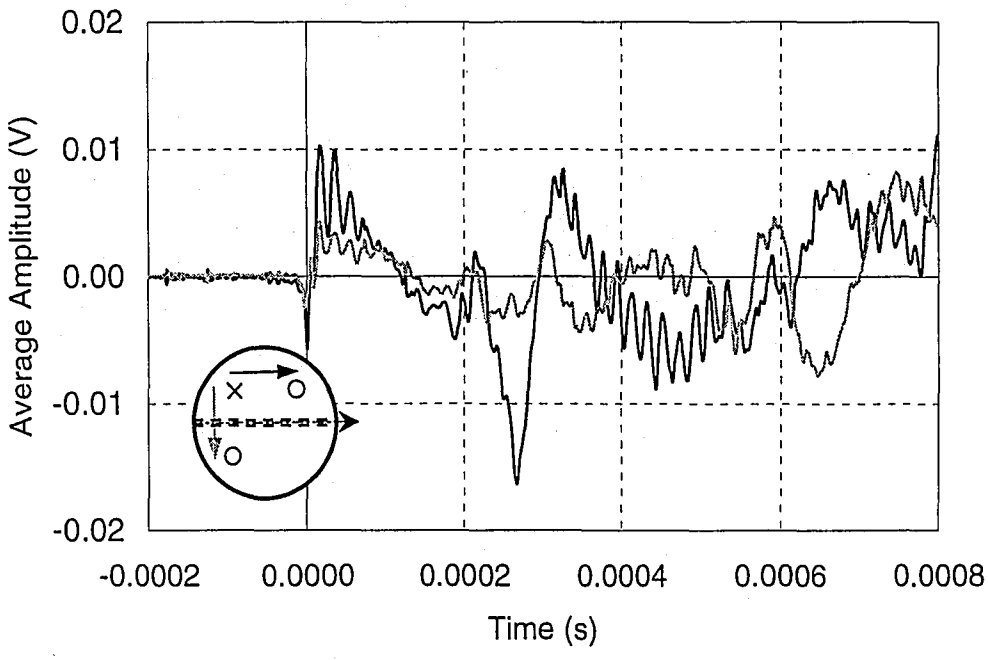

(b)

Figure 6.29 Effect of the web-to-flange connection on the opposite side of the plate (P6'): (a) resulting from impact in Q2; (b) resulting from impact in Q4.

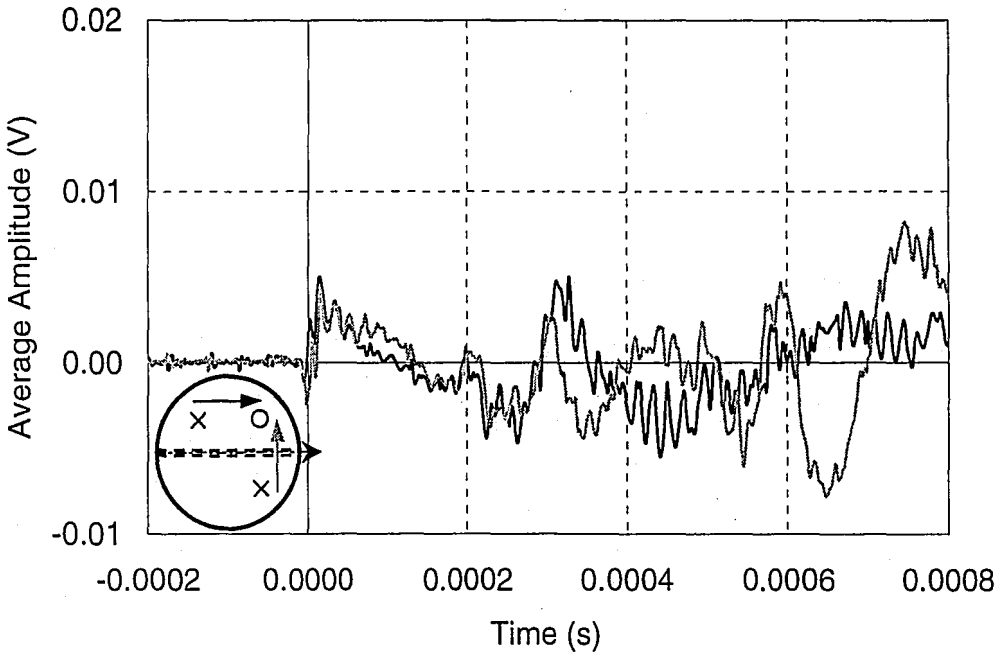

(a)

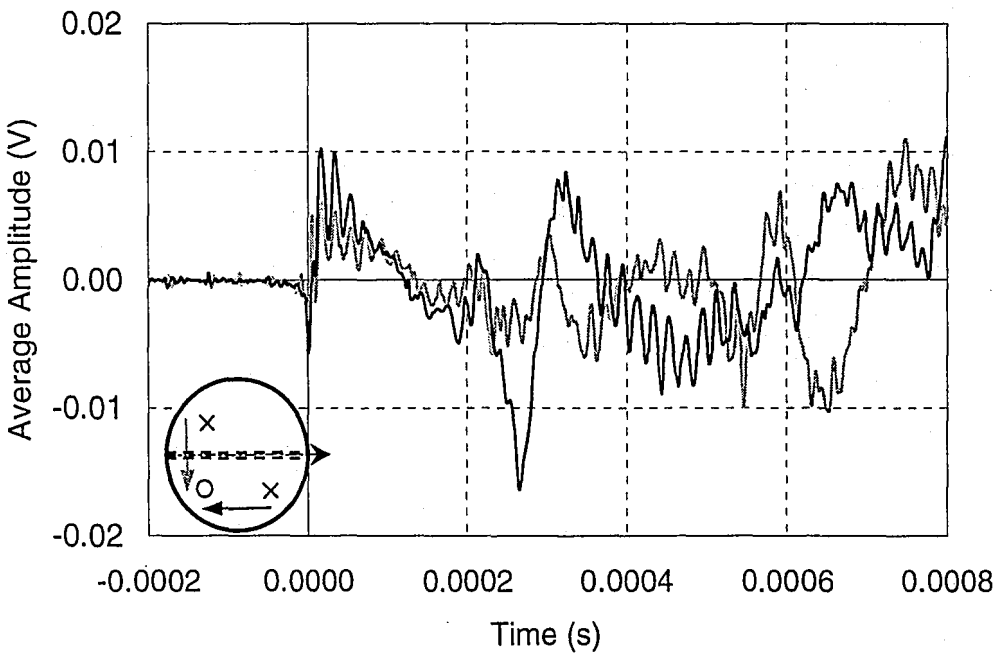

(b)

Figure 6.30 Effect of the web-to-flange connection on the opposite side of the plate (P6'): (a) recorded by a transducer in Q1; (b) recorded by a transducer in Q3.

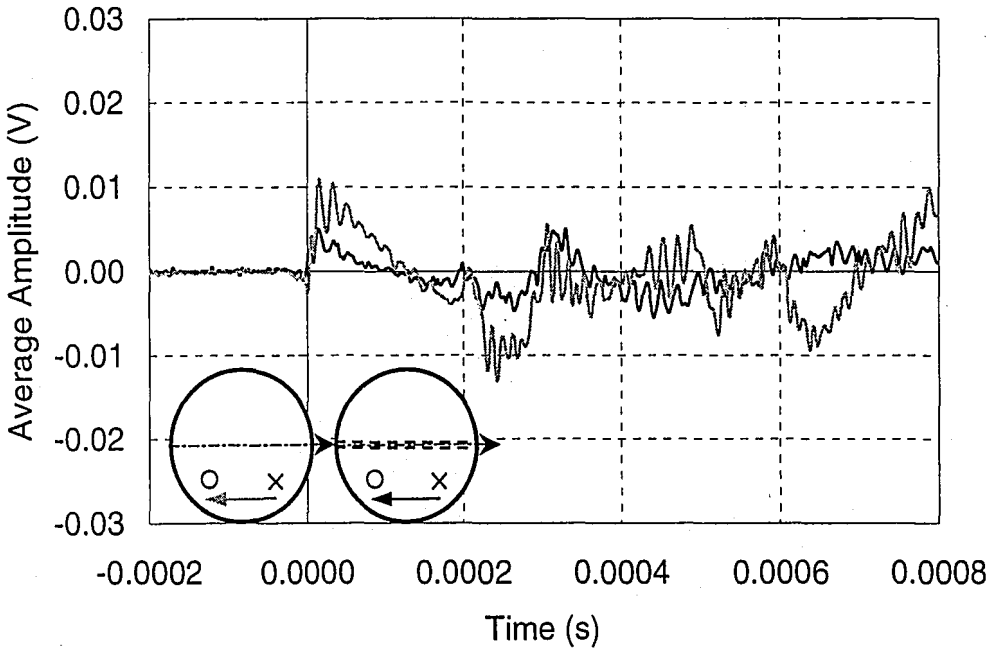

(a)

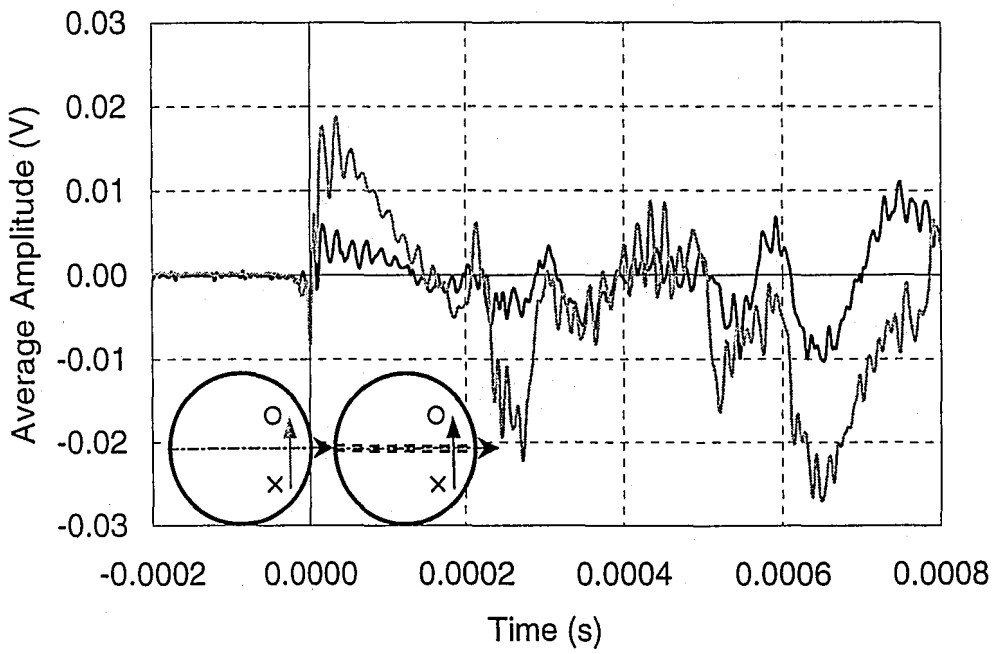

(b)

Figure 6.31 Effect of the presence of the web-to-flange welded attachment on the opposite side (P6') compared to the plain plate (P2): (a) parallel to the roll direction; (b) perpendicular to the roll direction.

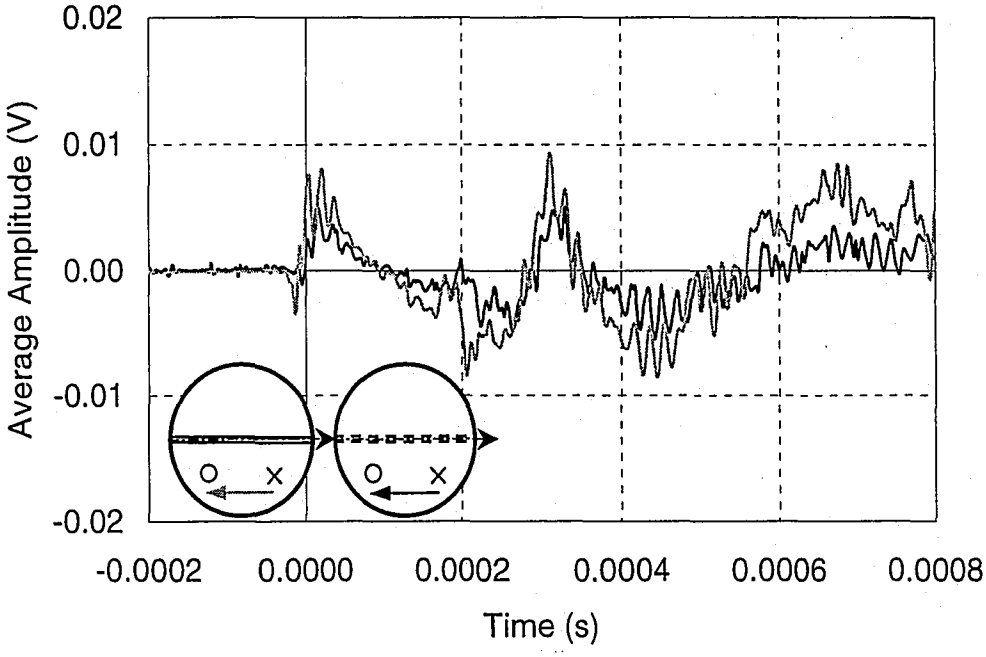

(a)

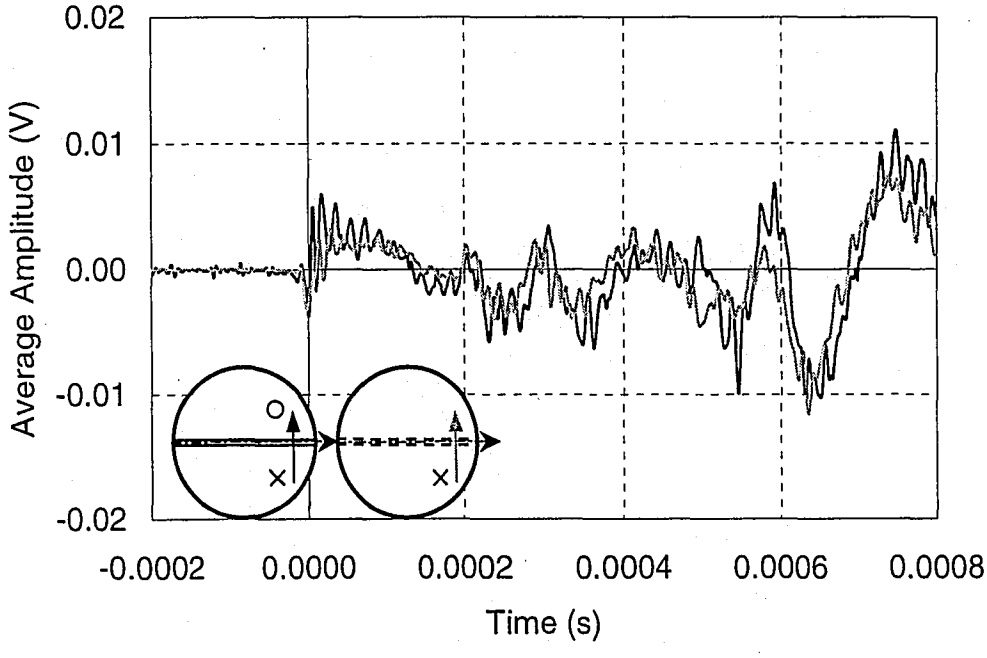

(b)

Figure 6.32 Effect of the orientation of the web-to-flange attachment (P6 versus P6'): (a) parallel to the roll direction; (b) perpendicular to the roll direction.

6.14 SUMMARY

Chapter 6 presents an analysis of the results of the testing done in this research. Waveforms are compared to determine the effect of welded details present between the source and transducer location on stress waves as they propagate in a steel plate girder. Impact from steel spheres is used as an input source, creating a highly repeatable surface displacement waveform. The results can be analyzed in the time domain using average waveforms created from repeated impacts. With repeated impacts, slight misalignment of the waveforms can occur in the time domain. The misalignment can be ignored in signal averaging.

The effect of the roll direction on stress waves as they propagate either parallel to or perpendicular to the roll is determined from the plain web and flange plates, P1 and P2. In the web plate (P1), the waveform is elongated on the time axis for waveforms traveling parallel to the roll direction. It is determined that the material is dispersive in that direction. This dispersion effect is small, and no significant attenuation occurs in either the amplitude or the shape of the surface displacement waveform due to the roll direction of the steel plates.

Plates P3 and P4 are used to show that the single V groove weld used for both the flange and the web splice have no effect on the amplitude or shape of the stress waves that are obstructed by it. The splice plates with the groove weld down (P3′ and P4′), show that the orientation of the weld (open upward or open downward) has no effect on the waveforms.

The stiffener-to-web and web-to-flange connections cause attenuation of both the shape and amplitude of the surface displacement waveform. The location of the connection with respect to the transducer and impact location does not affect the waveform. The attenuation of the signal is the same if the attachment is on the side of the plate with the transducers and impact, or on the opposite side.

CHAPTER 7

CONCLUSIONS AND FUTURE RESEARCH

7.1 INTRODUCTION

The objective of the research presented in this report was to experimentally study the attenuation of acoustic emission signals caused by welded details commonly used in welded steel plate girders. A series of small scale specimens were made to replicate the web and flange of a welded steel plate girder, as well as a web splice, flange splice, stiffener-to-web connection, and web-to-flange connection. Stress waves were created in the specimens by mechanical impact and the waveforms were recorded and compared.

Conclusions from this research are presented in Section 7.2, and areas of future research are discussed in Section 7.3.

7.2 CONCLUSIONS

The following conclusions are drawn from this research. The conclusions are applicable to the materials and geometries treated in this study.

1. Roll direction has no effect on the amplitude or shape of the surface displacement waveform in the 51 mm plate (P2). The roll direction has no significant effect on the amplitude or shape of the surface displacement waveform in the 13 mm plate (P1). However, the roll direction may cause dispersion in the 13 mm plate. The surface displacement waveform

caused by stress waves traveling in the direction parallel to the roll was observed to lag behind waveform caused by stress waves traveling perpendicular to the roll direction.

2. A web splice comprised of a single V groove weld (P3) has no effect on the amplitude and shape of the surface displacement waveform in the 13 mm plate. The orientation of the single V groove weld with respect to the impact and transducer placement (i.e. with the V up for P3, and with the V down for P3') does not effect the waveform.

3. A flange splice comprised of a single V groove weld (P4) has no effect on the amplitude and shape of the surface displacement waveform in the 51 mm plate. The orientation of the single V groove weld with respect to the impact and transducer placement (i.e. on the same side for P4, or on the opposite side for P4') does not effect the waveform.

4. A stiffener-to-web connection (P5) causes an attenuation of the amplitude and shape of the surface displacement waveform in the time domain. The attenuation of the waveform is independent of the stiffener location with respect to the impact and transducer placement (i.e. on the same side for P5, or on the opposite side for P5').

5. The web-to-flange connection (P6) causes an attenuation of the amplitude and shape of the surface displacement waveform in the time domain. The attenuation of the waveform is independent of the connection location with respect to the impact and transducer placement (i.e. on the same side for P6, or on the opposite side for P6').

7.3 FUTURE RESEARCH

There are several areas of future research that logically follow from the work that is described in this report. Progress in these future research areas will contribute to a greater understanding of the attenuation of acoustic emission signals in welded steel structures. Areas of future research are discussed below:

1. Only experimental results are presented in this report. Finite element analyses may be performed to study the propagation of the stress waves in the plates. This may be a useful way to explain the general shapes of the surface displacement waveforms in the plates in which attenuation of the signals was not observed. Finite element analyses may also be used to study the interactions of the stress waves with the plates at the stiffener-to-web and flange-to-web connections. This may lead to a further understanding of the attenuation that takes place at these details. If the finite element modeling is successful, then additional finite element analyses may be performed to treat other plate thicknesses and geometries not treated in this report.

2. The work described in this report used impact to impart stress waves to the test plates. While this lead to very repeatable inputs, other input sources with characteristics more like fatigue cracking (e.g. the use of pencil lead breaks on the surfaces of the plates) should also be explored.

3. The work described in this report used broadband displacement transducers. The tests described in this report should be repeated with other types of transducers such as resonant transducers (which are often employed in actual acoustic emission testing of structures).

4. The tests conducted in this research were made on small specimens that reproduced several details commonly found in actual welded steel plate girders. Reflections of stress waves from the boundaries of the test plates may have obscured some of the information that could have been obtained from the tests. The types of tests described in this report should also be conducted on full size welded plate girders to treat conditions that would be found in actual structures.

Appendix A

This sample calculation to determines the natural frequency of a free circular plate for n=3, s=2. Assuming a steel plate with a diameter of 915 mm has the properties given, the frequency and the location of the nodal diameters can be calculated as follows for the case of three nodal diameters and two nodal circles.

Material Properties:

$E = 207\ GPa = 207 \cdot 10^9\ kg/(m \cdot s^2)$
$\rho = 7850\ kg/m^3$
$\nu = 0.3$

Geometric Properties:

$R = (0.915\ m)/2 = 0.458\ m$
$t = 0.051\ m$

Equation 2-12 calculates the plate rigidity, D.

$$D = \frac{Et^3}{12(1-\nu^2)} = \frac{(207\times10^9 \frac{kg}{m\cdot s^2})(0.051m)^3}{12(1-0.3^2)} = 2485071\frac{kg\cdot m^2}{s^2}$$

From Table 2.1, the α value for a free circular plate with n=3 and s=2 is 111.30. Equation 2-11 yields the natural angular frequency associated with the mode shape n=3, s=2.

$$\omega = \frac{\alpha}{R^2}\sqrt{\frac{D}{\rho t}} = \frac{111.30}{(0.458m)^2}\sqrt{\frac{2485071\frac{kg\cdot m^2}{s^2}}{(7850\frac{kg}{m^3})0.051m}} = 42000\frac{rad}{s}$$

The natural frequency is obtained from the angular frequency by dividing by 2π.

$$f = \frac{\omega}{2\pi} = \frac{4200\,\frac{rad}{s}}{2\pi} = 6690Hz = 6.69kHz$$

The location of the nodal diameters is given in Table 2.3. For the n=3, s=2 case, the R′/R values are given as 0.925 and 0.605. The circles of zero deflection will occur at radii of

$$R'_1 = \frac{R'}{R} \times R = 0.925 \times 0.458 = 0.423m, \text{ and}$$

$$R'_2 = \frac{R'}{R} \times R = 0.605 * 0.458 = 0.277m.$$

The nodal diameters are equally spaced. Therefore, the three nodal diameters will be 60° apart. Figure A.1 shows the location of the nodal diameters and circles for this case.

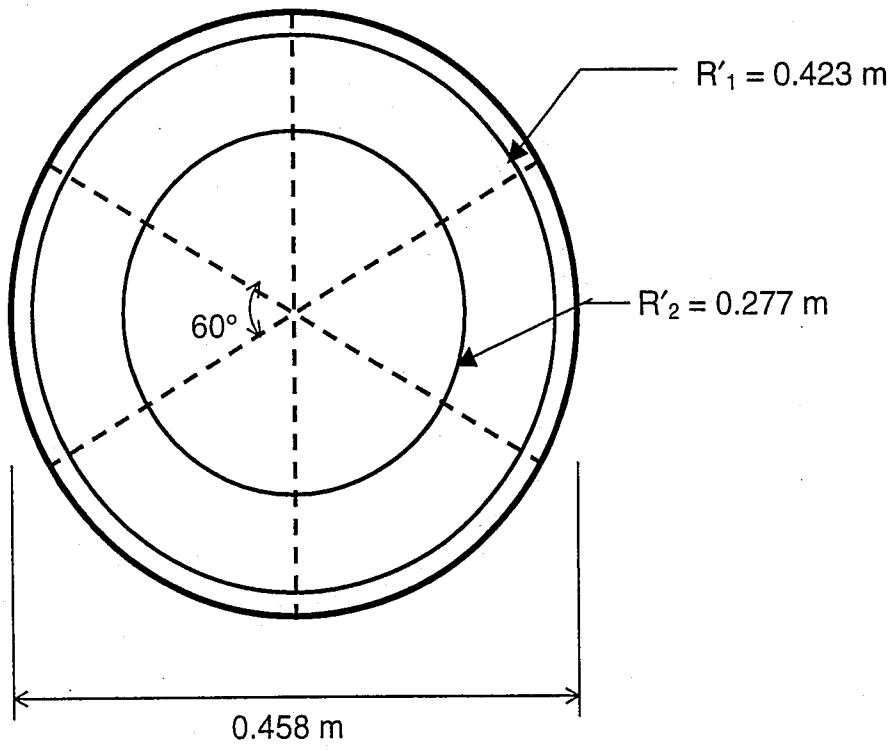

Figure A.1 Location of nodal circles and diameters for the s=2, n=3 mode.

REFERENCES

American Institute of Steel Construction, (1998) "Manual of Steel Construction: Load and Resistance Factor Design," 2nd Ed.

American Society for Nondestructive Testing, (1987) *Nondestructive Testing Handbook Volume 5: Acoustic Emission Testing 2nd Ed.*, ASNT, USA.

American Welding Society, (1995) "D1.5-95 Bridge Welding Code".

American Society for Testing and Materials, (2001) "Guide for Determining the Reproducibility of Acoustic Emission Sensor Response" E976.

American Society for Testing and Materials, (2001) "Standard Definition of Terms Relating to Acoustic Emission" E1316-00.

American Society for Testing and Materials, (2001) "Standard Test Method for Acoustic Emission Testing of Insulated Digger Derricks" E1797-98.

American Society for Testing and Materials, (2001) "Standard Test Methodfor Examination of Seamless, Gas-Filled, Pressure Vessels Using Acoustic Emission" E1419-00.

American Society for Testing and Materials, (2001) "Test Method for Acoustic Emission for Insulated Aerial Personnel Devices" F915.

Connor, R., (2000) Private Correspondence, November.

Gary, J., Hamstad, M, and O'Gallagher, A., (1994) "Computer Modeling of Waves Generated by Acoustic Emissions", National Institute of Standards and Technology.

Goldsmith, W., (1965) *Impact: The Theory and Physical Behavior of Colliding Solids*, Edward Arnold Press, Ltd., Vol. 33, pp. 725-757.

Heiple, C. R. and carpenter, S. H. (1983) "Acoustic Emission from Dislocation Motion" *Nondestructive Testing Monographs and Tracts Volume 2: Acoustic Emission*, Gordon and Breach Science Publishers.

Horn, D. T., (1992) *Designing and Building Electronic Filters*, Tab Books, Blue Ridge Summit, PA, pp. 1-58.

Jolly, W. D., (1992) "Status and future Directions for acoustic Emission Standards," N*ondestructive Testing Standards—Present and Future, ASTM STP 1151*, H., American Society for Testing and Materials, Philadelphia, pp 56-62.

Leissa, A. W., (1977) "Recent research in Plate Vibrations: Classical Theory" *Shock and Vibration Digest*, Vol. 9, No. 10, p.13.

Matthews, J. R., (1983) "Acoustic Emission Evaluation" *Nondestructive Testing Monographs and Tracts Volume 2: Acoustic Emission*, Gordon and Breach Science Publishers.

Miller G., and Pursey, H., (1955) "On the Partition of energy Between Elastic Waves in a Semi-Infinite Solid" *Proceedings of the Royal Society of London*, A, 233, pp. 55-69.

Miller, G., and Pursey, H., (1954) "The Field and Radiation Impedance of Mechanical Radiators on the Free Surface of a Semi-Infinite Solid," *Proceedings of the Royal Society of London*, A, 223, pp. 521-541.

Proctor, T. M., Jr., (1982) "Some Details on the NBS Conical Transducer," *Journal of Acoustic Emission*, Vol. 1, No. 3, pp. 173-78.

Rao, J.S., (1999) *Dynamics of Plates*, Narosa Publishing House, New Delhi.

Ravenhall, F. W., and Som, A. K., (1973) "Some Recent Observations on Chlandi's Figures" *Acustica*, Vol. 29, p 14.

Roberts, W. L., (1983) *Hot Rolling of Steel*, M. Dekker, New York.

Sansalone, M. J., and Streett, W. B., (1997) *Impact-Echo: Nondestructive Evaluation of Concrete and Masonry*, Bullbrier Press, Ithaca, NY, pp. 9-83.

Santamarina, J. C., and Fratta, D., (1998) *Introductrion to Discrete Signals and Inverse Problems in Civil Engineering*, ASCE Press, Reston, VA.

Weaver, W., Timoshenko, S. P., and Young, D. H., (1990) *Vibration Problems in Engineering, 5th Ed.*, John Wiley & Sons, Inc, New York.

VITA

Jacqueline Mayrosh was born September 15, 1977 in Easton, Pennsylvania. She is the only child to Mr. and Mrs. Daniel Mayrosh. In June of 1999, she received a Bachelor of Science in Civil Engineering from Lehigh University. The author remained at Lehigh University to pursue a Master of Science in Structural Engineering. She expects to graduate in January of 2002. The author has accepted employment with URS Corporation and will work in the Airport Division of their Hunt Valley, Maryland office.

END OF TITLE